Systems Identification of Sensorimotor Control for Visually Guided Wrist Movements

Chintan Poladia
Marquette University

SYSTEMS IDENTIFICATION OF SENSORIMOTOR CONTROL FOR VISUALLY GUIDED WRIST MOVEMENTS

by

Chintan Poladia, B.S.

A Thesis submitted to the Faculty of the Graduate School,
Marquette University,
in Partial Fulfillment of the Requirements for
the Degree of Master of Science

Milwaukee, Wisconsin

August 2009

ABSTRACT

SYSTEMS IDENTIFICATION OF
SENSORIMOTOR CONTROL
FOR VISUALLY GUIDED
WRIST MOVEMENTS

Chintan Poladia, B.S.
Department of Biomedical Engineering
Master of Science

The sensorimotor control system is a complicated system in which the neural controller uses the feedback information from sensory modalities (visual, proprioceptive, vestibular, auditory, etc.) to actuate the musculo-skeletal system in order to execute intended movements. It has been an ongoing research to decode this sensorimotor integration. The current study utilized a systems identification approach in conjunction with a one-degree-of-freedom robotic manipulandum to quantify (delays, noises, wrist dynamics and controller parameters) a simplified (linear time-invariant) model of sensorimotor control for visually guided wrist stabilization movements.

Four sensorimotor tasks were used to characterize the parameters of the sensorimotor control model. Open loop visual and proprioceptive delays along with effective feedforward delay (associated with motor processing and feedforward conduction) were estimated from subject's response to perturbation (Exp. 1) using cross-correlation analysis. Multiplicative feedforward (motor) noise was estimated by measuring the force variability in isometric torque contractions at 5 different torque levels (Exp. 2). Frequency response analysis (Exp.3 and 4) was used to obtain estimates of wrist dynamics (inertia, viscosity and stiffness), the feedback (visual and

proprioceptive) gains, the controller gains (proportional, integral and derivative) and an additive sensory noise. The experimental paradigms were validated by simulating and testing the experimental task along with the sensorimotor control model in SIMULINK®. The ability of the experiments to characterize the model was tested over a range of parameter values to determine the robustness of the approach. Model performance was measured by characterizing the sensorimotor control system in 11 subjects. Variance Accounted For (VAF) by the model was used as a performance metric to compare model's response (obtained using the parameters measured for each subject in the model) with subject's performance (Exp. 5).

The proposed model of sensorimotor control contained 13 parameters, which were measured successively to study their interaction during wrist stabilization in 11 neurologically-intact subjects. The model parameters estimated for human subjects resulted in accurate predictions of hand position, with a high percentage of variance accounted for (VAF) across all subjects (78.3±3.3 %). Future studies will use these techniques to quantify how the sensorimotor control changes across tasks (tracking vs. stabilization), age and neuro-motor disabilities.

ACKNOWLEDGEMENTS

Chintan Poladia, B.S.

I would like to acknowledge my funding sources, Falk Family Medical Research Trust and the Ralph and Marion Birnschein Foundation, NSF 0238442 and NIH HD53727. This study was carried out at Integrative Neural Systems Laboratory and Neuromotor Control Laboratory at Marquette University

I wish to thank my thesis director, Dr. Scott Beardsley, who suggested the topic and guided me through the entire process. Your help and ideas have been invaluable. Thanks for giving me the opportunity to be part of this research. I wish to thank Dr. Robert Scheidt for his guidance and advice, and for allowing me to use his 1-D wrist robot for this study. I also wish to thank Dr. Brian Schmit and Dr. Michelle Johnson for serving on my committee and for their constructive feedback.

A special thanks to my lab colleagues and friends for their help and support.

Finally, I wish to thank my parents and brother for all their advice and encouragement during the thesis process. I would like to dedicate this thesis to my mother who has been a great source of inspiration throughout my academic career.

TABLE OF CONTENTS

LIST OF TABLES

LIST OF FIGURES

1 INTRODUCTION & SPECIFIC AIMS

Sensorimotor control for posture and goal-directed movement is central to our ability to carry out activities of daily living (ADL), such as grasping and/or reaching for an object, driving, drinking and writing. Accurate and efficient execution of the stabilizing and tracking movements underlying such activities relies on feedback from sensory modalities (visual, proprioceptive, vestibular, auditory, etc.) to enable on-line corrections to errors in intended movement and changes in the environment. Deficits in the propagation and integration of sensory information to control movement can result in functional motor impairment within specific patient populations (e.g. Multiple Sclerosis (MS)). Thus, developing targeted treatments and therapies to improve ADLs requires a more detailed understanding of how the neural systems that implement sensorimotor control interact to produce smooth and precise movement across tasks and within neurologically intact subjects.

From the standpoint of control systems theory, sensorimotor control can be modeled in its simplest form as a negative feedback system consisting of a feedforward path and multiple feedback paths. Hitherto, investigators have developed qualitative models of sensorimotor control (Kawato 1999; Miall et al. 1993b; Wolpert and Miall 1996a; Mehta and Schaal 2002), but few have attempted to systematically quantify the parameters that characterize the model (Peterka 2002; Schouten et al. 2008). The current study builds on the generalized sensorimotor control framework proposed for goal-oriented stabilization and tracking (Miall et al. 1993b; Wolpert and Miall 1996a; Mehta and Schaal 2002; Peterka 2002) to develop a linear time-invariant model of sensorimotor control during visually guided wrist stabilization.

In the current study, a systems identification approach was developed to experimentally measure the temporal delays, internal noises, feedback gains, neural controller, and wrist dynamics that characterize sensorimotor control in human subjects. In a series of visually-guided wrist stabilization tasks, subjects used a one-degree-of-freedom robotic manipulandum to maintain a user-controlled cursor on a visual target in the presence of externally applied perturbations. Cross-correlation and frequency response function analyses across experimental conditions were then used to estimate the parameters of the 1-D model of wrist control developed in parallel with the experiments. Accordingly, the aims of the research were:

Aim 1: Develop a model of sensorimotor control for 1-D wrist movement.

Aim 2: Use system identification techniques to develop a set of visuo-motor control tasks that can be used in conjunction with the model and a 1-D robotic wrist manipulandum to characterize sensorimotor control in neurologically-intact subjects.

Aim 3: Validate the model and the subsequent experimental approach by comparing the results of subjects obtained experimentally with those obtained from model simulations on an individual performance basis.

In the future, the methodological approach developed here will be used to characterize the sensorimotor control system in neurologically impaired patients (MS with tremors). Significant deviations in the parameter estimates of the patient population could help discern the underlying source(s) of tremor.

2 BACKGROUND & SIGNIFICANCE

2.1 Motivation

Human sensorimotor control is a highly complex system capable of performing goal-oriented movements with multiple degrees of freedom. To achieve smooth and precise movement, the brain utilizes feedforward planning and sensory feedback (visual, proprioceptive, vestibular, auditory etc.) of the intended movement, to actuate the musculo-skeletal system and make online corrections during movement. Multiple brain areas are involved in this process including the visual, somatosensory, parietal, pre-motor, and motor areas of the cerebral cortex, cerebellum, spinal cord, basal ganglia and thalamus. The sensory information (about the location of the limb) processed by the brain then drives multiple groups of muscles to perform an intended movement. The accuracy and precision of the control system is time-varying as it changes with age, training and adaptation (Miall and Jackson 2006; Bock and Girgenrath 2006). Owing to input from multiple feedback modalities, multiple muscle groups involved in making the movement and various regions of the brain involved in processing, the sensorimotor system is, in its most general form, a highly complex, nonlinear time varying system.

Of particular interest to a number of researchers has been to develop quantitative models of sensorimotor control and its interaction with physical systems. Early studies were focused on the development of human operator control models to explain the behavior of pilot-vehicle control systems (McRuer and Krendel 1959). The purpose of these models was to understand the control actions of the pilot, such that it could be used in conjunction with vehicle dynamics in forming predictions. Other studies were more general wherein they modeled human operator dynamics to predict human performance

to different tracking tasks (Osafo-Charles et al. 1980; Shinners 1974).

More recently, research has shifted toward characterizing sensorimotor control associated with activities of daily living The main motivation underlying most of these studies has been to decipher the function (sensorimotor integration, limb trajectories, interaction forces, joint torques, stability, muscle activations) of the complex system under different task conditions (Kawato 1999; Mehta and Schaal 2002; Peterka 2002; Flanders and Cordo 1989; Harris and Wolpert 1998; Wolpert et al. 1995). Other studies have focused on understanding the changes in control strategy that occur in response to neurological impairment (Beppu et al. 1984; Feys et al. 2003a; van Donkelaar and Lee 1994) and developing focused rehabilitation strategies to account for dysfunctional behavior (Morgan et al. 1975; Kotovsky and Rosen 1998; Rocon et al. 2004). Hitherto, these studies have developed simplified qualitative models of the system (Kawato 1999; Miall et al. 1993b; Mehta and Schaal 2002; Miall and Reckess 2002; van Beers et al. 1999; Wolpert and Miall 1996b), but few have attempted to fully quantify the parameters that together characterize the model (Peterka 2002; Schouten et al. 2008).

Results from previous studies suggest that as a first order approximation, sensorimotor control can be considered to be a linear system (Mehta and Schaal 2002; Peterka 2002; Schouten et al. 2008; Fitzpatrick et al. 1996). The current study builds on this approach to define and quantify a simplified (linear time-invariant) 1-D model of sensorimotor control during feedback stabilization of wrist position For the purpose of our model, the following simplifying assumptions were made: i) the system was considered to be a time-invariant such that learning or adaptation was minimized during an experimental session; ii) subjects' performance was ergodic; iii) system properties

(e.g., conduction delays, noise sources) could be expressed as a single lumped parameter; iv) to a first order approximation, sensorimotor control could be modeled as linear system.

Relative to the shoulder and elbow joints, the selection of the wrist joint as a model to characterize sensorimotor control offers several advantages, including simplicity in devising the experimental setup and ease in performing 1-D movements. An additional advantage is that it is a more distal joint, and impairments such as tremor are disproportionately larger in the distal limb (Deuschl et al. 1998; Smaga 2003). Thus, the use of wrist movement to characterize a model for sensorimotor control will enable future studies to investigate the impact of such impairments on 1-D movement control.

2.2 Visually-guided posture stabilization and goal-directed movements

Hogan and Sternad have recently provided clear definitions of two distinct motor behaviors, limb posture stabilization and goal-directed movements (Hogan and Sternad 2007). The tasks we are studying in these experiments is one of posture stabilization where an external stimulus drives the hand and/or the cursor representing the location of the hand from its intended target. As we will show, subjects respond by performing discrete corrective actions or in terminology of Hogan and Sternad, by performing goal-directed movements.

Daily activities including writing, drinking, reaching for an object, and using a computer mouse, can be classified as visually-guided goal-directed movements involving the use of sensorimotor control. From the viewpoint of control system theory, a visually-guided goal-directed movement can be separated into two control phases: i) an initial

feedforward phase, which brings the limb to a position in the neighborhood of the target; ii) followed by a feedback directed phase, in which the limb homes in on the target (Woodworth 1899; Elliott et al. 2001; Ghez et al. 2007; Scheidt and Ghez 2007). During the feedforward phase, pre-planned movements are made by the limb and accompanied by movements of the eye, while during the feedback phase, movements are adjusted to compensate for errors in position (and/or velocity) detected via the sensory pathways (e.g., visual and proprioceptive).

2.3 Sensory feedback for goal-directed movements

Typically, an eye movement precedes the motion of the limb (Helsen et al. 1998) in order to bring the region of interest (external environment) into the foveal vision (Binsted and Elliott 1999). The information (about the external environment) flashed onto the retina in the form of patterns of lights is then converted into neural impulses which are processed in a hierarchical fashion by the eye, lateral geniculate nucleus, striate and extrastriate visual cortices, and subsequently used by higher brain areas to guide movement. During the movement, proprioceptive signals encoding the spatial location of the limb are fed back to the somatosensory cortex to update the intended movement. The visual and proprioceptive sensory modalities are the two primary sources for providing feedback during visually-guided goal-directed movement which is in turn compared to the desired movement to generate an error signal that is used by the neural controller to achieve the desired movement. For visually-guided movements, visual feedback plays a greater role in updating movement than proprioceptive feedback (Boff et al. 1986). However, it is still not clear how these weightings are assigned to each path. The weighting could depend on the precision of the information in each modality (van Beers

et al. 1999; Pick et al. 1969; Welch et al. 1979) or may be a function of the attention directed to each modality (Kelso et al. 1975; Uhlarik and Canon 1971; Warren and Schmitt 1978). Other studies have shown that the weightings change based on the experimental condition suggesting a dependence on the task at hand (Mon-Williams et al. 1997; Plooy et al. 1998).

Delay and noise are inherent properties within any physiological system including sensory processing. Prior to its use in motor action, the incoming sensory information is delayed. The feedback delay, i.e. the delay in the incoming sensory information prior to its involvement in computing motor action, encompasses afferent delays associated with the propagation of signals from the peripheral nervous system and the delays associated with processing the sensory information in the cortex. Feedback delays typically range from 80-150 ms for proprioceptive control (Flanders and Cordo 1989; Paillard 1996) and 200-500 ms for visuomotor control (Flanders and Cordo 1989; Paillard 1996; Keele and Posner 1968). Additionally, the representation of high-level spatial information within sensory systems is not exact. Variations in the neuronal representation associated with nonlinear transduction, synaptic transmission and network (neuron) interactions (Faisal et al. 2008), as information propagates through sensory subsystems can manifest as uncertainties in sensory feedback estimates of position and velocity during goal-directed movement and can be attributed to the presence of noise sources within the sensory sub-systems (Izawa and Shadmehr 2008).

The current model is based on an implicit assumption that the position information propagated through the feedback paths consists of four components: an unbiased estimate of the limb's actual position, lumped parameter models of the

propagation delays and additive internal noise sources within each path, and a gain (weighting) reflecting the relative contribution of different sensory sources to the position estimate. The current study aims to quantify these parameters in order to understand the interactions that occur between sensory feedback paths during the control of movement.

2.4 Feedforward path

Figure 2.1 shows a simplified block-diagram representation of the sensorimotor control system comprised of visual and proprioceptive feedback path and a feedforward motor path. In the model, the integrated feedback information is used by the neural controller (representing areas of the brain involved in error processing and initiation of corrective movement) to generate a set of motor commands to the muscles around the joint whose patterns of contraction produce the desired movement. Studies have shown

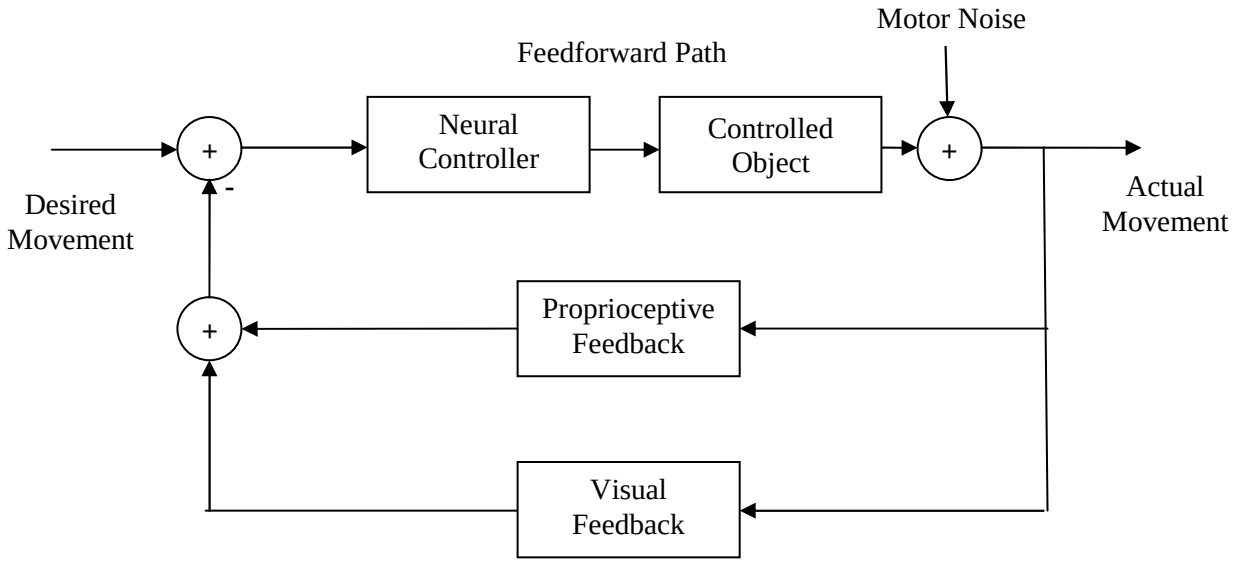

Figure 2.1 Simplified block diagram representation of sensorimotor control. The current state of movement is measured by the sensory modalities (visual and proprioceptive) and combined to generate an estimate of the actual movement. The sensory estimate is compared to the desired or intended movement and the resulting error is processed by the neural controller to produce a set of motor commands to achieve the desired movement.

that in its most basic form, the feedforward path is comprised of a controller (corresponding to the cortical processing of and in-line correction for perceived error), the plant or controlled object (corresponding to the limbs and their mechanical environment) and the conduction delay associated with the time taken for the motor commands to reach the plant from the controller (Peterka 2002; Izawa and Shadmehr 2008; Wolpert et al. 1998). Trial-by-trial variability in performing the same movement has been observed in a number of studies (Harris and Wolpert 1998; Jones et al. 2002a; van Beers et al. 2004) suggesting the presence of a (motor) noise source within the forward path between the neural controller and the plant (limb). The current study incorporates these elements into the sensorimotor control model and estimates the controller parameters, limb (wrist) dynamics and motor noise to characterize how they change across neurologically intact subjects and task conditions.

2.5 Forward Model

Owing to what are relatively large propagation and processing delays, if one were to rely solely on sensory feedback to control movement, fast movements such as catching a moving ball would not be possible. Understanding how the relative slowness of sensory feedback can be used for precise control has been the area of active research since Woodworth (1899) first proposed dissociating the target-directed movement into feedforward (ballistic) and feedback phases. Over the last three decades, studies to dissociate the role of feedforward and feedback paths in the execution of goal-directed movement have suggested the involvement of prediction mechanisms to compensate for the inherent delays in sensorimotor processing (Kawato 1999; Miall et al. 1993b; Wolpert et al. 1995; Wolpert et al. 1998). The prediction mechanisms, generally referred to as a

"Forward Models" (Mehta and Schaal 2002; Wolpert and Miall 1996b), models the behavior of the sensorimotor system to provide a noiseless estimate of predicted position and/or velocity using an efference copy of the motor commands sent to the controlled limb (Wolpert and Miall 1996a). The predicted output is compared to the actual feedback response and if the two position estimates are not matched, a new set of motor commands based on the error between the two estimates is generated to correct for erroneous movement and stabilize the system. The advantage of this type of predictive system is that it eliminates the effect of feedback delays by predicting the output of the feedback system, thereby making it possible to generate faster movements.

Neural implementation of the forward model has been attributed to the cerebellum (Miall et al. 1993b; Ito 1970). Cerebello-cortical circuits have also been shown to play an important role in the coordination and on-line control of visually guided movements (Miall and Reckess 2002; Stein and Glickstein 1992), especially in processing sensory information for, and resulting from, motor action. This has led to speculation that cerebellar systems may act as a comparator, contrasting intended movements with actual movement. Impairment of the cerebellum by disease can lead to improper functioning of the sensorimotor control system as a whole, potentially causing unstable movements. This is consistent with the reports of patients with cerebellar damage who have impaired goal-directed arm movements (Beppu et al. 1984; van Donkelaar and Lee 1994). As part of the research we test the assumption (based on previous literature) that the inclusion of the forward model acts to stabilize the system and successfully replicates human performance during a wrist stabilization task.

2.6 Current study

In parametric studies of sensorimotor control, research has typically focused on specific aspects of sensory (van Beers et al. 1999) and motor (Jones et al. 2002a; Notley et al. 2007) systems while others have used an indirect approach to estimate the parameters of the system (van Beers et al. 1999). Peterka (2001) proposed a system identification approach to characterize sensorimotor control for the maintenance of whole-body posture during stance. His model was structurally similar to that proposed here, however, it did not incorporate internal noises sources within the sensorimotor control system or attempt to isolate and estimate the delays within sensory feedback paths.

In the current study, we propose a detailed model of single-joint (1-D) sensorimotor control that builds on and extends the techniques developed by Peterka (2002). We employ system identification techniques to experimentally characterize the parameters of the model control system. Through a series of computer simulations we first validate the experimental approach by comparing the known values of the parameters used in the model with those estimated through simulation of the experiments and data analyses. The ability of the experiments to characterize the underlying model parameters was subsequently tested over a range of values to quantitatively determine the robustness of the experimental and analytical techniques. Finally, the basic structure of the model was validated by fully characterizing the sensorimotor control system in 11 subjects and measuring the Variance Accounted For (VAF), obtained by comparing the parameter–matched responses of the model with each subject's actual performance.

2.7 Methodology

Previously, a system identification approach has been used to quantify the contribution of sensory information to postural control (Peterka 2002) and proprioceptive reflexes during human arm control (Schouten et al. 2008). In system identification, an external disturbance (input to the system) is applied and the system's response (output) to the disturbance is measured to identify the transfer function that parametrically relates the input to the output. Here, a grey box modeling approach was used, since a mathematical relationship between the input and the output was assumed. The general structure of the model was derived from the sensorimotor literature (Kawato 1999; Miall et al. 1993b; Peterka 2002; Flanders and Cordo 1989; Beppu et al. 1984) and the mathematical relationship was formulated from the resulting control model. In grey box modeling, the parameters of the model are treated as free variables and estimated using either time-domain or frequency-domain analyses. In the current study, a time domain cross-correlation analysis was used for the estimation of system delays, while a frequency response function analysis was used to estimate other system parameters.

Tracking paradigms have been used previously to characterize human postural control (Peterka 2002), to measure adaptation in the subjects' response to delayed visual feedback (Foulkes and Miall 2000), and to study intention tremor in Multiple Sclerosis patients (Feys et al. 2003a). The advantage of choosing a tracking paradigm is its similarity (in terms of the strategy used) with activities of daily living. Furthermore, it provides unmatched simplicity in terms of experimental setup and input signal implementation. Two kinds of tracking tasks have been reported in literature; pursuit tasks (Miall and Reckess 2002; Foulkes and Miall 2000; Feys et al. 2003b), wherein the

subject tracks a moving target, and compensatory tasks (Peterka 2002; Schouten et al. 2008; Miall and Jackson 2006), wherein the error between the input and the output is displayed, and the subject's task is to minimize the error. In the compensatory task (referred to subsequently as a stabilization task), the target is normally held static. Such tasks have been extensively studied for the purposes of modeling pilot-vehicle systems in which the pilot produces a control action based on the displayed error between a desired command input and the comparable vehicle output motion (McRuer et al. 1965); and also for modeling human operator performance (Osafo-Charles et al. 1980; Shinners 1974). Here we employ a similar methodology to characterize stabilization about the wrist through the introduction of continuous sensory perturbations that cannot be predicted á priori.

The current study develops methods to experimentally characterize sensorimotor control through a series of four experiments which were designed to be similar in nature. External random perturbations were either introduced to the visual cursor (representing the limb position) or to the hand via a robotic manipulandum (force perturbation) and subjects were required to correct for the perturbation in order to place the cursor on a static target. Continuous perturbations were chosen over impulse perturbations to eliminate transient response effects and to constantly engage subjects in performing continuous online corrections.

2.8 Significance

Our results show that wrist stabilization using visual and proprioceptive feedback is essentially a linear process over the range of movements examined. This study also provides quantitative measures of the model parameters (delays, motor noise, feedback

gains, wrist dynamics and controller gains) associated with 1-D wrist stabilization. This study provided a better understanding of sensorimotor processing and integration, and demonstrated that the system for neurologically-intact subjects was inherently stable.

The techniques developed here to characterize wrist stabilization can be extended to other tasks and movement conditions - to compare and differentiate the strategies used for different tracking paradigms (pursuit tracking vs. compensatory tracking), study sensorimotor integration in 2-D movements, characterize the effects of age on sensorimotor control and to create humanoid robotic applications. In the long term, the above approach will be used to characterize the contributions of impaired sensory and motor processing to the phenomena of instability (in form of tremors) during goal-directed movement. Significant deviations in the parameter estimates of the patient population could help discern the underlying source(s) of tremor. This information could then be used to develop focused intervention and rehabilitation strategies for patients with movement disorders.

2.9 Workflow of the Thesis

The entire project was divided into different stages. The first stage was aimed towards developing the sensorimotor control model and a set of visuo-motor tasks that could be used in conjunction with 1-D robotic manipulandum to quantify the parameters of the model. The design and development of experimental tasks was an iterative process wherein an experiment was designed and tested via simulation using SIMULINK® until the error in the parameter estimation was within a predefined bound (of ± 25%). Pilot data was then collected on human subject to assess the sensorimotor control model and modifications were made in the model if its performance (measured in form of Variance

Accounted For (VAF) by the model) was not good (< 60%). Once the experimental tasks and the model were finalized, data was collected from a group of neurologically intact subjects to quantify the parameters of the sensorimotor control system. The model's performance was then evaluated by comparing each subject's performance with the model's prediction (obtained using the estimated parameters from the subject) to the same perturbation sequence. Finally, the robustness of the experimental paradigms was tested via simulation over a range of parameter values encompassing the experimentally measured parameter estimates.

2.10 Thesis Layout

As part of the Methods, Chapter 3 details the proposed model, the experimental setup used and the experimental design structure. During the process, all experimental paradigms were designed and tested first, followed by human data collection. However, in order to maintain a proper flow and for better understanding, each experiment (Chapters 4-7) is presented separately as a chapter. Within each chapter, a detailed description of the experimental task and data analysis is followed by simulations and experimental results (of one representative subject) and discussion. In Chapter 9, the proposed model's performance is evaluated by comparing its response to the human response. A separate discussion of the overall model, its importance and possible applications is presented as an additional chapter (Chapter 10). Results of the EMG analysis and future directions are presented in Chapter 8 and 11 respectively.

3 METHODS

3.1 Dual Feedback 1-D Model

To characterize the contribution of visual and proprioceptive pathways to motor control, a feedback model of 1-D wrist movement is proposed whose parameters were measured experimentally.

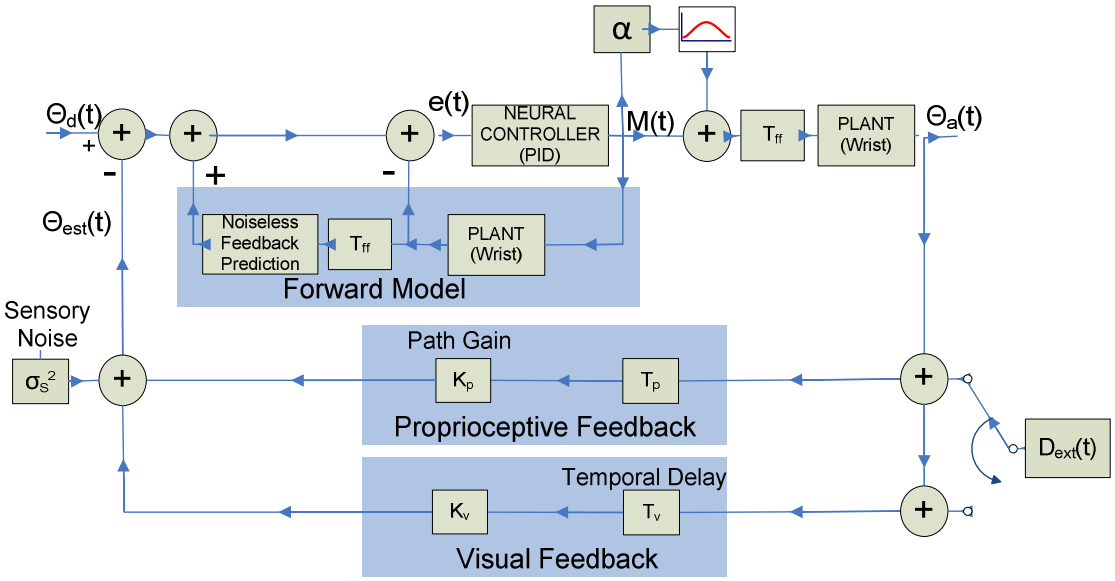

Figure 3.1 "Dual Feedback" model of sensorimotor control for 1-D wrist movements. The model consists of two sensory feedback paths (visual and proprioceptive). Each feedback path consists of a weight (K_v, K_p) and delay (T_v, T_p). A common block of additive noise was incorporated to represent cumulative sensory noise (σ_S^2). The feedforward path consists of neural (PID) controller, signal dependent feedforward noise (α), conduction delay (T_{ff}), plant (wrist) and a forward model. $\theta_d(t)$ and $\theta_a(t)$ indicate desired and actual movements respectively. External perturbations, $D_{ext}(t)$, were added to the cursor or the manipulandum depending upon the type of experiment.

The "dual feedback" model (Figure 3.1) uses negative feedback from two sensory inputs, visual and proprioceptive, to determine the position of wrist at any point of time. The visual system provides feedback of the wrist position based on the location of a cursor presented on a computer screen. The proprioceptive system on the other hand is an

interoceptive sense, which provides feedback of the wrist position based on the signals sent by the stretching of muscles. Each feedback path has a delay (T) and a weight (K) associated with it. The sensory noise (σ_S^2) is a lumped parameter that incorporates the cumulative noise within the feedback paths. In the current study, the sensory noise has been modeled as an additive source. The sum of the feedback weights is constrained to one, forming a unity-gain feedback system. The estimate of wrist position, $\theta_{est}(t)$, obtained from the feedback paths is compared to the desired wrist response, $\theta_d(t)$ to form an error signal, e(t), which forms the input to the feedforward path. The feedforward path consists of a controller (PID), multiplicative motor noise (α), feedforward conduction delay (T_{ff}) and plant characterizing the dynamic properties of the wrist (inertia, J; viscosity, B; stiffness, K). The forward model acts as a prediction mechanism for making fast movements. The subject's task was to stabilize the wrist in the presence of externally applied perturbations, $D_{ext}(t)$.

3.1.1 Neural Controller

Neural controller is part of the central nervous system which processes the error information of the limb and is involved in initiation of a movement. The neural controller

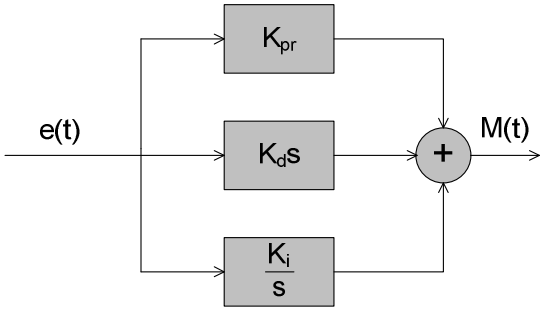

Figure 3.2 Neural Controller

was modeled as a proportional-integral-derivative (PID; Figure 3.2) controller to allow simultaneous correction of transient response properties and steady state error. A PID controller attempts to correct the error, e(t), between a feedback signal and a desired response by generating a controlling torque signal, M(t), to the plant such that the error is reduced. The transfer function of the neural controller is

$$\frac{M(s)}{e(s)} = \frac{K_d s^2 + K_{pr} s + K_i}{s} \qquad \text{eq. (1)}$$

where K_d, K_{pr} and K_i correspond to the derivative, proportional and integral gains respectively.

3.1.2 Plant

Second order models have been used successfully to replicate the performance of 1-d joint movements (Becker and Mote 1990; Bennett et al. 1992; Grey 1997). In this study, the flexion-extension movement of the wrist (plant) was modeled as a linear second order system having inertia, viscosity and stiffness. The parameters of the model were assumed to be constant over the time duration of the experiments. The net muscle torque sent from the neural controller is transformed by the plant into actual wrist position, $\theta_a(t)$, by the transfer function

$$\frac{\theta_a(s)}{M(s)} = \frac{1}{Js^2 + Bs + K} \qquad \text{eq. (2)}$$

where J is moment of inertia, B is viscosity and K is stiffness of the wrist joint.

3.1.3 Signal Dependent Feedforward Noise (α)

The signal dependent feedforward noise was modeled as a multiplicative noise

(Harris and Wolpert 1998) which scaled linearly with the applied torque (Jones et al. 2002a). For the same task (for e.g. reaching) performed multiple times, the torque generated at the limb joint will thus be a stochastic variable whose variance is a function of the applied torque.

3.1.4 The Forward Model

The forward model compensates for the time delays in the system by predicting the output of the feedforward path based on the current command and an estimate of current plant state (e.g. θ_a). This type of predictive mechanism is common in systems with long feedback delays. In the brain, the existence of such mechanisms can be illustrated by the ability to catch a moving ball. Catching a ball can be considered in the context of a visually-guided tracking task in which the moving ball is the visual target. Sensory feedback of the target position is delayed due to visual information processing and feedback of the hand position relative to target is only available to the brain after this processing delay. Nevertheless, subjects are able to make a fast arm movement in order to catch the ball suggesting presence of prediction mechanisms. The brain could have multiple forward models for motor planning and online movement correction (Miall et al. 1993b); however in our model the prediction mechanism is associated with instantaneous online correction of limb position (rather than motor planning).

Several studies have proposed cerebellum as the underlying neural substrate for making feedforward predictions in visually guided tasks (Miall et al. 1993b; Wolpert et al. 1998; Ito 1970). In the current study, the forward model was formed from a cascade of two stages (Miall et al. 1993b). The first stage models the Plant, capturing the wrist dynamics and providing a prediction of instantaneous wrist position which is negatively

fed back to the neural controller. This stage excludes the delays present in the feedforward (T_{ff}) and feedback (T_v and T_p) path. The output of the first stage forms input to the second stage. The second stage models the feedback gains along with the temporal delays (T_{ff}, T_p and T_v) in the system, associated here with feedforward conduction, proprioceptive and visual information processing, and provides a delayed prediction of the noiseless wrist position. The output of the second stage is delayed and fed back positively matching temporally to feedback response. If the prediction is accurate, the output of the second stage cancels out the effect of the feedback response, thereby producing faster movements. If the prediction is not perfect, the controller generates command signals (based on the error between the two responses) to compensate for the error and the process continues.

3.1.5 Transfer Function of Dual-Feedback model

The overall transfer function relating desired wrist angle, $\theta_d(t)$, to actual wrist angle, $\theta_a(t)$ is given as

$$\boldsymbol{\theta_a(s)} = \boldsymbol{\theta_d(s)}\left[\frac{(K_d s^2 + K_{pr} s + K_i)e^{-T_{ff}s}}{Js^3 + Bs^2 + Ks + K_d s^2 + K_{pr} s + K_i}\right]$$

$$+\boldsymbol{D_{ext}(s)}\left[\frac{(K_d s^2 + K_{pr} s + K_i)(K_v e^{-(T_{ff}+T_v)s})}{(Js^3 + Bs^2 + Ks + K_d s^2 + K_{pr} s + K_i)}\right]$$

$$+ [\propto \boldsymbol{M(s)}]\left[\frac{e^{-T_{ff}s}\left(Js^3 + Bs^2 + Ks + K_d s^2 + + K_{pr} s + K_i - (K_d s^2 + K_{pr} s + K_i)(K_p e^{-(T_{ff}+T_p)s} + K_v e^{-(T_{ff}+T_v)s})\right)}{(Js^2 + Bs + K)(Js^3 + Bs^2 + Ks + K_d s^2 + K_{pr} s + K_i)}\right]$$

$$- \boldsymbol{D_S}\left[\frac{(K_d s^2 + K_{pr} s + K_i)e^{-T_{ff}s}}{Js^3 + Bs^2 + Ks + K_d s^2 + K_{pr} s + K_i}\right]$$

eq. (3)

The equation can be broken down into four components. The first component corresponds to the transfer function associated with desired wrist position, $\theta_d(t)$. The

second component corresponds to the transfer function associated with external perturbations, $D_{ext}(t)$. The third component corresponds to transfer function associated with multiplicative feedforward noise, α, and the forth component corresponds to transfer function associated with sensory noise, D_S. Here, D_S is the average magnitude of the power spectrum of sensory noise (σ_S^2), used to estimate the sensory noise in the model. The relationship between the two is explained in detail in section 7.4.1. During stabilization against external perturbation, $D_{ext}(t)$, the desired wrist response, $\theta_d(t) = 0$.

3.2 Subjects

Eleven healthy volunteers (3 female; Mean age – 24.3 yrs, SD – 2.1 yrs) participated in the study. Nine subjects were right-handed, one left-handed and one subject was ambidextrous according to the Edinburgh Handedness Inventory (Oldfield 1971). Subjects taking psychoactive medications or those with neurological or psychiatric disorders were excluded from the normative study. Written informed consent was obtained from each subject in accordance with institutional guidelines approved by Marquette University and the experiments were performed in accordance with the Declaration of Helsinki.

3.3 Experimental Setup

All experiments were performed on a custom made robotic manipulandum (Figure 3.3). The system consisted of three main components: the robot (which includes wrist manipulandum, motors, external frame and instrumentation), the controller (data collection, real-time control, and safety monitoring) and the display screen for presenting target and cursor. The manipulandum rotated in the horizontal plane about a central axis that was aligned with the primary axis of the subjects' wrist.

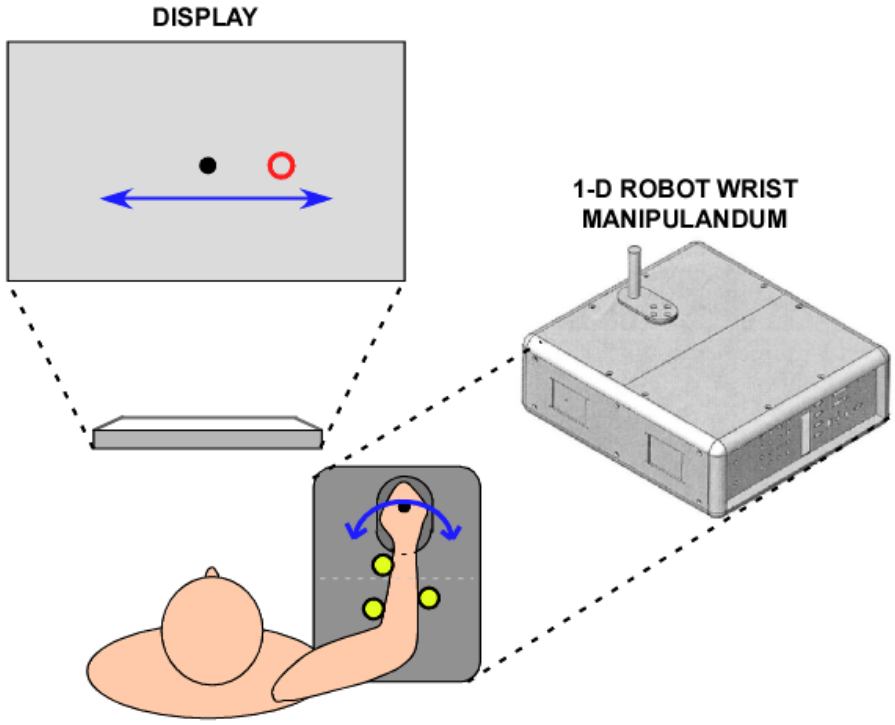

Figure 3.3 Experimental Setup (Top View). 1-D robot wrist manipulandum rotates in the horizontal plane. The rotation of the wrist was transformed into linear horizontal motion to control the position of a cursor presented on the display screen. The subject's task was to use the wrist manipulandum to place a user-controlled cursor (red ring) on a target (black dot) presented on the display screen. Direct view of the wrist was obstructed by an opaque shield. EMG was collected from ten muscles of the upper arm.

The robotic system recorded wrist position, velocity, and torque and could apply user defined torques to perturb wrist position. The wrist manipulandum was a planar one degree-of-freedom device that could generate a commanded torque at the handle using a DC motor. It consisted of an aluminum handle mounted above a Kollmorgen D061A DC brushless torque motor (Kollmorgen Inc., Radford, Virginia) such that the rotational axis of the handle and the motor are aligned with the subject's wrist joint. The DC motor was capable of generating 16.9 Nm peak torque at the rotational axis in response to a command torque provided by a Kollmorgen Servostar CD motor drive. The motor could

be configured to operate in either ‘Position Mode’ or in ‘Torque Mode’ based on the movement parameter being controlled. In Position Mode, the motor (along with the wrist manipulandum) was either held fixed or moved to a predefined position with a constant angular velocity (used to bring the manipulandum to home position before start of each trial). In torque mode, the motor could be rotated freely by the subject using the wrist manipulandum (to do tracking or stabilization tasks). In this mode, external torque perturbations could be applied to the wrist manipulandum by sending appropriate current commands to the motor. The angular position of the manipulandum was measured using a 19-bit optical encoder attached directly to the motor shaft. Forces and torques were measured at the manipulandum using a six-degree of freedom load cell with analog outputs (Model 67M25A-I40-A-200N12, JR3 Inc., Woodland, CA). The load cell measured forces in the x, y, and z direction, and moments about the x, y, and z axes. The robot housing contained all hardware related to data collection, signal conditioning, real-time control, and safety monitoring.

The experiments were controlled via two PCs: a target computer (mounted in the robot), which ran XPCTarget® for real-time control/data collection and a host computer running SIMULINK® and STATEFLOW®, which provided a GUI for controlling the experiment and was used to save recorded data to a file. The target PC communicated with the host PC via a dedicated 100Mbps Ethernet connection. Since powerful motors were being used with human subjects, it was necessary to take precautions to ensure subject safety. Safety features, in the form of electrical limit switches, software disable control signals and mechanical stops were implemented to protect the subject from injury by disabling the motors if the robot entered an unsafe operating mode or an unexpected

control state.

During the experiments, the subject was seated on a height adjustable chair in an upright position. The subject rested his/her lower arm on the 1-D robot with their wrist placed on the manipulandum such that the wrist joint and the rotation axis of the manipulandum were vertically aligned. A target (black dot) and user-controlled cursor (red ring) were presented on a 19" monitor (spatial resolution of 1280 x 1024 pixels and a refresh rate of 60 Hz), whose height was adjusted such that the center of the screen was aligned with the subject's normal direction of gaze (Figure 3.3) and was placed at a viewing distance of 60 cm. The cursor position was yoked to the angular position of the wrist manipulandum controlled by the subject. The subject's task was to place the cursor on the target by flexing and extending their wrist to control the manipulandum. The rotational motion of the wrist was translated into horizontal movement on the screen. For a viewing distance of 60 cm, the wrist angle of 1 degree corresponded to the visual angle of 0.286 degrees on the screen. The lower arm was constrained using three magnetic clamps to minimize elbow movement (Figure 3.3). Direct view of the wrist was obstructed by means of an opaque screen stand placed between the subject and the robot to prevent direct visual feedback of the subject's wrist position.

Data was collected at a sampling frequency of 1000 Hz. For each experiment, the following data was collected: input signal (tracking and/or perturbation signal), $x(t)$, the position of the wrist manipulandum, $y(t)$, the torque generated at the wrist manipulandum, $M(t)$, velocity and acceleration profile of the movement, $v(t)$ and $a(t)$, and EMGs from ten arm muscles. Cross-correlation and frequency response analyses across experimental conditions were used to estimate the parameters of the 1-D wrist control

model and validate the approach in neurologically intact subjects. All data analysis was performed using MATLAB® and Simulink®.

3.4 EMG Data Collection and Analysis

During the experimental session, EMGs were recorded from ten arm muscles using differential surface electrodes (Delsys DE-2.1 electrodes and Delsys Bagnolli 16 system; Delsys, Taunton, MA). The EMG data were collected to measure the degree of antagonist muscle co-activity (CoA) at the wrist, elbow, and shoulder joints for each subject across different experimental conditions. Muscle CoA increases the stiffness in the joint (Kornecki 1992). CoA was estimated for two purposes; first was to make sure that the subjects' were not co-contracting (or stiffening their wrist joint) during the tasks and second was to compare the CoA of the wrist muscles across experimental conditions to verify the homogeny of the dynamic properties of the wrist.

The monitored muscles included wrist extensors and flexors (flexor carpi radialis (FCR); flexor carpi ulnaris (FCU); flexor digitorum superficialis (FDS); extensor carpi radials (ECR); extensor carpi ulnaris (ECU); and extensor digitorum communes (EDC)), single-joint elbow flexors and extensors (short head of biceps (BICS); brachioradialis (BRD); lateral head of triceps (TRILT)) and single-joint shoulder muscles (anterior deltoid (ADL); posterior deltoid (PDL)). EMG signals were band-pass filtered between 10 and 450 Hz, amplified (x1000) and sampled with 16-bit resolution at 1000 Hz prior to being stored off-line for further analysis.

Post processing of the EMG signals was performed using the approach employed by Suminski et al. (2007). After removing the residual offsets from the digitized EMGs,

the EMG data was rectified and low pass filtered at 4 Hz (4th-order Butterworth). Within each subject, EMG signals were normalized to facilitate comparisons across the study population for each muscle. For each subject, EMG signals were normalized to their respective maximum voluntary isometric contractions (MVIC) measured prior to start of the experimental session. Two MVIC trials each were obtained for wrist flexion, wrist extension, elbow flexion, elbow extension, shoulder flexion, and shoulder extension.

During measurements of subjects' MVICs, the wrist manipulandum was held fixed and the subjects were asked to produce maximum wrist flexion and extension, with their upper hand resting as shown in Figure 3.3. MVICs for the biceps were measured by having subjects flex their elbow against an opposing (restricting) force applied by the experimenter. MVICs for the triceps were measured by having subjects place their dominant hand on the center of their chest and then extend their arm about the elbow joint against an opposing force applied by the experimenter. MVICs for the anterior and posterior deltoids were measured by having subjects raise their shoulder in front and behind their torso respectively against restrictions applied by the experimenter. The peak value (average of 2 trials) of the rectified and filtered EMG signals for MVICs of each muscle was subsequently used for normalization. For our analysis, FCR and ECR muscles were considered as wrist antagonists, BIC and TRI as elbow antagonists, and AD and PD as shoulder antagonists. Co-activity was estimated by selecting the minimum value of the normalized EMG signals for each pair of antagonist muscles at each sampling instant such that co-activity at time nT was given by

$$CoA(nT) = min\left(EMG_{flexor}^{norm}, EMG_{extensor}^{norm}\right)$$

where n is the temporal index and T is the sampling interval (= 1 millisecond).

3.5 Experimental Design

The data were collected over two experimental sessions spanning two days. Each experimental session lasted for 90 min during which a series of experiments were performed in order to quantify the model parameters summarized in Table 3.1 .

Exp.	Parameter	
Exp. 1	T_v (ms)	Visual feedback delay
	T_p (ms)	Proprioceptive feedback delay
	T_{eff} (ms)	Effective Feedforward delay ($T_{ff} + T_{cp}$) T_{ff} (ms) → Feedforward conduction delay T_{cp} (ms) → Controller and plant delay
Exp. 2	α	Multiplicative feedforward noise
Exp. 3	J (kgm^2)	Wrist's Rotational Inertia
	B (Nms/rad)	Wrist's Damping coefficient
	K (Nm/rad)	Wrist's Stiffness coefficient
Exp. 4	K_v	Visual feedback gain
	K_p	Proprioceptive feedback gain
	K_d (Nms/deg)	Derivative Gain
	K_{pr} (Nm/deg)	Proportional Gain
	K_i (Nms/deg.s)	Integral Gain
	σ_S^2 (deg^2)	Sensory noise
Exp. 5	VAF (%)	Variance Accounted for by the Model

Table 3.1 Model parameters measured experimentally

On day one, Exp. 1 and 2 along with experiments for proprioceptive stabilization, visuo-proprioceptive stabilization and a tracking task to estimate Variance Accounted For by the model (description and results of these experiments are not presented in this thesis) were tested. On day two (non-consecutive), Exp. 2, 3, 4 and 5 were tested. The subject's task was to use the wrist-manipulandum to place a user-controlled cursor on a target presented on the display. Based on the experimental condition, visual feedback (via the cursor) was either provided ($K_v + K_p = 1$) or not provided ($K_p = 1$). Input sequences were

generated in frequency domain over the frequency and amplitude (SD) ranges specified for each experiment. Since the visual display updated every 16.6 ms (60 Hz refresh), input sequences were generated with the temporal resolution of 17ms. For Exp.1, the high frequency cutoff of the perturbation sequence was set to 0.5 Hz to enable visual smooth pursuit (Leist et al. 1987). Previously, frequencies ranging from 0.06 Hz to 1.5 Hz have been used effectively for visually-guided tracking paradigms (Miall and Jackson 2006; Notley et al. 2007; Foulkes and Miall 2000; Hefter and Langenberg 1998) . Since, the refresh rate of the screen was 60 Hz, the maximum possible frequency of the visual perturbation was 30 Hz (Nyquist criteria). Hence, for Exp.3 and 4, the upper cutoff of the perturbation sequence was set to 30 Hz.

A brief practice session preceded the experimental session in order to familiarize the subject with the experimental setup and the tasks. The order of the experiments was randomized for each subject in order to minimize any sequential bias. In order to avoid fatigue, brief rest periods were provided between the trials and experiments. In the subsequent chapters we describe each of the experimental conditions tested and the corresponding analysis used to estimate control model parameters.

3.6 Simulations for Validation of Experimental Methods

To validate the systems identification approach, the experiments and model (see Appendix F for SIMULINK® implementation of the model) were simulated and tested in SIMULINK®. Extensive simulations were performed to characterize the robustness of the approach over a range of parameter values (Table 3.2). Nominal values of the parameters are shown in Table 3.2 based on results from the human subject studies. The high-dimensional parameter space was coarsely explored on an experiment-specific basis

using the ranges specified in Table 3.2. Parameters not fit by a particular experiment were held fixed at their nominal values.

Parameter	Nominal Value	Range
T_v (ms)	200	50-600
T_p (ms)	60	20-240
T_{ff} (ms)	30	10-100
J (kgm^2)	0.009	0.001-0.1
B (Nms/rad)	0.2	0.03-0.7
K (Nm/rad)	1	0.5-5
K_v	0.8	0.5, 0.75, 1
K_d (Nms/deg)	0.001	0.0001-0.01
K_{pr} (Nm/deg)	0.05	0.005-0.5
K_i (Nm/deg.s)	0.5	0.02-5
α	0.03	0.01-0.1
σ_S^2 (deg^2)	0	1-1000

Table 3.2 Nominal values and range of the parameters explored in the model simulations. For each experimental condition, the fitted parameters were varied over the ranges specified to assess the robustness of the approach. Parameters not fit by a particular experiment were held fixed at their nominal values.

4 EXPERIMENT 1: SYSTEM DELAYS

The proposed model contains three explicit delays, a visual delay (T_v), proprioceptive delay (T_p) and feedforward conduction delay (T_{ff}). The feedback delays (T_v and T_p) reflect a cumulative delay comprising of the afferent delays associated with the propagation of signals from the peripheral nervous system and the delays associated with processing the sensory (visual and proprioceptive respectively) information in cortex. The feedforward conduction delay is associated with the time taken for the motor commands to reach the wrist muscles and the excitation/contraction coupling delay associated with the generation of force within the muscle fibers. In addition to these delays, the system contains an implicit delay associated with controller and the plant. This implicit delay (T_{cp}) along with the feedforward conduction delay (T_{ff}) forms the effective feedforward delay (T_{eff}) of the system.

4.1 Experimental Task

Experiment 1 was divided into 3 sub-experiments to estimate the open loop visual delay (T_v+T_{eff}), open loop proprioceptive delay (T_p+T_{eff}), and effective feedforward delay (T_{eff}) respectively. The subsections below detail each experimental task.

4.1.1 Experiment 1a: Estimation of open loop visual delay (T_v + T_{eff})

In this experiment, subjects were required to stabilize the cursor on the target (held static at the center of the screen). Pseudorandom visual perturbations (Bandwidth = 0.05 – 0.5 Hz; SD = 5 degrees) were added to the cursor position. To perform the task, subjects were required to continuously correct for the perturbation by applying counter movement in order to keep the cursor on the stationary target. Since, the perturbations

were applied to the visual feedback path, and the output was measured at the end of feedforward path, the delay measured between input and output was $T_v + T_{eff}$. Subjects completed ten trials of 20 seconds each which were individually correlated with the underlying perturbation sequence to estimate the open loop visual delay.

4.1.2 Experiment 1b: Estimation of open loop proprioceptive delay ($T_p + T_{eff}$)

In this experiment, subjects were required to stabilize the wrist manipulandum so as to place a virtual cursor on the target (held static at the center of the screen). No visual feedback (cursor) was provided. Pseudorandom torque perturbations (Bandwidth = 0.05 – 0.5 Hz; SD = 0.25 NM) were applied to the wrist manipulandum during the task and subjects were required to continuously correct for the applied torque by applying counter torques in order to keep the wrist manipulandum at the center of the display. Since, the perturbations were applied to the proprioceptive feedback path, and the output was measured at the end of feedforward path, the delay measured between input and output was $T_p + T_{eff}$. Subjects completed ten trials of 20 seconds each which were individually correlated with the underlying perturbation sequence to estimate the open loop proprioceptive delay.

4.1.3 Experiment 1c: Estimation of effective feedforward delay (T_{eff})

In this experiment, subjects performed rhythmic tracking task in which the target moved back and forth at a frequency of 0.5 Hz (Amplitude = 20 degrees). Rhythmic tracking ensured the use of prediction mechanism by the subjects, thereby eliminating the feedback delays associated with perceiving the target. In order to avoid anticipation, subjects were instructed not to lead the target. It was assumed that the subjects' perfectly predicted the target motion and did not anticipate the target. Subjects completed ten trials

of 20 seconds each which were individually correlated with the underlying tracking sequence to estimate the effective feedforward delay. Subjects typically required 5 seconds to adapt to the synchrony of the input signal and therefore first five seconds of the data was discarded from the analysis for each trial.

4.2 Data Analysis

Cross-Correlation analysis is conventionally used to estimate time delays between two signals (Figure 4.1). In our study, we used cross-correlation analysis to estimate the delay parameters (T_v, T_p and T_{eff}) of the sensorimotor control model. The cross-correlation, $\hat{R}_{xy}[n]$, between two discrete signals, x(N), and y(N) delayed by T samples is

$$\hat{R}_{xy}[n] = \sum_{m=-N}^{m=N} x^*[m]\, y[m+n]$$

$\hat{R}_{xy}[n]$ will be maximum at $n = T$ (Figure 4.1 inset). Hence T can be estimated from the position of the maximum peak in $\hat{R}_{xy}[n]$. When $\hat{R}_{xy}[n]$ is normalized (obtained by dividing $\hat{R}_{xy}[n]$ by product of the square root of autocorrelation of x and y) to range from -1 to 1, the cross-correlation coefficient provides a measure of the similarity between the two signals such that identical signals have a cross-correlation coefficient of 1 and random signals have a coefficient near zero.

Prior to analysis, the position data was low-pass filtered at 30 Hz using a 4th order Butterworth filter to eliminate the noise induced by the motor of wrist manipulandum. The cross-correlation was computed using the MATLAB function “xcorr” to return a normalized cross-correlation vector. Measurement of the peak and position of the peak of the cross-correlation was used to estimate the co-variation between the perturbations and

subjects' responses and the time delay associated with the initiation of corrective movements following the perturbation.

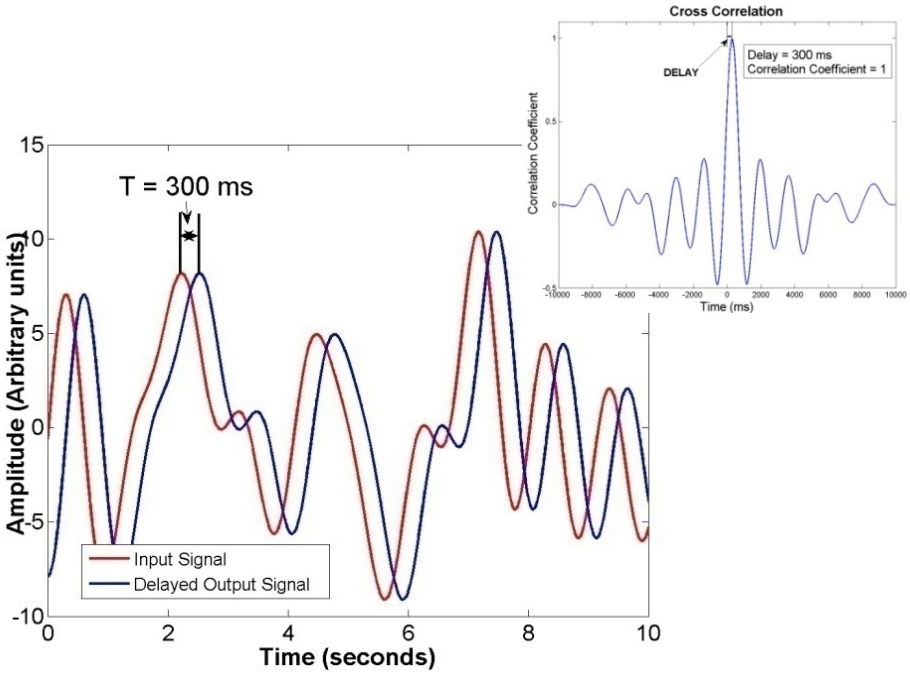

Figure 4.1 Cross-Correlation Analysis. The Output signal (blue) is a delayed (by 300 ms) version of input signal (red). [Inset] The cross correlation plot illustrates that the maximum peak occurs at T = 300 ms with a correlation coefficient = 1 for the noiseless signals illustrated here.

In Exp. 1a the open loop visual delay ($T_v + T_{eff}$), was measured by applying visual perturbations to the cursor and comparing subjects' corrections via the position of the wrist manipulandum position. The shift in the peak of the cross-correlation signal between the visual perturbation sequence and subject's correction was used to measure the open loop visual delay. Since, the perturbations were applied to the visual feedback path, and the output was measured at the end of feedforward path, the delay measured between input and output was $T_v + T_{eff}$ (Figure 4.2A).

Similarly, proprioceptive delay ($T_p + T_{eff}$) was measured by applying torque perturbations (Exp. 1b) to the wrist manipulandum and measuring subject's correction (counter torque measured by the torque sensor) to the perturbation as the output. Cross-correlation between the torque perturbation sequence and the subject's counter torque was used to measure the open loop proprioceptive delay. Since, the perturbations were

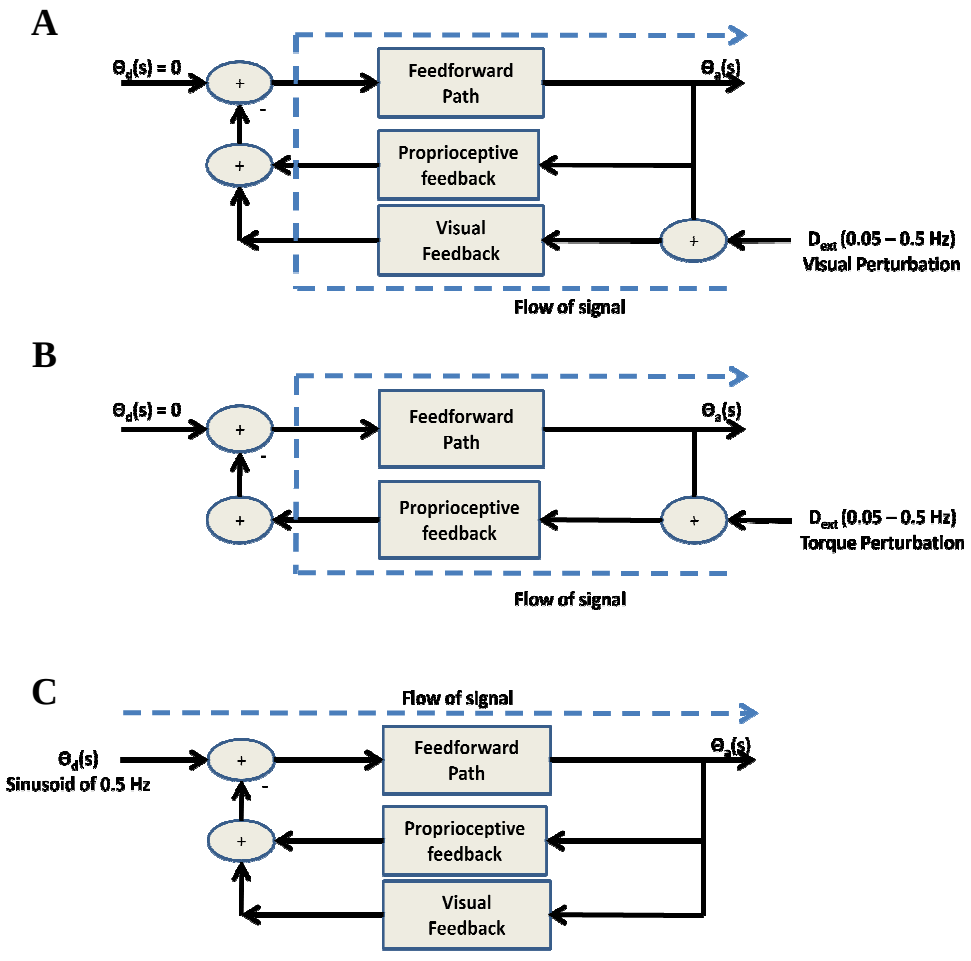

Figure 4.2 Block diagram representation of the control subsystems isolated in Exp 1 to measure open-loop delays. A) Open loop visual delay was estimated by measuring the subject's response to the perturbations applied to visual feedback. B) Similarly, open loop proprioceptive delay was estimated by measuring the subject's torque response to the torque perturbations applied to proprioceptive feedback. C) Effective feedforward delay was estimated by measuring subject's response to a sinusoid of 0.5 Hz

applied to the proprioceptive feedback path, and the output was measured at the end of feedforward path, the delay measured between input and output was $T_p + T_{eff}$. (Figure 4.2B).

In order to estimate the effective feedforward delay (Teff), subjects were required to perform a rhythmic tracking task (Exp. 1c). Cross-correlation between the target sequence and the subject tracking response (wrist manipulandum position) gave an estimate of effective feedforward delay (Figure 4.2C). The reason for selecting rhythmic tracking (single frequency of 0.5 Hz) was to completely predict the feedback delays thereby allowing estimation of T_{eff} alone. The initial five seconds of the data was discarded from analysis to account for time required by the subject to become familiarized with the single frequency target movement.

4.3 Simulation

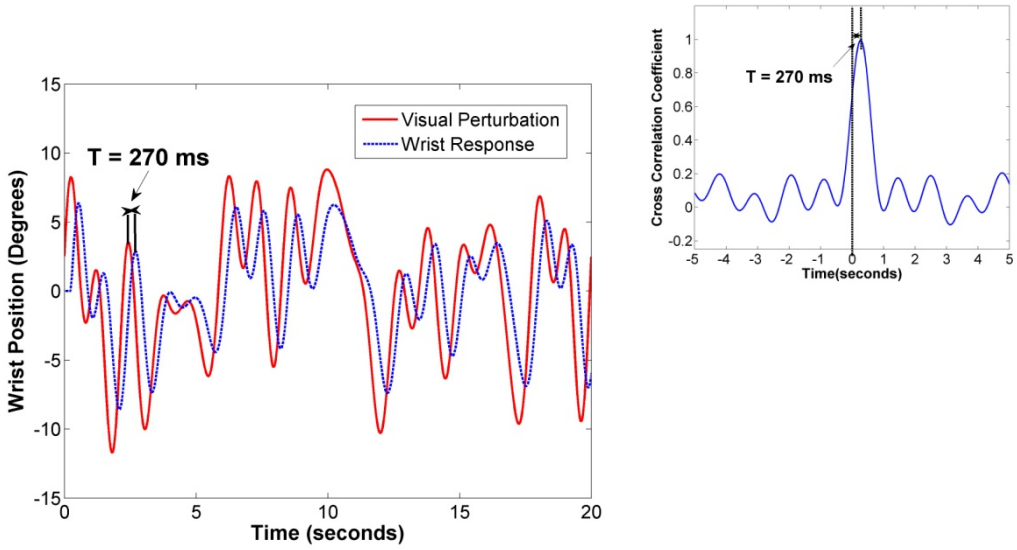

Figure 4.3 Estimation of open loop visual delay via simulation of Exp. 1a. Visual perturbations (red line) were applied to the cursor and the model (e.g. subject) response (blue line) was measured. Cross-correlation (inset) between the two signals yielded the open loop visual delay.

In order to validate the experimental approach to estimate the delays, Exp. 1 in conjunction with the model was tested via simulations in SIMULINK®. Figure 4.3 shows a simulated wrist response to visual perturbation for one trial. For this simulation, the visual delay (T_v) was set to 200 ms, feedforward conduction delay (T_{ff}) was set to 30 ms and the delay associated with the plant and the controller (T_{cp}) was 40 ms, corresponding to open loop visual delay ($T_v + T_{eff}$) of 270 ms. The cross-correlation (inset) analysis for this trial resulted in an estimate of 270.6 ms. The high cross-correlation coefficient (r^2 = 0.98) indicates that the two signals were identical (Figure 4.3 inset). Simulations over ten trials resulted in a mean delay of 268.4 ms and a standard deviation of 5.02 ms.

Validation over a range:

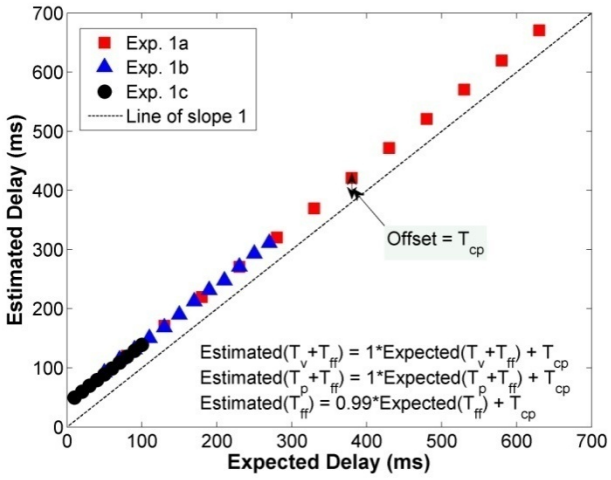

Figure 4.4 Validation of Exp. 1 used in conjunction with cross-correlation analysis to estimate open-loop delays. The experimental approach proposed to estimate the delays was tested over a range of values; T_v = 50-600 ms (red squares), T_p = 20-240 ms (blue triangles) and T_{ff} = 10-100 ms (black circles). The estimated delays were linearly related to the expected delays. A least-squares linear fit returned a slope of 1(r^2 >0.99) and an offset of 40.5 ms corresponding to the delay associated with the controller and plant (T_{cp}).

The simulations were repeated for visual delays (T_v) ranging from 50 ms to 600 ms in step of 50 ms while all other parameters where kept constant. Figure 4.4 (red squares) shows the relation between the estimated and expected open loop visual delays. A linear fit resulted in a slope of 1 (r^2>0.99) and an offset of 41 ms corresponding to delay associated with the plant and the controller (T_{cp}).

Similarly, simulations were performed to estimate open loop proprioceptive delay (T_p +T_{eff}; Exp. 1b) and effective feedforward delay (T_{eff}; Exp. 1c). Figure 4.4 shows simulation results for a range of proprioceptive delays (20-240 ms in steps of 20 ms; blue triangles) and feedforward delay (10-100 ms in steps of 10 ms; black circles). The best-fit lines relating the estimated to the expected delays had slopes of 1 (r^2>0.99) and 0.99 (r^2>0.99) with offsets of 41.9 ms and 40.1 ms corresponding to delay associated with the plant and the controller (T_{cp}) respectively (refer Appendices A1, A2 and A3 for simulation results).

4.4 Experimental Results

Figure 4.5 shows a typical position response of a subject to the addition of a visual perturbation to the cursor (Exp. 1a). For this trial the open loop visual delay (T_v + T_{eff}) estimated using cross-correlation analysis was 286 ms. The cross correlation (Figure 4.5 inset) coefficient between the visual perturbation and the subject's position response was high (r^2 = 0.92), suggesting that the estimate of the delay was reliable. An average over ten trials for the same subject yielded a mean of 293.5 ms with a standard deviation of 25.3 ms. Figure 4.7 shows the estimated (mean ± std) system delays for the 11 subjects tested. The open loop visual delay (black circle) ranged from 232 to 375 ms across subjects with a mean of 287.1±42.1 ms. The average cross correlation coefficient

(r^2) across trials for all subjects was greater than 0.7 with the exception of one subject whose correlation coefficient was 0.47 (refer Appendix B for experimental results of all subjects).

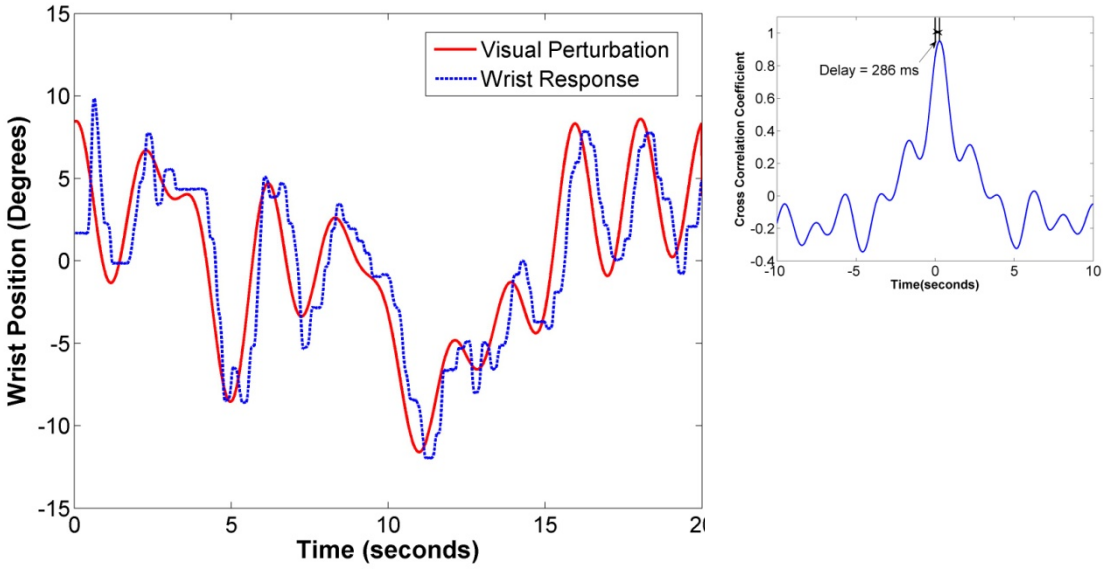

Figure 4.5 Estimation of open loop visual delay ($T_v + T_{eff}$) from Exp. 1a for a subject. Visual perturbation (red solid line) was applied to the cursor and subject's response (blue dashed line) was measured. For this trial, the delay estimated was 286 ms with a correlation coefficient of 0.96

Estimates of open loop proprioceptive delays ($T_p + T_{ff}$; red square in Figure 4.7) were obtained by cross correlating the applied torque perturbation and subject's response (counter torque; Figure 4.6A), (Exp. 1b). The torque perturbation signal profile was similar to that shown in Figure 4.7. Across subjects, the open loop proprioceptive delay ranged from 80 to 155 ms with a mean of 121.8±18.8 ms. The average correlation coefficient was high (r^2 = 0.77-0.92) for all the subjects (refer Appendix B for experimental results of all subjects).

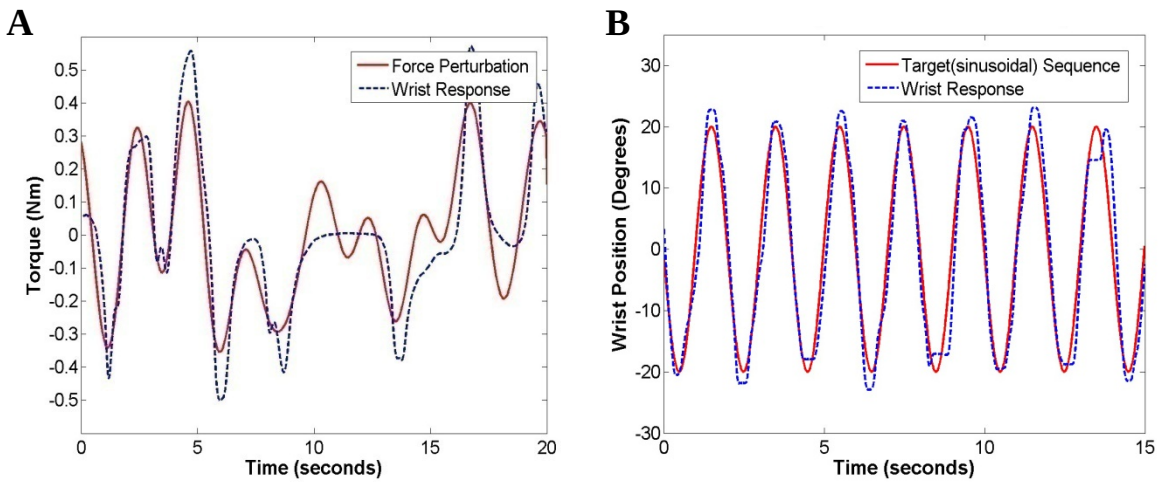

Figure 4.6 Proprioceptive stabilization (Exp. 1b) and target tracking (Exp. 1c) trials for a single subject. A) Subject's response to torque perturbation used to measure open loop proprioceptive delay (T_p+T_{eff}) B) Subject's response to a rhythmic moving target used to measure effective feedforward delay.

Effective feedforward delays (T_{eff}; blue diamond in Figure 4.7) were measured using the shift in the cross correlation between the sinusoidal target motion and subject's

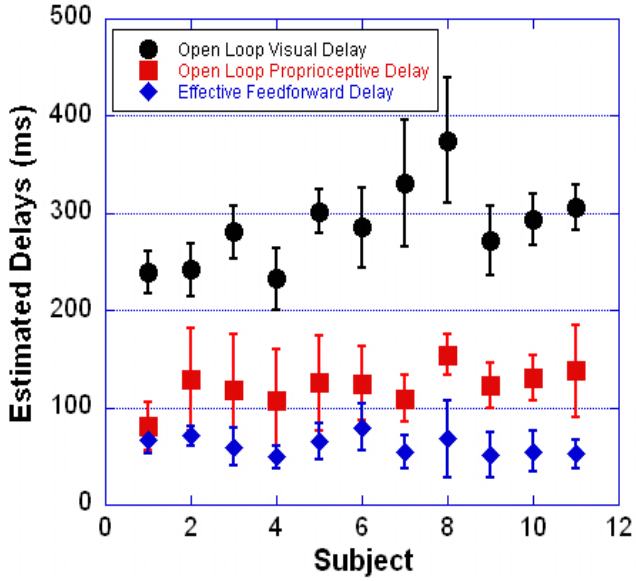

Figure 4.7 Estimated open loop delays across subjects. The system delays were measured using Exp. 1 for 11 subjects. Black circle denotes the open loop visual delay (T_v+T_{eff}), red square denotes open loop proprioceptive delay (T_p+T_{eff}) and blue diamond denotes effective feedforward delay (T_{eff}) estimated from 11 subjects

cursor position as they tracked the target (Exp. 1c; Figure 4.6). For 11 subjects, the effective delay ranged from 49 to 80 ms with a mean of 61.1±9.7 ms. The mean correlation coefficient was high (r^2 = 0.92 to 0.98) for all the subjects (see Appendix B for experimental results of all subjects).

4.5 Discussion

Open loop delays (visual and proprioceptive) were measured from the subjects' responses to external perturbations introduced within the visual (Exp. 1a) and proprioceptive (Exp. 1b) feedback paths respectively. A stabilization task was used to ensure the continuous use of feedback mechanisms with minimal dependence on the prediction mechanisms inherent in visually-guided tracking. External perturbations were applied within a particular feedback path whose delay was to be measured. This allowed us to make accurate measurements of the open-loop feedback delays that were combinations of the respective sensory feedback delay and the effective feedforward delay associated with initiation of corrective action. Estimates of the effective feedforward delay were obtained using a sinusoidal tracking task (Exp. 1c), which enabled the prediction of the feedback delays. Simulations of Exp. 1c suggested that the forward model was able to predict feedback delays only, thereby giving us an estimate of the effective feedforward delay. For experimental data, it was assumed that the subject's perfectly predicted the target motion thereby eliminating the feedback delay associated with target perception. Also, we assumed that our instruction to not lead the target avoided anticipation of the target by the subject. Further, it was assumed that tracking and stabilization are inherently similar in nature requiring use of same strategy. This assumption was important as the task for measuring open loop delays (visual and

proprioceptive) was stabilization, whereas the task to measure effective feedforward delay was tracking.

The simulation results suggested that the stabilization and tracking tasks in conjunction with the cross-correlation analysis can be successfully used to characterize the delays within human sensorimotor control system. The open loop delays measured across subjects ranged from 232 - 375 ms and 80 – 155 ms for visual and proprioceptive delays respectively. Flanders and Cordo (1989) reported a similar range wherein the measured open loop visual delay varied from 186 - 285 ms and open loop proprioceptive delay varied from 108 – 175 across six subjects. Subtraction of the effective feedforward delay from the open loop delays resulted in estimates of visual and proprioceptive delays ranging from 170 – 307 ms (mean = 226.1±46.7 ms) and 14 – 87 ms (mean = 79.8±20.2 ms) respectively. For one subject, the feedback delays were relatively high (307 ms for visual feedback and 87 ms for proprioceptive feedback) compared to others. It is interesting to note that this subject was the only ambidextrous participant in the study, as measured by the Edinburgh Handedness Inventory.

Previously, feedback delays have been estimated by measuring the reaction time to initiate a movement (Flanders and Cordo 1989; Keele and Posner 1968). The current study used a continuous task enabling a direct and accurate measurement of the feedback delays. Based on our review of the sensorimotor literature, estimation of effective feedforward delay by means of non-invasive methods is novel. Using the model, the feedforward conduction delay can be estimated by subtracting out the phase shift induced by the controller and the plant (T_{cp}) from the estimate of effective feedforward delay (T_{eff}). We discuss this point in more detail in Chapter 10 (see section 10.3).

5 EXPERIMENT 2: FEEDFORWARD NOISE

Studies have shown that the motor-unit variability in muscle responses (labeled as feedforward noise in the model), is a function of the mean torque generated by the muscles (Jones et al. 2002a; Slifkin and Newell 2000). Jones et al. (2002) showed that this relationship was linear; though the motor-unit variability was studied in isolation. In the current study this variability was incorporated as a part of a sensorimotor control model to replicate variable (noisier) human performance.

In our study we replicated the experimental approach used by Jones et al. (2002) to estimate multiplicative feedforward noise. The experimental paradigm is explained in detail in the section below, followed by the simulation and experimental results.

5.1 Experimental Task

In experiment 2, subjects flexed their wrist to produce a constant isometric torque contraction while the position of the wrist manipulandum was held fixed at center. The visual cursor was controlled by the amount of torque applied to the manipulandum by the subject. A static target displaced from the center (corresponding to a pre-defined torque level) was shown on the screen and subjects were required to place the cursor on the target by applying the appropriate isometric contraction (Jones et al. 2002). Visual feedback of the target and cursor was shown for the first 3 seconds after which the target and cursor were removed and subjects were required to maintain that torque level for next 5 seconds. Only the last 5 seconds of data (corresponding to feedforward control) was used for the estimation of multiplicative feedforward noise. Subjects performed five trials for each of five torque levels ranging from 20% to 60% of their MVIC.

5.2 Data Analysis

Torque measurements (output data) were low pass filtered at 30 Hz using a 4^{th} order Butterworth filter to remove high frequency noise induced by the motor system of the manipulandum. A drift in the torque measurements was observed for most subjects when visual feedback was removed; consistent with a previously reported study by Jones et al. (2002). In order to remove the drift, trend removal using a second order polynomial (Jones et al. 2002) was performed on each 5 second trial. Standard deviation in the force measurements about the constant torque level was measured to estimate the variability in torque commands as a function of torque level. Estimates were averaged over 5 trials for each force level. A scaling factor (α) relating the torque level and measured standard deviation was used to estimate the variability in the multiplicative feedforward noise. This scaling factor was estimated by performing a linear fit to the data (Constant torque level vs. Standard Deviation).

5.3 Simulation

Using Exp. 2, multiplicative feedforward noise was characterized by performing isometric torque contraction and measuring the variability in the torque output. Figure 5.1 shows simulation results for the estimation of multiplicative feedforward noise (α). The simulation consisted of five trials for each of five torque levels. For the simulation results shown, α was set to 0.03. The measured α estimated from the slope relating the variability (SD) in the torque output to constant torque level was 0.0302. The variability in estimate of SD across trials for same torque level was less than 1.2% of the average torque. The red dots in Figure 5.1 obscured the variability in SD such that the corresponding error bars are not visible.

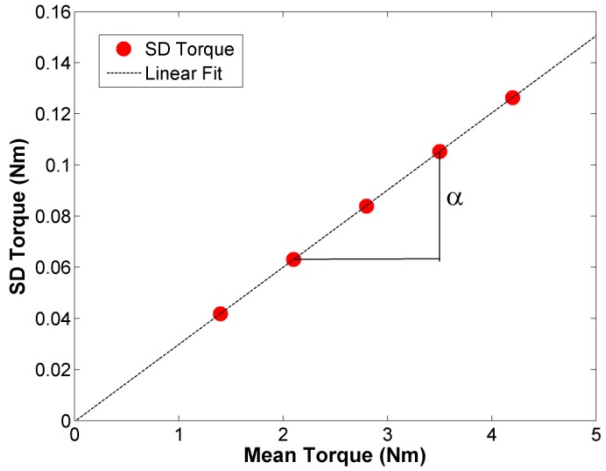

Figure 5.1 Estimation of Multiplicative Feedforward Noise (α) via simulation of Exp. 2. The standard deviation (SD) of the torque output was linearly related to the average torque level being maintained. The estimated slope (α) of 0.0302 was well-matched to the expected slope of 0.03.

Validation over a range:

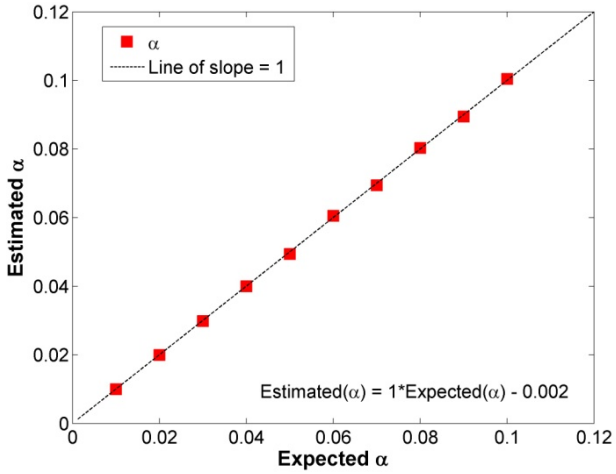

Figure 5.2 Validation of Exp. 2 and the linear fit estimate of α. The approach to estimate signal dependent (multiplicative) feedforward noise was tested over a range of values (0.01-0.1). The estimated α was linearly related to the expected α with a slope of 1.

The approach to estimate the multiplicative noise was tested over a range of α value from 0.01 to 0.1. Figure 5.2 shows the relation between the estimated and expected estimates of α used to characterize the multiplicative feedforward noise. A linear fit returned a slope of 1 (r^2 >0.99), meaning the approach was able to estimate the expected α with minimal error (see Appendix A4 for additional simulation results).

5.4 Experimental Results

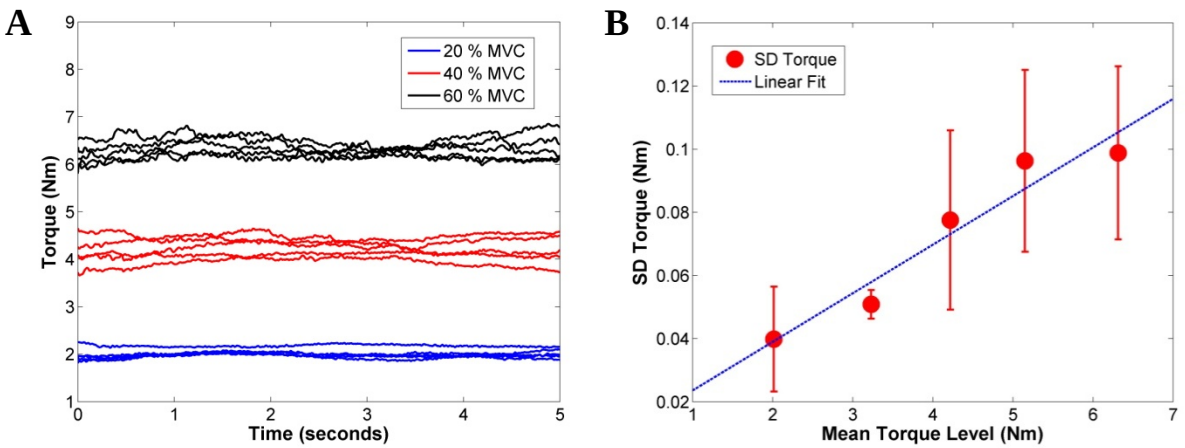

Figure 5.3 Estimation of Multiplicative Feedforward Noise (α) from Exp. 2 for a subject. A) Torque output (5 trials each) after de-trending for three torque levels (20% (blue), 40% (red) and 60% (black) of MVC for clarity) for subject #10. Output is for last 5 seconds when no feedback was provided. SD was calculated over the de-trended trials. B) The SD (Standard Deviation) of the torque output was linearly related to Torque level to be maintained (plot representative of data from one subject). The slope (α) estimated was 0.017.

Figure 5.3 shows the analyzed data obtained from one subject (#10) performing voluntary isometric torque contraction (Exp. 2) to measure the feedforward noise (α). Figure 5.3A shows a time plot (de-trended) of torque output for 5 seconds when no visual feedback was present. For clarity, the plot shows 3 of the 5 torque levels used for the task, where each line corresponds to a trial. For this subject, the variability in torque

response, expressed as standard deviation, during steady-state contraction increased linearly with mean torque level (Figure 5.3B). Similar results were obtained for all subjects. For this subject, torque SD increased linearly ($r^2 = 0.933$, p=0.008) with mean torque with a slope (α) of 0.017, which corresponds to the multiplicative scaling between the torque signal and variability associated with the torque signal. Table 5.1 shows the measured scaling factors (α) and results of the regression analyses across subjects.

Subject #	**α**	**r^2**
1	0.0207	0.948 (p=0.005)
2	0.0354	0.835 (p=0.030)
3	0.0210	0.934 (p=0.007)
4	0.0354	0.956 (p=0.004)
5	0.0592	0.900 (p=0.014)
6	0.0280	0.924 (p=0.009)
7	0.0378	0.925 (p=0.009)
8	0.0270	0.974 (p=0.002)
9	0.0152	0.985 (p=0.001)
10	0.0170	0.933 (p=0.008)
11	0.0196	0.964 (p=0.003)

Table 5.1 Estimated feedforward noise (α) and regression analysis results for 11 subjects.

5.5 Discussion

The simulation results suggested that the isometric torque contraction task could be successfully used to characterize the feedforward multiplicative noise within human sensorimotor control system. The experimental results indicate that the torque variability (SD) is linearly related to the mean torque level (Table 5.1), consistent with Jones et al. (2000). In our study ranged from 0.017 to 0.06 for neurologically intact subjects. At 100% MVC, this value of α results in torque variability from 1.7 to 6, which is well matched with the values (0.8 to 4.6) reported by Jones et al (2000).

The signal dependent (multiplicative) nature of the feedforward noise has been argued to optimize motor performance and minimize error. With repetition, movements tend to become smoother which can be attributed to a decrease in the driving signal coming from the brain (Harris and Wolpert 1998). As a consequence, the variability in the output position due to motor-unit noise scales linearly, reducing the impact of feedforward noise in neurologically intact subjects during repetitive movements.

Studies have shown that this motor-unit variability (Laidlaw et al. 2000) increases with age. However, the underlying source of this variability is not well understood. Within the model, multiple factors could result in an increased error signal going into the neural controller and/or control signal coming from the controller; either of which would lead to an increase in motor unit variability, *vis à vis* the signal dependent noise (□). Characterizing the sensorimotor control model as a function of age using the current approach could thus provide important insights into the driving factors responsible for the increased variability observed in motor responses.

6 EXPERIMENT 3: WRIST DYNAMICS

For the proposed sensorimotor control system, the wrist (plant) was modeled as a second order linear time invariant system consisting of inertia (J), viscosity (B) and stiffness (K). Frequency domain analysis was used in conjunction with a passive wrist perturbation experiment, to characterize the wrist model. The sections below detail the experimental task and explain the frequency response analysis employed to estimate the parameters of the wrist model. Simulation results are subsequently presented to validate the experimental approach, followed by experimental estimates of the wrist model across subjects and discussion of the results.

6.1 Experimental Task

In experiment 3, subjects were asked to hold the wrist manipulandum passively, using the same grip and levels of co-contraction applied in the other experiments, and were instructed “do not intervene” in response to force perturbations applied by the robot. Pseudorandom band-limited torque perturbations (Bandwidth = 0.033 – 30 Hz; SD = 0.25 Nm) were applied by the manipulandum and the wrist angle (Figure 6.1) was measured as a function of time. Passive wrist movements were recorded across five trials (30 seconds each) and the resulting power spectra were averaged to facilitate frequency response analysis.

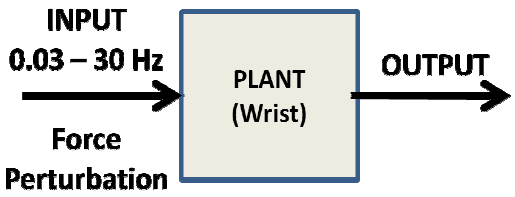

Figure 6.1 Block diagram representation of Exp 3 used to characterize passive wrist dynamics. Force perturbations were applied to the wrist manipulandum while subjects maintained a normal grip without making corrections.

6.2 Frequency Response Analysis (Exp. 3 and 4)

Frequency response analysis was used to estimate wrist dynamics, controller parameters, feedback gains and sensory noise (Exp. 3 and 4). For Exp. 3, frequency response functions (FRF) and coherence functions were calculated over the frequency range of the perturbing signal (0.033 – 30 Hz (in steps of 0.033 Hz) for each trial and an average FRF calculated across trials. The parameters characterizing the passive wrist dynamics (inertia, J, viscosity, B and stiffness, K) were then obtained by fitting the model (Eq. 2) to the magnitude of the averaged FRF. A bootstrap analysis was then performed to characterize the statistics and uncertainty (mean/median, standard deviation/percentile, skewness and kurtosis) in each of the parameter estimates.

6.2.1 Frequency Response Function (FRF)

The Frequency Response Function (FRF) describes the input-output relationships of a LTI system. For our analysis, pseudorandom (uniform band-limited) torque or visual perturbations were the input, x(t), and the position of the wrist manipulandum was the output, y(t). To calculate the FRFs, position and perturbation sequences in the time domain were transformed to the frequency domain using a Fast Fourier Transform (FFT). The FRF was calculated from the power spectra of the input and output signals.

$$\hat{H}(j\omega) = \frac{\hat{G}_{xy}(j\omega)}{\hat{G}_{xx}(\omega)}$$

where $H(j\omega)$ is the frequency response function, $\hat{G}_{xx}(j\omega)$ and $\hat{G}_{xy}(j\omega)$ are the average input spectral density and cross spectral density functions

$$\hat{G}_{xx}(\omega) = \frac{1}{N}\sum_{n=1}^{N} X_n^*(j\omega) \cdot X_n(j\omega)$$

$$\hat{G}_{xy}(j\omega) = \frac{1}{N}\sum_{n=1}^{N} X_n^*(j\omega) \cdot Y_n(j\omega)$$

where N is the number of trials, and $X_n(j\omega)$ and $Y_n(j\omega)$ are the input perturbation and output response of nth trial. Since, $H(j\omega)$ is a complex term, it can be represented in terms of a magnitude and phase response.

$$\left|\hat{H}(\omega)\right| = \sqrt{\hat{H}(j\omega)^* \cdot \hat{H}(j\omega)}$$

$$\angle\hat{H}(\omega) = \tan^{-1}(Imag(\hat{H}(j\omega))/Real(\hat{H}(j\omega)))$$

where $Real(H(j\omega))$ and $Imag(H(j\omega))$ are the real and imaginary components of the FRF respectively. For parameter estimation, only the magnitude response was used.

6.2.2 Coherence Function

The Coherence function (γ^2) provides a measure of the noise and non-linearity within the system.

$$\hat{\gamma}^2(\omega) = \frac{\left|\hat{G}_{xy}(j\omega)\right|^2}{\hat{G}_{xx}(\omega) \cdot \hat{G}_{yy}(\omega)}$$

where $\hat{G}_{yy}(j\omega)$ is the average output spectral density. The coherence metric spans the range from zero to one, with 1 indicating a linear relationship between input and the output without the presence of noise, and 0 indicating no linear relationship between the input and the output.

6.2.3 Parameter Estimation

Experimental estimates of the control parameters were obtained by fitting the

transfer function of the proposed model of 1-D wrist movement with the frequency response functions of individual subjects. In Exp. 3 and 4, combinations of parameters were isolated and estimated. Based on the experimental condition, parameters were kept as free variable for the curve fit. The other parameters (delays and feedforward noise) obtained from previous experiments were kept constant. In Exp. 4, J, B and K triplets were randomly selected from the distributions obtained via the Exp. 3 bootstrap analysis to account for the propagation of errors across successive parameter estimates. Table 6.1 shows the parameters estimated from the FRF by experiment. Least-square curve fits to the FRF were performed for each subject using the *lsqcurvefit* function in MATLAB® to minimize the least square error between the FRF and the model transfer function. Due to presence of random noise sources in the system (Feedforward noise and Sensory Noise), the phase response contained abrupt phase transitions that could not be automatically unwrapped without imposing *á priori* assumptions regarding the phase profile. Therefore, curve fits were performed only on the magnitude component of the FRF.

Experiment	Parameters Estimated
3	J, B and K
4	FRF1 – K_v, K_d, K_{pr} and K_i FRF2 – σ_S^2

Table 6.1 Sensorimotor control parameters estimated experimentally using frequency response analysis

6.2.4 Bootstrap Analysis

A single least-squares curve fit of the FRF provides a single estimate of the model parameters, making meaningful interpretation of the accuracy of the estimates problematic within subjects. Bootstrapping allows characterization of the uncertainty in the curve fit process through successive rounds of data re-sampling and curve fitting to

assess the variation in parameter estimates arising from the combined variability of the data and least-squares estimates based on random initial conditions. The resulting distributions provide an estimate of the uncertainty in the fitted parameters that can be used to statistically test within and across subject differences.

Bootstrapping is achieved by generating thousands of datasets, each of which is obtained by random sampling of the data points with replacement from the original dataset. A curve fit is then obtained for each dataset yielding thousands of estimates for each parameter whose distribution metrics (mean/median, standard deviation/percentile, kurtosis and skewness) can be used to quantify the uncertainty in the parameter estimate. For our analysis, ten thousand sampling iterations were performed to obtain a distribution of each parameter estimate. The initial parameter values for the curve fit were randomly selected (varying over an order of magnitude about the estimate) to minimize bias. Curve fits that exceeded the maximum iterations (400) or whose correlation between the data and fitted curve was less than 0.8 were discarded from further analysis. No *á priori* assumptions of the type of distribution were made for bootstrap results. Distribution metrics such as mean/median, standard deviation/percentile, kurtosis and skewness were then calculated for each parameter for each subject.

6.3 Simulation

Wrist dynamics (inertia, J, viscosity, B and stiffness, K) were characterized from the passive wrist response to the applied torque perturbations using the frequency response function analysis outlined for Exp. 3.

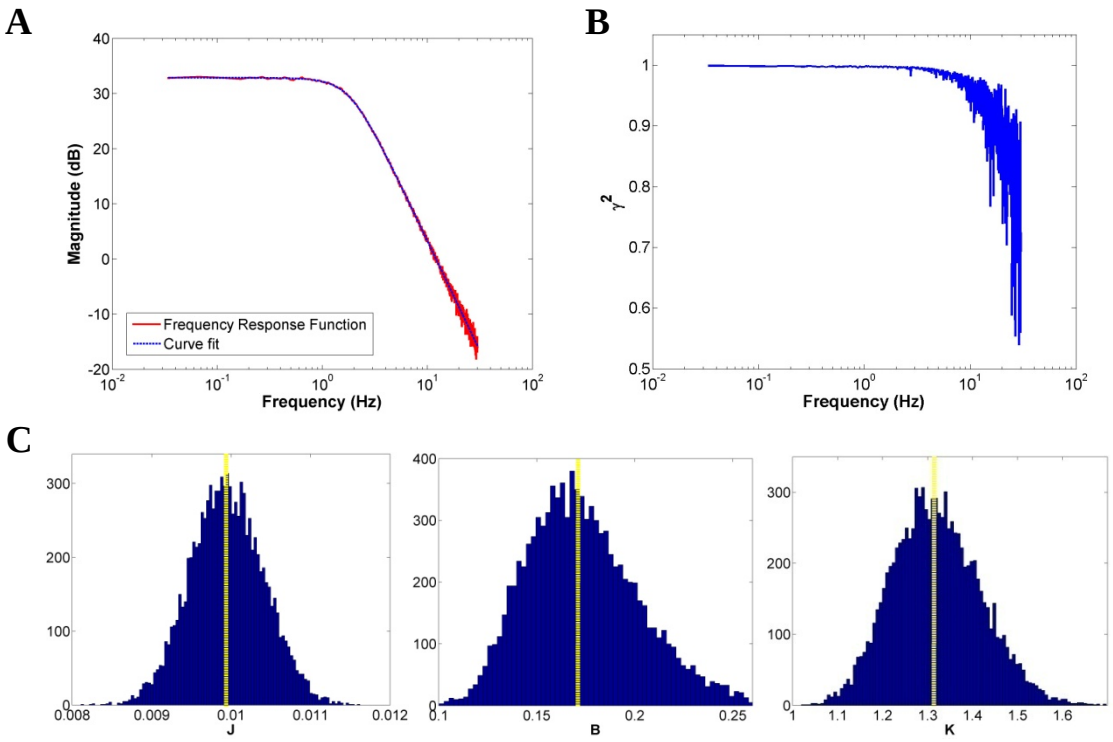

Figure 6.2 Characterization of Passive Wrist Dynamics via simulation of Exp. 3. A) Shows a typical Frequency Response Function (magnitude) plot (red solid line) for one simulated data set. The data was fitted (blue dashed line) in least squares sense to estimate J, B and K. B) Coherence plot for the same data set averaged over five trials. C) Distributions of J, B and K obtained from Bootstrap analysis performed over 10000 iterations. The peak of the distributions coincided with the median (yellow dashed line) of the estimates obtained from bootstrap analysis. The median values of the estimates were approximately equal to the values used for simulations.

Figure 6.2 shows the estimated FRF (Magnitude Response) of the passive wrist dynamics (Figure 6.2A) and the coherence plot (Figure 6.2B) for one simulation averaged over 5 trials. The FRF was estimated over the frequency range of 0.033-30 Hz. For the simulation shown, the coherence was high (γ^2>0.9) up to 10 Hz, after which it dropped systematically. The curve fit (r^2 > 0.99) to the FRF using Eq. 2 (relating the motor input to the wrist and wrist position response) yielded estimates of J, B and K that were well matched to the values specified in the model (Table 6.2). Figure 6.2 shows the distributions of each of the three parameters obtained from a bootstrap analysis of the

simulation results. For the bootstrap analysis, a dataset was discarded if the correlation coefficient between the FRF and the curve fit was less than 0.8 or if the curve fit function exceeded predefined number of iterations (400; default value of *lsqcurvefit*).

To characterize the distributions obtained from the bootstrap analysis we measured the skewness and kurtosis of the resulting distributions. Skewness is a measure of asymmetry of the probability distribution. For a normal distribution the skewness is zero. A negative skew suggests that left tail is longer and the mass of the distribution is located on the right, while a positive skew would suggest that the distribution has a longer right tail with mass of the distribution is located to the left. Kurtosis is a measure of peakedness of a distribution and is equal to three for a normal distributed random variable. As kurtosis increases (>3), the peak of the distribution becomes sharper and the tails become fatter, while as kurtosis decreases (<3), the distribution has a more rounded peak and shorter thinner tails. The kurtosis of the J, B, and K distributions was 2.95, 3.91 and 3.03 respectively and the skewness was 0.04, 0.69 and 0.27, suggesting that the distributions (for J, B and K) for this simulation were close to normal.

For the simulations using frequency response analysis (Exp. 3 and Exp. 4), median and percentiles (2.5% and 97.5%) of the distribution were estimated as opposed to mean and standard deviation to limit bias in the central estimates for skewed distributions (which were observed in a small number of cases). Table 6.2 shows the results for the same simulation. The median of the estimates (yellow dashed line) was well matched to the values specified in the simulations, indicating that the approach was able to estimate the parameters correctly. In Table 6.2, the percentiles (2.5% and 97.5%) define the ranges of J, B, and K within which 95% of the estimates fell.

Parameters	Expected	Estimated	
		Median	Percentile [2.5 97.5]
J	0.01	0.0099	[0.0091 0.011]
B	0.17	0.174	[0.125 0.243]
K	1.3	1.319	[1.139 152]

Table 6.2 Expected versus estimated parameters, J, B, and K, of the wrist (plant) for a single simulation of Exp. 3.

Validation across the parameter space:

To characterize the robustness of the approach to estimate passive wrist dynamics, a series of simulations were performed encompassing range of values for each parameter (J = 0.005-0.05; B = 0.03-0.7; K = 0.5-5). The range was selected such that it incorporated the estimates obtained from experimental data across the 11 subjects tested (See Section 6.4). The sample space formed a cube encompassing the ranges specified for J, B and K. 125 triplets of J, B and K were sampled from this space (5 values per parameter) for the subsequent simulations. Figure 6.3 shows the percentage error in estimating each parameter (median obtained from bootstrap analysis) as a function of the expected value across simulations. Each triangle represents the median obtained from bootstrap analysis of one simulation. In the figure, simulation results are collapsed across two dimensions (parameters) to characterize the error in third dimension (parameter). As seen in Figure 6.3A, the percentage error in estimation of J increased with increasing values of J (results collapsed across B and K). Similarly, Figure 6.3B shows percentage error in estimation of B collapsed across J and K. The percentage error increased with decreasing values of B. Figure 6.3C shows that the error estimation in K increased with decreasing values of K.

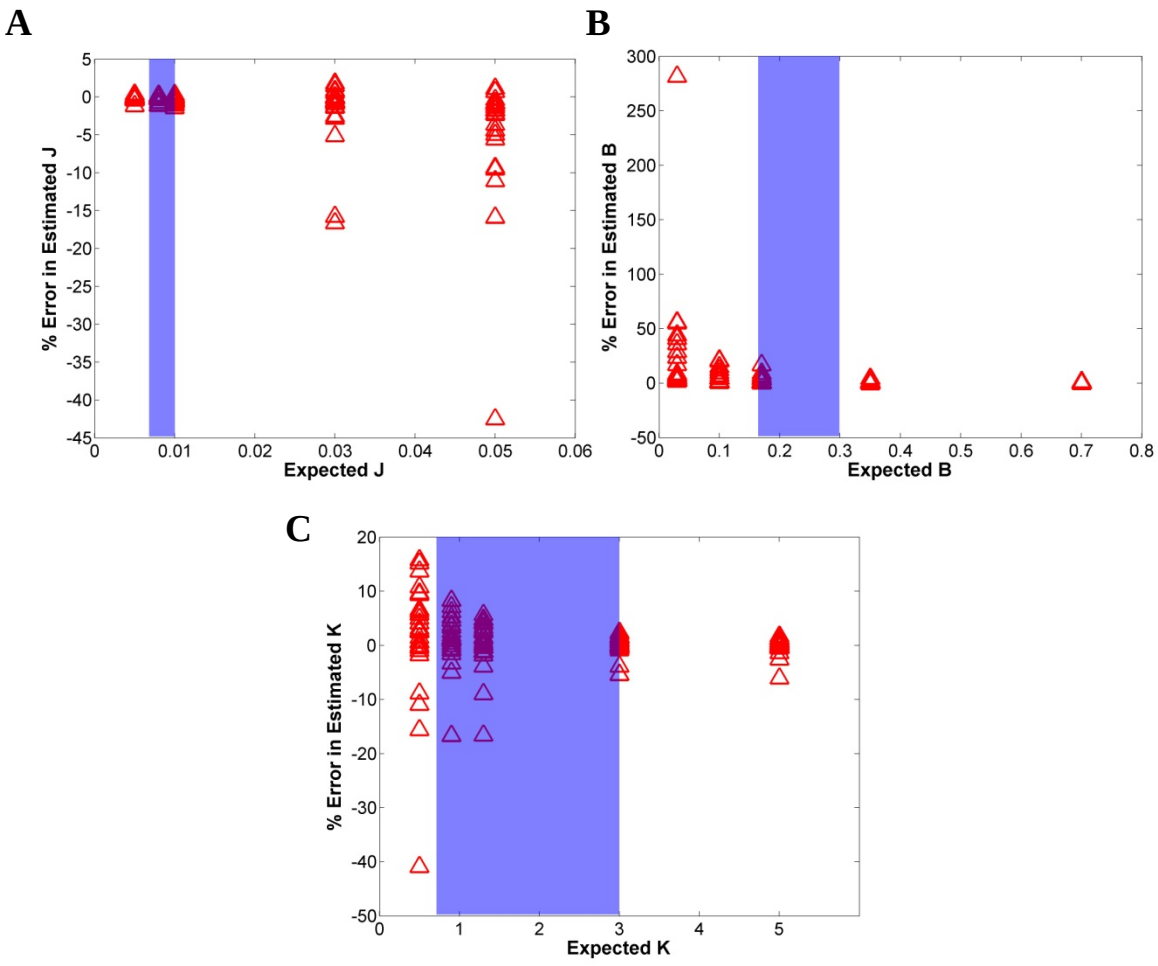

Figure 6.3 Validation of Exp. 3 used in conjunction with frequency response analysis to characterize passive wrist dynamics (Exp. 3). The approach to estimate passive wrist dynamics was tested over a range (J = 0.005-0.05; B = 0.03-0.7; K = 0.5-5) of values. The sample space formed a cube encompassing the range of J, B and K. Figure A, B and C show percent error in the median estimates of the J, B and K respectively. In each plot, simulation results were collapsed across two dimensions (parameters) to characterize the error in third dimension (parameter). Highlighted areas indicate the ranges of parameter estimates obtained across 11 subjects.

While Figure 6.3 provides insight into the errors in estimating the parameters of the wrist model, this representation makes it hard to comprehend the effect of one parameter on the estimates of another. In order to visualize this effect, we did a surface plot of error in one parameter as function of the other two parameters (refer Appendix A5

for surface plots). Percentage error for each value of J (e.g. for J = 0.05) as a function of B and K suggested that at low values of B (< 0.1) and K (< 1), J was underestimated by as much as 40%. Similarly the viscosity, B, was systematically underestimated as the moment of inertia (J) of the system increased. For low values of the plant stiffness, K, the error in the estimated values systematically shifted from a 15% overshoot to a -40% undershoot as the moment of inertia varied across an order of magnitude. However, it is important to note that for the (J, B, K) triplets estimated experimentally (see Section 6.4), the percentage error in the estimated parameters was less than 10 % (highlighted in Figure 6.3). These results suggest that Exp. 3 accurately estimated the wrist model parameters within neurologically intact subjects.

6.4 Experimental Results

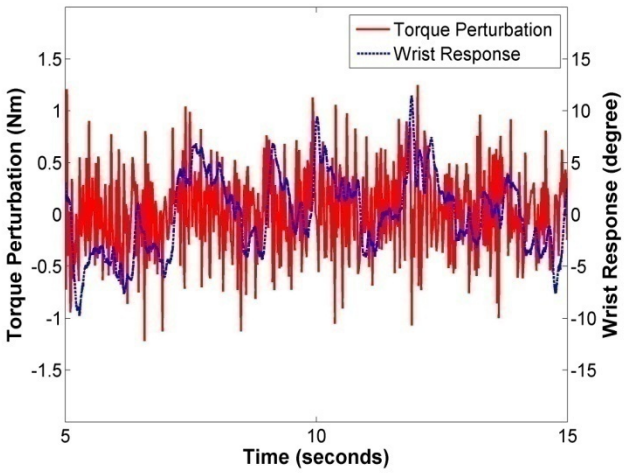

Figure 6.4 The temporal profile of applied torque and wrist position in Exp. 3 is shown for a representative trial in subject # 10. Each trial was 30 seconds long. In the plot, a 10 second subset of the trial is shown for clarity.

Figure 6.4 shows time plot of subject's response to the perturbation from one of the five trials. Figure 6.5A shows the estimated FRF (Magnitude Response) of the passive wrist dynamics (Figure 6.5A) and coherence plot (Figure 6.5B) for Subject 10

averaged over 5 trials.

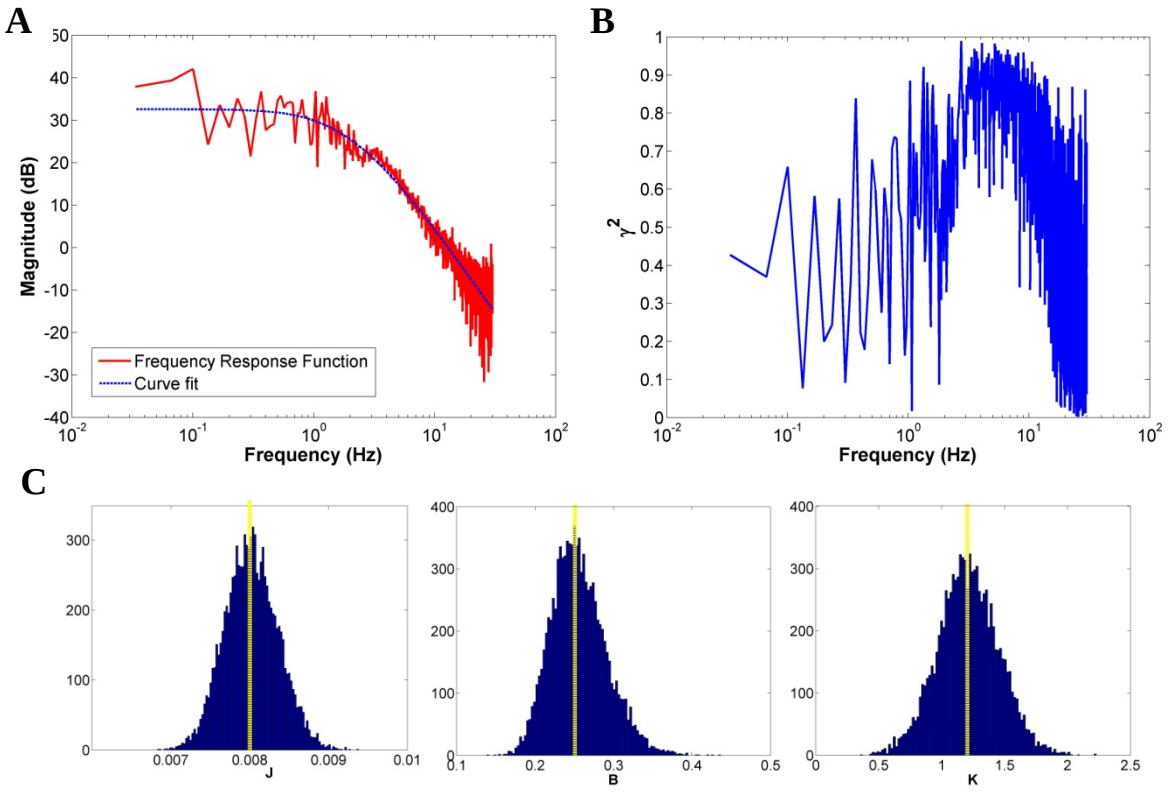

Figure 6.5 Characterization of Passive Wrist Dynamics using Exp. 3 for a subject. A) A typical frequency response function (magnitude) plot (red solid line) for data from one subject (Subject 10). A least-squares fit to the wrist model (Eq. 2) (blue dashed line) was used to estimate J, B and K. For the values reported, the measured dynamics included the combined effect of the wrist and wrist manipulandum B) Coherence plot for the same data set averaged over ten trials C) Distributions of J, B and K obtained from a bootstrap analysis over 10000 iterations. The peak of the distributions coincided with the mean (yellow dashed line) of the estimates (J = 0.008, B = 0.256 and K = 1.21) obtained from the Bootstrap analysis.

As with the simulations, the FRF was estimated over the frequency range 0.033-30 Hz. The coherence estimate is an indicator of linearity of the system, and for this subject, the coherence was high (>0.5) up to 15 Hz, beyond which it dropped systematically. This would support our assumption of a linear model for wrist dynamics over the specified range of frequency. The curve fit (r^2=0.91) to the FRF using eq. 2 (representing input-output relationship between torque command signal sent to the wrist

and position response of the wrist) yielded estimates of moment of inertia, J, viscosity, B, and stiffness, K, of the wrist. During the bootstrap analysis, datasets were discarded if the correlation coefficient between the FRF and the curve fit was less than 0.8 or if the curve fit function exceeded predefined number of iterations (400).

Figure 6.5C shows the distributions of each of the three parameters obtained from the bootstrap analysis. For the experimental data, the bootstrap distributions of all estimated parameters were normal or close to normal. Hence for the human subject studies we report the parameter estimates in terms of their means and standard deviations. For Subject 10, the estimated parameters of the wrist model were J = 0.008 ± 0.0003 kgm^2, B = 0.256 ± 0.035 Nms/rad and K = 1.21 ± 0.244 Nm/rad. For the values reported here, the measured dynamics included the combined effect of the human wrist and the manipulandum handle. The distributions were normal with kurtosis values of 2.97, 3.43 and 3.11, and skewness values of 0.10, 0.49 and 0.04 for J, B and K respectively. In all distributions, the peak of the distribution coincided with the mean (yellow dashed line) of the parameter estimate

Figure 6.6 shows the estimated parameters of the wrist model for all eleven subjects (Refer Appendix B for experimental results for all subjects). The distributions of parameters obtained from bootstrap analyses for each subject were normally distributed. Across subjects the kurtosis ranged from 2.96-3.01, 3.29-3.71 and 2.89-3.42, and the skewness ranged from 0.06-0.14, 0.44-0.63 and 0.04-0.58 for J, B and K respectively (refer Appendix B).

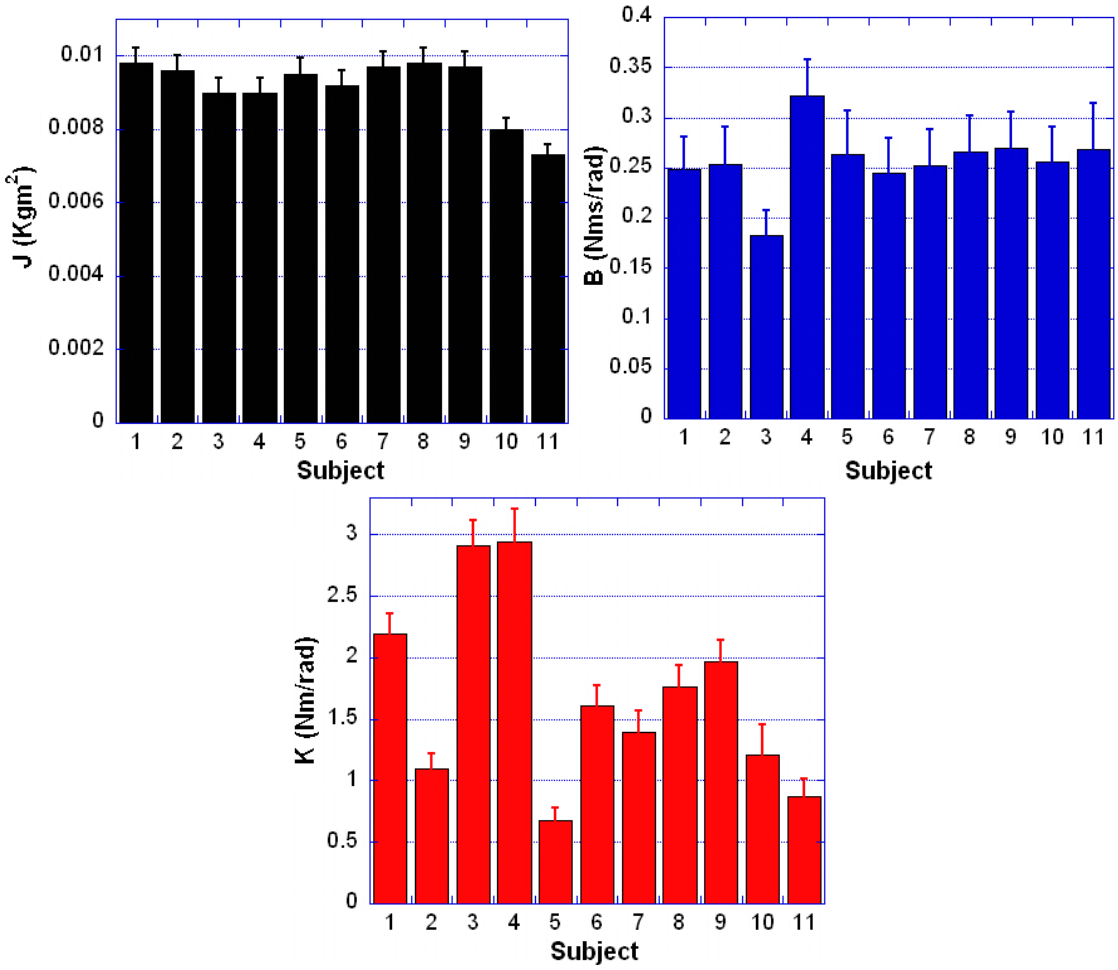

Figure 6.6 Passive wrist dynamics measured across subjects (Exp. 3). The estimates (mean ± std) of the wrist moment of inertia, J, viscosity, B and stiffness, K measured across 11 subjects. For the values reported, the measured dynamics included the combined effect of the wrist and wrist manipulandum.

In order to segregate the passive dynamics of the human wrist and the wrist manipulandum, Exp. 3 was performed using just the manipulandum under a no load condition. Subsequent analysis (FRF, curve fit and bootstrap) yielded a J_{WM} = 0.0066 ± 0.0004 kgm^2, B_{WM} = 0.323 ± 0.057 Nms/rad and K_{WM} = 0.215 ± 0.106 Nm/rad for the wrist manipulandum (WM). The passive dynamics of the human wrist (after removal of wrist manipulandum dynamics) ranged from 0.0007 to 0.0032 Kgm^2, -0.001 to -0.14 Nms/rad and 0.45 to 2.73 Nm/rad for J, B, and K respectively across subjects.

6.5 Discussion

In the current study, the wrist dynamics were modeled as a linear second order system containing an inertia (J), viscosity (B) and stiffness (K). The usage of a second order linear model for wrist dynamics was justified by coherence measures > 0.5 for frequencies up to 15 Hz (Figure 6.5) in all subjects and by use of visual stabilization task (for which the reflex response was very minimal). These results are consistent with a previous study (Halaki et al. 2006), which showed that human wrist dynamics were linear over this range. The linear model was subsequently fitted to the frequency response function (FRF) for each subject to quantify the passive dynamics of the wrist. Results from the model simulations suggest that measurement of applied perturbations without conscious correction is a robust way to estimate the wrist dynamics, presuming the dynamics under tasks conditions are similar.

When used in conjunction with a bootstrap analysis the systems identification approach returned accurate estimates across a wide range of parameter values with distributions that were either normal or close to normal. The technique (of bootstrapping) thus provides an additional tool to quantify the underlying sensorimotor control properties by characterizing the uncertainty associated with applying a curve fit to a particular dataset. The resulting distributions provide a means to apply parametric and nonparametric statistical analysis techniques to compare parameters across experimental conditions, tasks, subjects, or across subject populations (e.g., patients vs. neurologically intact subjects).

Exploration of the three-dimensional (J, B, K) parameter space via simulation revealed regions of reduced accuracy in estimating the parameters of the wrist model.

Specifically, the FRF analysis began to break down for larger moments of inertia (J>0.3 Kgm^2) and lower values of viscosity (B<0.05 Nms/rad) and stiffness (K<0.7 Nm/rad), as demonstrated by increase in percentage error (Figure 6.3). While current sampling of the parameter space was somewhat coarse (5x5x5), the results did show that the region of the (J, B, K) space encompassing the wrist dynamics of neurologically intact subjects was accurately estimated using the system identification approach. More extensive simulations, with finer sampling of the parameter space, will be required to allow accurate assessment of subjects and task conditions that fall outside normative range, however, the current simulations provide confidence that the values estimated in the neurologically intact population are accurate.

The inertia (J), viscosity (B) and stiffness (K) measured experimentally varied from 0.0007-0.0032 Kgm^2, -0.001 to -0.14 Nms/rad and 0.45-2.73 Nm/rad respectively. Grey (1997) obtained similar estimates (0.002-0.0041 Kgm^2) for the moment of inertia about the wrist. In his study, the stiffness measured across ten subjects ranged from 4-8 Nm/rad, which was generally higher than the values reported here. We believe this difference could be due to the type of task used to measure the parameters. Grey (1997) measured stiffness while performing a target reaching task (by means of 1-D wrist robot) using velocity feedback provided on the screen. This suggests that the stiffness was measured during active control of the movement as opposed to the passive control employed in our study. His interpretation is consistent with other studies, which have reported ranges of 2-5 Nm/rad (Gielen et al. 1984) and 1.5-4 Nm/rad (De Serres and Milner 1991), for the stiffness that are consistent with the values reported here.

The negative viscosities estimated for all subjects were unexpected. The effect

may be due to reflex activity generated in response to the high frequency components of the applied torque perturbations. During the task, counter-torques resulting from reflex activity were delayed with respect to the input torque, potentially inducing movements in the direction of the perturbation at the current time-step. As a result, for higher frequency torque perturbations the resulting delay coupled with the fast changes in perturbation direction could end up assisting the movement instead of opposing it, giving rise to negative viscosity. A similar finding has been reported previously for the wrist (Grey 1997) and elbow (Bennett 1994). Incorporation of a reflex path within the model may provide insight into the effect of reflex responses during continuous movement on the viscoelastic properties of the wrist. Future modeling efforts will incorporate a reflex path and additional experimental conditions to characterize the reflex model.

7 EXPERIMENT 4: CONTROLLER GAINS, FEEDBACK GAINS AND SENSORY NOISE

In Experiment 4, a visual stabilization task was used in combination with frequency response analysis to estimate the controller gains, feedback gains and the sensory noise of the system. In the current study, the controller was modeled as a PID controller, having a proportional gain (K_{pr}), integral gain (K_i) and a derivative gain (K_d). Owing to the use of a unity feedback system, the feedback gains (K_v and K_p) summed to 1 and where thus constrained to a single parameter. The internal noise within the sensory feedback path was lumped into a single noise source having a variance of σ_S^2.

The sections below detail the experimental task and explain the frequency response analysis employed to estimate the parameters of the wrist model. Simulation results are subsequently presented to validate the experimental approach, followed by experimental estimates of the wrist model across subjects and discussion of the results.

7.1 Experimental Task

This experiment was similar to previously described Experiment 1a. In this experiment, subjects were required to stabilize the cursor on the target (held static at the center of the screen) as pseudorandom visual perturbations (Bandwidth = 0.0033 – 30 Hz filtered (1^{st} order) at 1 Hz; SD = 15 degrees) were added to the cursor position. Filtering of the visual perturbation was done to make the task doable without losing the data points at high frequency (>1 Hz) which were required for curve fitting. To perform the task, subjects were required to continuously correct for the perturbation by applying counter movement in order to keep the cursor on the stationary target. To facilitate a subtraction analysis, stabilization responses were recorded across two sets of ten trials (32 seconds

each) and the resulting power spectra were averaged to improve the frequency response analysis (see Section 6.2).

7.2 Data Analysis (Subtraction Analysis)

In order to characterize the neural controller parameters (K_d, K_{pr} and K_i), feedback gains (K_v and K_p) and sensory noise (σ_S^2), the analysis was divided into two parts based on the form of the subtraction analysis. Estimates of K_v, K_d, K_{pr} and K_i (FRF1) were obtained from first part, whereas the second part was used to estimate σ_S^2 (FRF2) as described below.

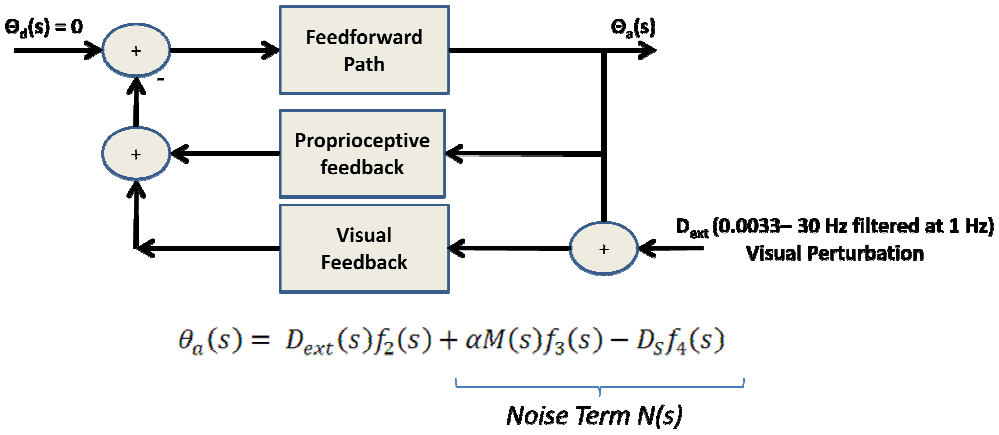

Figure 7.1 Block diagram representation of Exp 4 for characterization of controller parameters, feedback gains and sensory noise. Visual perturbations were added to the cursor and the subject's task was to correct for the perturbations in order to place the cursor on a target located at the center of the display.

A single visual perturbation sequence (Bandwidth = 0.0033 – 30 Hz filtered (1st order) at 1 Hz; SD = 15 degrees) of 302 seconds was generated and broken down into ten sequences of 32 seconds each such that the last 2 seconds of the previous sequence (trial) overlapped with first 2 seconds of next sequence (trial). For estimation of sensory noise (σ_S^2), all (ten) trials were concatenated to form a single continuous input-output sequence

of 300 seconds. For concatenation, the initial 2 seconds of each trial were discarded to minimize transient effects in the subject's response to the trial onset. During concatenation, artifacts associated with discontinuities were introduced at (1/30) Hz and its harmonics. The power of these artifacts was small in comparison with that of the signal and hence had no impact on the analysis. If required, these frequencies could be masked from the analysis. The purpose for using a single long sequence was to increase the frequency resolution (starting at 0.0033 Hz) used to estimate the sensory noise (σ_S^2), which was dominant at lower frequencies compared to the multiplicative feedforward noise (α). For estimation of controller and feedback gains, trials were separated into two groups of ten trials each and averaged within groups (similar to Exp. 3).

In the Laplace domain, Eq. 3 (Section 3.1.5) can be written generally

$$\begin{aligned}\mathbf{\Theta_a(s)} &= \mathbf{\Theta_d(s)}\, f_1(K_d, K_{pr}, K_i, J, B, K, T_{ff}) \\ &+ \mathbf{D_{ext}(s)}\, f_2(K_d, K_{pr}, K_i, J, B, K, K_v, T_v, T_{ff}) \\ &+ \boldsymbol{\alpha}\, \mathbf{M(s)}\, f_3(K_d, K_{pr}, K_i, J, B, K, K_v, K_p, T_v, T_p, T_{ff}) - \mathbf{D_S}\, f_4(K_d, K_{pr}, K_i, J, B, K, T_{ff})\end{aligned}$$

where for the visual stabilization task, the desired position, $\theta_d(t)$ was zero. The third and the fourth terms can be combined to form a single term corresponding to overall noise, N(s), within the sensorimotor system, simplifying the above equation to

$$(\theta_a(s))_i = \left(D_{ext}(s)\right)_i f_2(s) + N(s)$$

where *i* indexes the group of trials (obtained either by averaging or concatenation of 10 trials) , $\theta_a(s)$ is actual wrist position, $D_{ext}(s)$ is the applied visual perturbation, and $f_2(s)$ and $N(s)$ are transfer functions associated with external perturbation, $D_{ext}(s)$, and sensorimotor noise(s) (Eq. 3). For our analysis, the two data sets

$$(\theta_a(s))_1 = \left(D_{ext}(s)\right)_1 f_2(s) + N(s) \rightarrow \text{Set 1}$$

$$(\theta_a(s))_2 = \left(D_{ext}(s)\right)_2 f_2(s) + N(s) \rightarrow \text{Set 2}$$

where used together with a subtraction analysis to segregate estimation of sensory noise and other parameters (K_d, K_{pr}, K_i and K_v). Solving simultaneously for $f_2(s)$ and N(s), in terms of the applied perturbations (input) and subjects' wrist position (output),

$$f_2(s) = \frac{(\theta_a(s))_2 - (\theta_a(s))_1}{(D_{ext}(s))_2 - (D_{ext}(s))_1} \rightarrow \textit{FRF 1} \qquad \text{…Eq. (4)}$$

$$N(s) = \frac{\frac{(\theta_a(s))_2}{(D_{ext}(s))_2} - \frac{(\theta_a(s))_1}{(D_{ext}(s))_1}}{\frac{1}{(D_{ext}(s))_2} - \frac{1}{(D_{ext}(s))_1}} \rightarrow \textit{FRF 2} \qquad \text{…Eq. (5)}$$

where FRF1 was averaged over 10 trials (30 seconds each) and FRF2 was evaluated over one (concatenated) trial of 300 seconds. System delays measured in Exp.1 were held constant. During bootstrap analysis, fitted (J, B, K) triplets estimated from Exp. 3 were randomly selected from their respective bootstrap distributions and were kept constant during each bootstrap iteration in Exp. 4. This was done to propagate the uncertainty in estimates of J, B, and K to the subsequent parameter estimates in Exp. 4. Least-squares fits (see Section 6.2) to $f_2(s)$ for the FRF1 dataset were made over a frequency range of 0.033-10 Hz (Frequency resolution = 0.033 Hz) to estimate K_v, K_d, K_{pr} and K_i. Least-squares estimates of the sensory noise (D_S), via FRF2, were made over a frequency range of 0.0033-0.2 Hz (Frequency resolution = 0.0033 Hz), keeping the parameter estimates from FRF1 constant.

7.3 Estimation of controller parameters (K_d, K_{pr}, K_i) and feedback gains (K_v, K_p)

7.3.1 Simulation

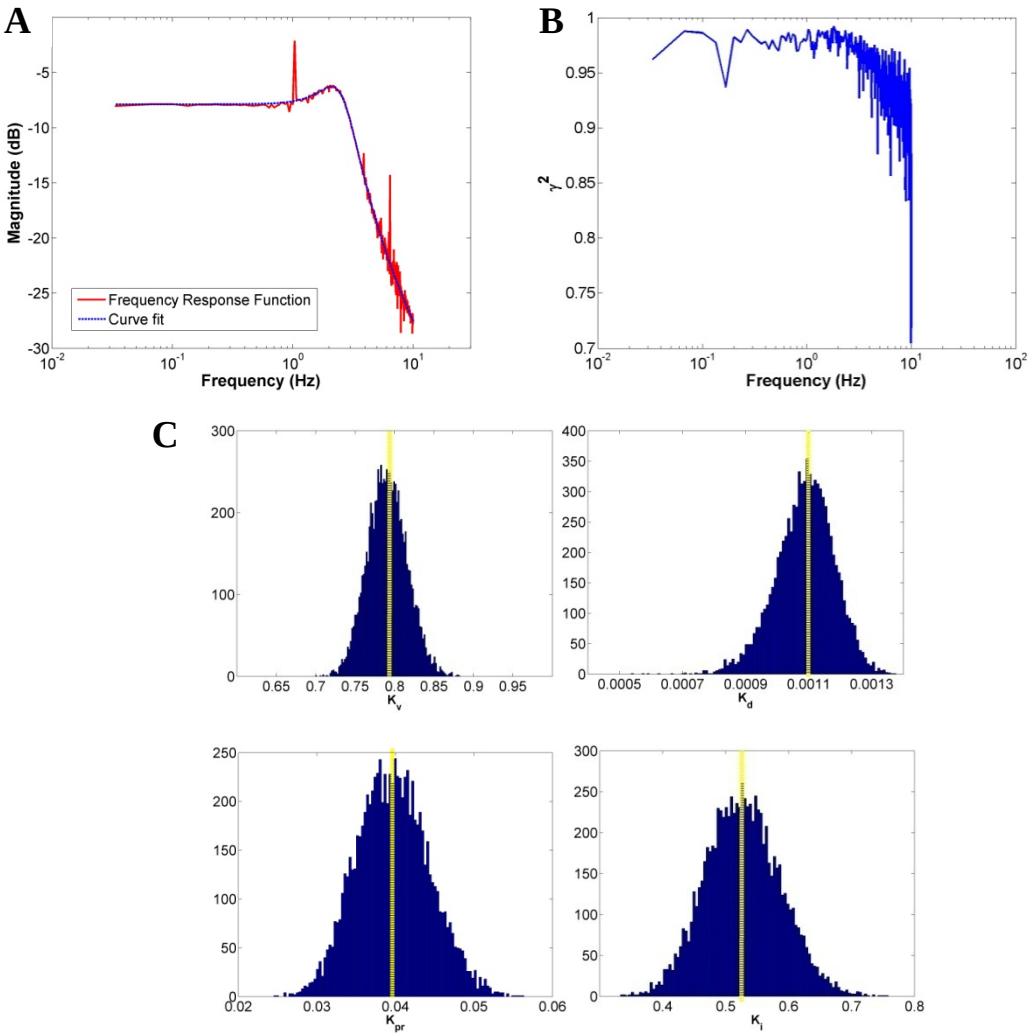

Figure 7.2 Characterization of controller parameters and feedback gains via simulation of Exp. 4a. A) A typical Frequency Response Function (FRF 1 magnitude) plot (red solid line) after subtraction analysis for one simulated data set. A least-square fit (blue dashed line) to the transfer function of the perturbing input, $f_2(s)$, (eq. 4) was used to estimate K_v, K_d, K_{pr} and K_i. B) Coherence plot for the same data set averaged over ten trials. C) Distributions of K_v, K_d, K_{pr}, and K_i obtained from bootstrap analysis performed over 10000 iterations. The peak of the distributions coincided with the median (yellow dashed line) of the estimates obtained from the bootstrap analysis.

For this set of simulations, the delays and feedforward noise were held constant. Since the delay term was a multiplicative factor in the transfer function (Eq. 3; transfer

function associated with $D_{ext}(t)$), it did not contribute to the least-squares fit of $f_2(s)$. This is advantageous because, unlike the estimation of J, B, and K, uncertainty in the estimates of the temporal delays in the model did not impact estimation of the visual feedback gain, K_v, derivative gain, K_d, proportional gain, K_{pr}, integral gain K_i and sensory noise, D_S obtained from experiment 4.

The first part of the FRF analysis estimated the controller parameters, K_d, K_{pr} and K_i, and feedback gain, K_v. FRF1 was estimated over a frequency range of 0.033-10 Hz. Frequencies from 10 Hz to 30 Hz were discarded because the input signal at those frequencies was very small (caused by low pass filtering of the input signal at 1 Hz; see Section 7.1), resulting in increased noise in the FRFs at those frequencies. Figure 7.2 shows the magnitude response and coherence of FRF1 and the corresponding least squares-fit to Eq. 4 ($r^2 = 0.94$) for one set of simulations. For the current simulation, the coherence was high ($\gamma^2>0.95$) up to 2.5 Hz, beyond which it systematically decreased. Since the model was assumed to have a unity feedback gain K_v was constrained to lie within [0, 1] for the curve fits. Figure 7.2C shows the distributions of each of the four fitted parameters obtained from bootstrap analysis of FRF1 shown in Figure 7.2A. The distributions were normally distributed with kurtosis values of 2.98, 3.66, 2.85 and 2.99, and skewness values of 0.09, -0.39, 0.15 and 0.14 for K_v, $K_{d,}$ K_{pr} and K_i respectively. The peak of the distribution coincided with the median (yellow dashed line) of the parameter estimate which was in turn well matched to the values set in the sensorimotor model. Table 7.1 shows the median and the percentile ranges of the estimates of the bootstrap results shown in Figure 7.2C.

Parameters	Expected	Estimated	
		Median	Percentile [2.5 97.5]
K_v	0.8	0.791	[0.744 0.841]
K_d	0.001	0.0011	[0.0009 0.0013]
K_{pr}	0.05	0.0396	[0.031 0.049]
K_i	0.5	0.526	[0.414 0.647]

Table 7.1 Simulation results for estimation of feedback gain and controller parameters (median, percentile [2.5 97.5]) obtained using the bootstrapping analysis (Figure 7.2C).

Validation across the parameter space:

To validate the approach for estimating the controller parameters and feedback gains, a series of simulations were performed encompassing a range of values for each parameter (K_v = 0.5, 0.75 and 1; K_d = 0.0001-0.01; K_{pr} = 0.005-0.5; K_i = 0.02-5). The range was selected such that it incorporated the estimates obtained experimentally from the the human subjects (see Section 7.3.2). The (K_d, K_{pr}, K_i) space was sampled uniformly (five values per dimension) resulting in 125 triplets of K_d, K_{pr} and K_i. For this sample space, K_v was constant and set to 0.5. Additional simulations using the same sample space for K_d, K_{pr} and K_i were repeated for K_v values of 0.75 and 1.

Figure 7.3 shows the percentage error in estimating each parameter (median obtained from bootstrap analysis) as a function of the expected value across simulations for K_v of 0.5. Each triangle represents one simulation and subsequent FRF bootstrap analysis where simulation results were collapsed across two parameter dimensions to characterize the error in third dimension. For example in Figure 7.3B, results were collapsed across K_{pr} and K_i to visualize the percentage error in estimation of K_d. As the value of K_d decreased the percentage error in the estimate systematically increased. Similar effects were seen for K_{pr} and K_i. The percentage error in estimation of K_v was

within 20% for all simulations (Figure 7.3A). Similar results were obtained for K_v values of 0.75 and 1 (refer Appendix A9 & A10). Over the range of the controller parameters estimated experimentally, the percentage error in the estimation was less than 25 % for K_d, K_{pr} K_i, and K_v.

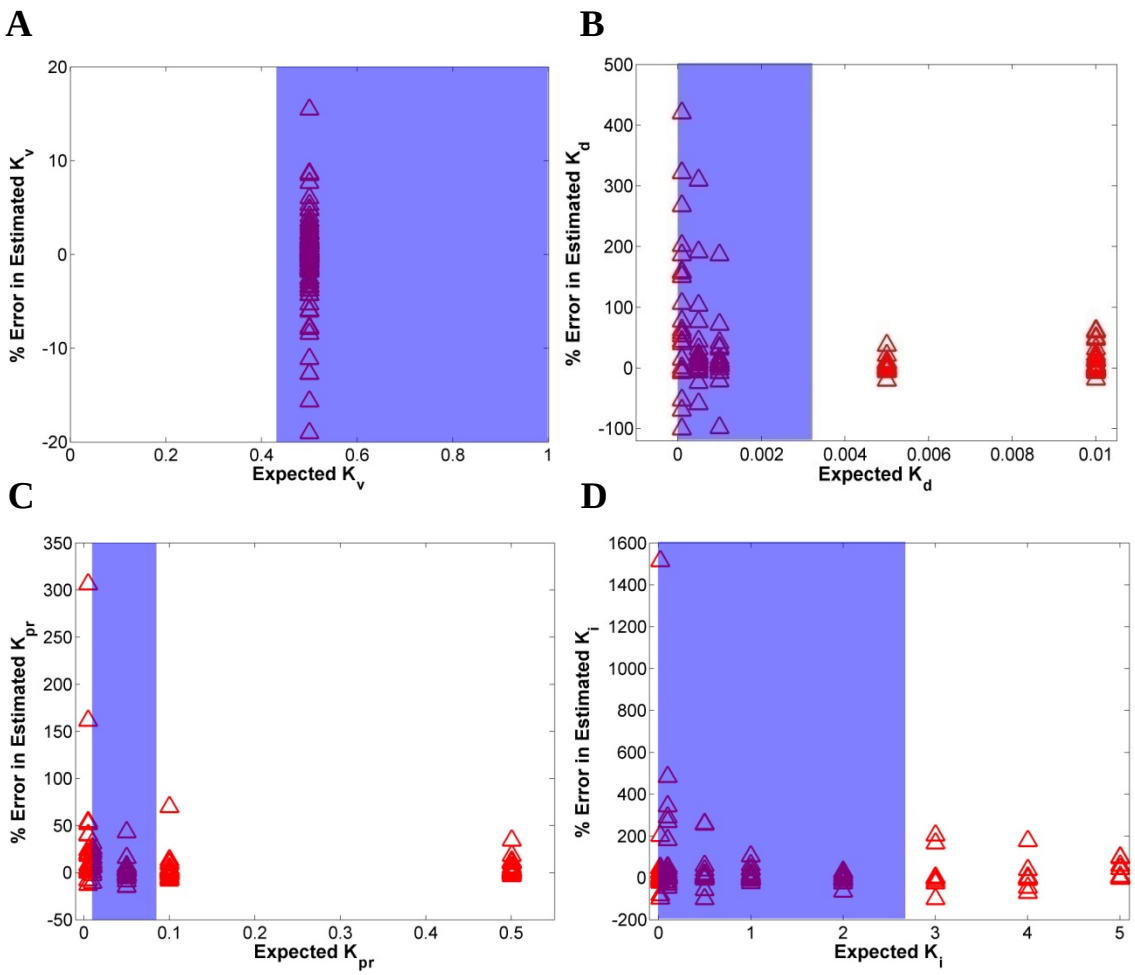

Figure 7.3 Validation of Exp. 4a used in conjunction with frequency response analysis to characterize controller and feedback gains. The approach to estimate controller parameters and feedback gain was tested uniformly (five values per parameter) over a range of values (K_d = 0.0001-0.01; K_{pr} = 0.005-0.5; K_i = 0.02-5) for K_v=0.5. Figure A, B, C and D show percent error in the median estimates of the K_v, K_d, K_{pr}, and K_i respectively. In each plot, simulation results were collapsed across two parameter dimensions to characterize the error in third dimension. Similar results were obtained for K_v values of 0.75 and 1. Highlighted area indicates the range of parameter estimates obtained across 11 subjects.

Similar to Exp. 3, surface plots of error across two parameter dimensions were used to visualize the effect of one parameter on the estimate of the other (refer Appendix A6, A7 & A8). For some triplets of K_d, K_{pr} and K_i, the system became unstable (represented by white space in the plots shown in Appendix A6, A7 & A8). However, for the (K_d, K_{pr}, K_i) triplets measured experimentally, the system was stable. Simulations showed that the percentage error for low values of K_d (=0.0001) was high (>150%) for low values of K_{pr} (< 0.1) and K_i (< 1). For higher values of K_d (>0.0005), the error in K_d increased with increasing K_{pr} (refer Appendix A6). Error in the estimation of K_{pr} increased with large values of K_d (>0.005) and small values of K_i (<0.1) (refer Appendix A7). For K_i = 0.02 error increased systematically with K_d and K_{pr}. However, for other values of K_i, no specific trend was observed (refer Appendix A8). Not all distributions of K_d, K_{pr} and K_i were normal. For some triplet of K_d, K_{pr} and K_i, the distributions of K_d and K_i were bimodal (but connected). In these simulations, the median of the principal distribution was approximately equal to the expected value of the model.

7.3.2 Experimental Results

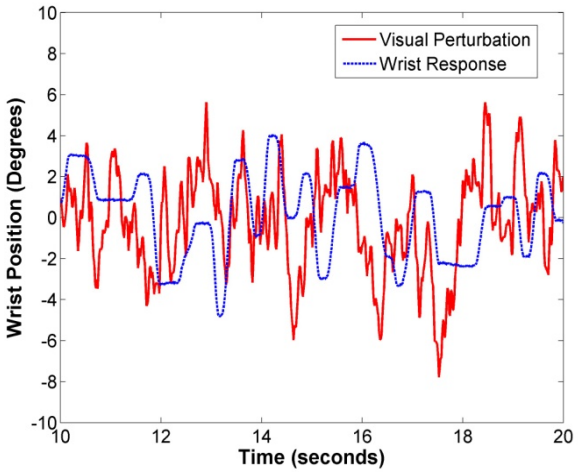

Figure 7.4 Example of a visual perturbation sequence and a subject's corresponding response for Exp. 4. For clarity, the plot shows 10 seconds of a typical 32 second trial.

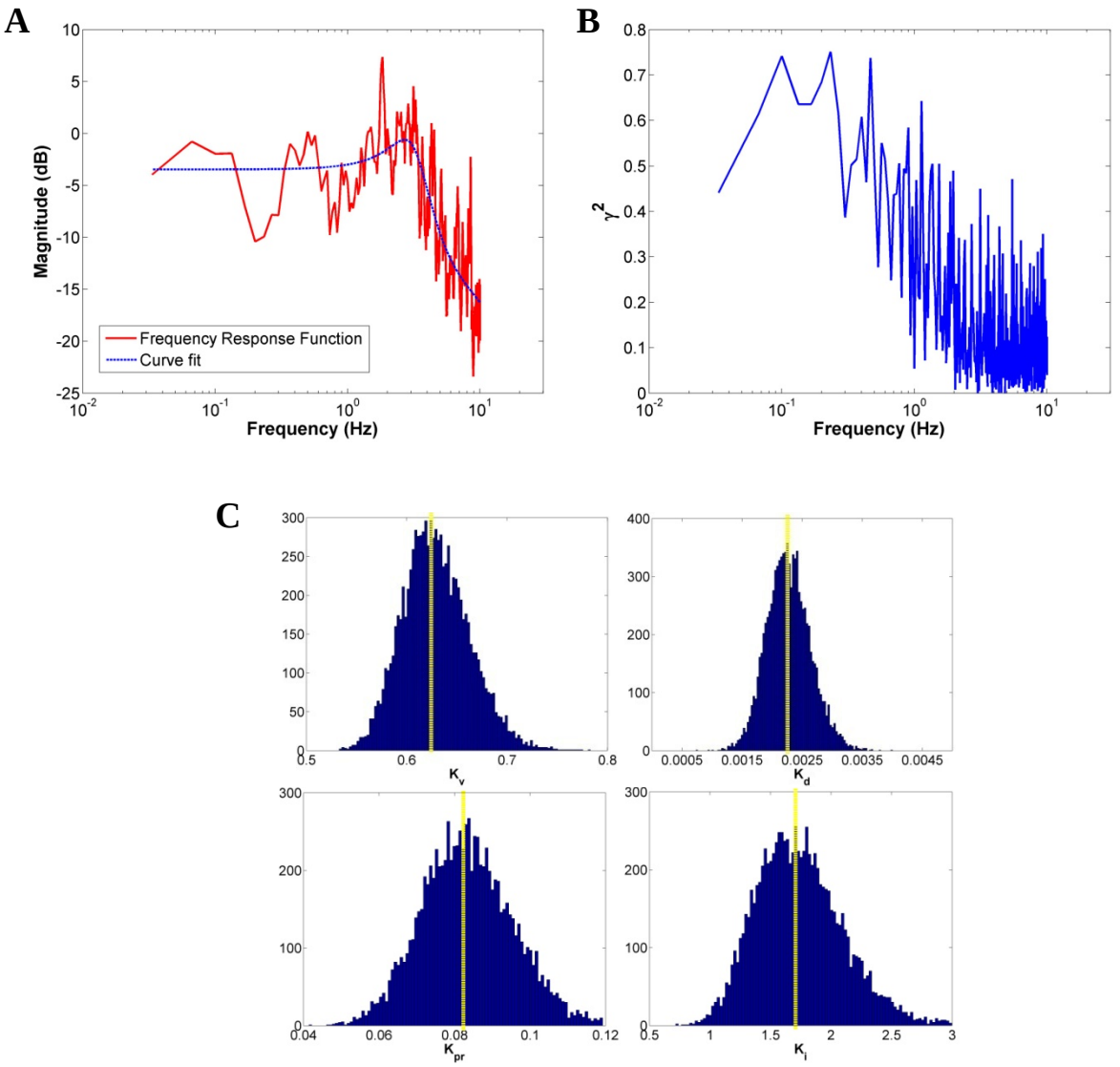

Figure 7.5 Characterization of controller parameters and feedback gains using Exp. 4a for a single subject. A) A typical frequency response function (magnitude – FRF1) plot (red solid line) obtained from visual stabilization task (Exp. 4) for subject 10. A least-squares fit to the external perturbation model (Eq. 4) (blue dashed line) was used to estimate K_v, K_d, K_{pr} and K_i. B) Coherence plot for the same data set averaged over ten trials C) Distributions of K_v, K_d, K_{pr} and K_i obtained from Bootstrap analysis over 10000 iterations. The peak of the distributions coincided with the mean (yellow dashed line) of the estimates (K_v = 0.63, K_d = 0.0023, K_{pr} = 0.083 and K_i = 1.71) obtained from the bootstrap analysis.

Figure 7.5 shows the estimated FRF1 (Magnitude Response; Figure 7.5A) and coherence plot (Figure 7.5B) for Subject 10, obtained using the subtraction analysis of two data sets averaged over 10 trials each (Exp. 4). Figure 7.4 shows time plot of

subject's response to the visual perturbation from one of the 20 trials. For all subjects the FRF1 was estimated over the frequency range 0.033-10 Hz. For this subject, the coherence was moderately high (>0.4) up to 1 Hz, beyond which it dropped systematically. Estimates of the neural controller parameters, K_d, K_{pr} and K_i and the visual gain, K_v, were obtained from the least-squares fit of Eq. 4 to FRF1 (r^2=0.72).Figure 7.5C shows the distributions of each of the four parameters obtained from bootstrapping analysis. The estimates (mean ± std) for this subject were K_v = 0. 63 ± 0.038, K_d = 0.0023 ± 0.0004 Nms/deg, K_{pr} = 0.083 ± 0.012 Nm/deg and K_i = 1.71 ± 0.377 Nm/deg.s. For subject 10 the distributions obtained from the bootstrap analysis were normal with kurtosis values of 3.26, 3.23, 2.87 and 3.32, and skewness of 0.36, 0.25, 0.16 and 0.51 for K_v, K_d, K_{pr} and K_i respectively. The peak of the distribution coincided with the mean (yellow dashed line) of the parameter estimate. In subjects whose estimated mean K_v was >0.9 (Subjects 1, 3, 5 and 8), the parameter distributions deviated from normal due to ceiling effects associated with an upper limit on the value of K_v of one.

Figure 7.6 shows the estimated feedback gain and controller parameters for all subjects. The distributions of the parameters obtained from the bootstrapping analyses for 10 subjects were normally distributed (except distribution of K_v for subjects 1, 3, 5 and 8) with kurtosis value ranging from 2.35-3.74, 2.85-3.75 and 3.04-3.74, and the skewness ranging from -0.42-1.28, -0.25-51 and 0.22-0.74 for K_d, K_{pr} and K_i. For subject # 11, the distributions of Kd, Kpr and Ki were not normal and they had kurtosis values of 6.29, 5.16 and 3.70 and skewness values of -0.63, 1.34 and 0.82 respectively (refer Appendix B for detailed experimental results).

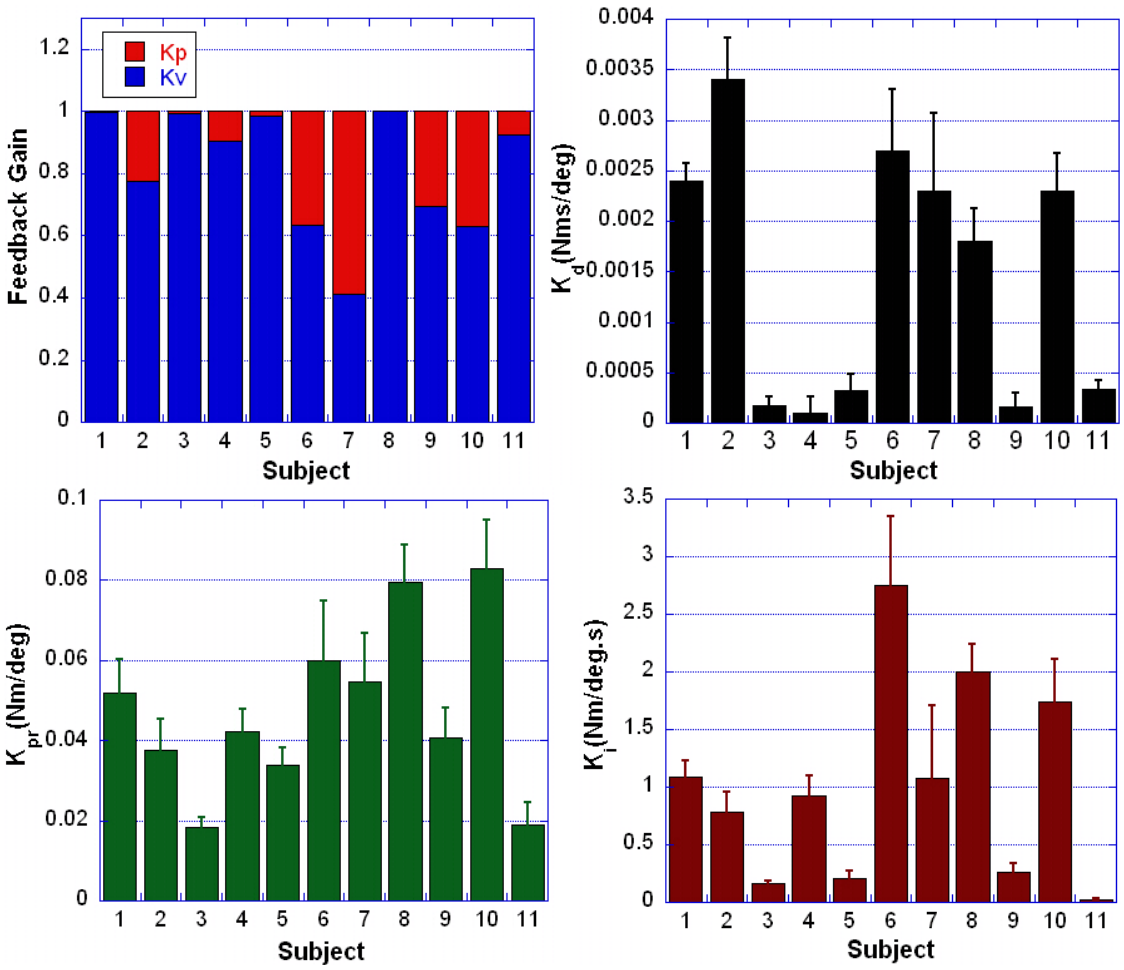

Figure 7.6 Estimated controller parameters and feedback gains across subjects. The estimates (mean ± std) of the controller parameters (derivative gain, K_d, proportional gain, K_{pr} and integral gain, K_i) and feedback gains (K_v and K_p) measured across 11 subjects were obtained using Exp. 4. Since the feedback had a unity gain, K_v+K_p was constrained to 1.

7.4 Estimation of Sensory Noise (σ_S^2)

7.4.1 Simulation

The second part of the analysis in Exp. 4, estimation of FRF 2 (Eq. 5; refer Section 7.2), was used to estimate the sensory noise (σ_S^2). During estimation of σ_S^2, all other parameters were fixed to the median bootstrap values determined from the previous experiments. Figure 7.8A shows the estimated magnitude response of FRF 2 for one set of simulations obtained using subtraction analysis. At lower frequencies the sensory noise was dominant while at higher frequencies the multiplicative feedforward noise dominated the response. Hence, FRF 2 was estimated over a much lower frequency range from

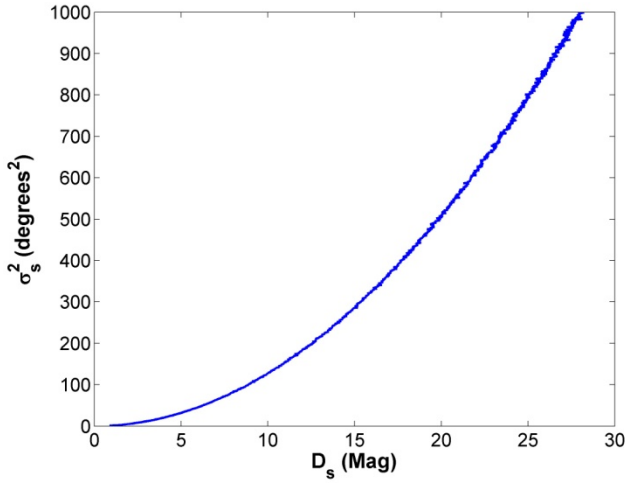

Figure 7.7 Mapping between the internal variance of the sensory noise (σ_S^2; degree^2) and the average magnitude of the sensory noise power spectrum (D_S).

0.0033-0.2 Hz. For the purposes of the model the additive sensory noise was assumed to be white and the mapping between the variance of the internal sensory noise source (degrees^2) and the average magnitude of the corresponding power spectrum (D_S) was determined to relate internal model variance (σ_S^2) to the average power of the noise in the

frequency domain (Figure 7.7).

The sensory noise can also be defined in terms of its effective position variability at the output of the plant, more commonly referred to as end point variability. This measure not only depends on internal sensory noise variance, but also on the properties of the wrist and neural controller which are subject specific, making it difficult to directly compare internal noise sources across subjects using this measure. For this reason, here we focus on reporting the sensory noise in terms of internal variance (σ_S^2; degrees^2). However, when interpreting the internal source variance (in degrees^2) it is important to note that its value does not directly correspond to the level of variability seen in the position output of the system. For a given set of controller and plant parameters, an internal sensory noise variance of 200 degree^2 could potentially correspond to an effective position variance of 3 degree^2 at the output of the model.

Figure 7.8A shows the estimate of FRF2 and the corresponding curve fit to Eq. 5 used to estimate D_S for a single simulation. The estimated value of D_S was subsequently converted to its equivalent internal noise variance (in degrees^2) using a polynomial fit (2^{nd} order) to the internal noise variance vs. average power spectrum (Figure 7.8). For the bootstrap analysis, datasets were discarded if the correlation coefficient between the FRF2 and the curve fit was less than 0.8 or if the curve fit function exceeded predefined number of iterations (400).

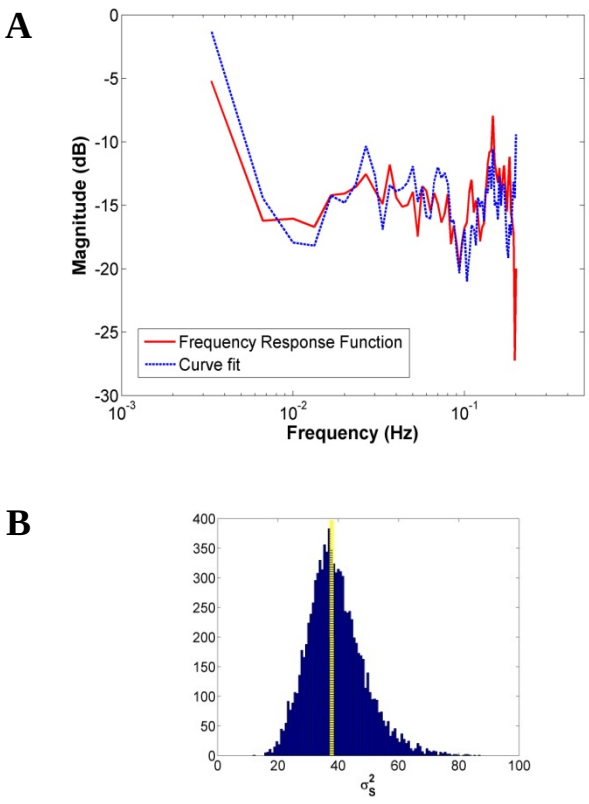

Figure 7.8 Characterization of the sensory noise via simulation of Exp. 4b. A) A typical Frequency Response Function (FRF 2 magnitude) plot (red solid line) after subtraction analysis for one simulated data set. A least-square fit (blue dashed line; Eq. 5) to the transfer function of the internal sensory noise, N(s), was used to estimate D_S. B) Distribution of σ_s^2 (obtained after conversion from D_S) obtained from Bootstrap analysis performed over 10000 iterations. The peak of the distribution coincided with the median (yellow dashed line) of the estimates obtained from Bootstrap analysis.

Figure 7.8B shows the distributions of σ_s^2 (estimated from Exp. 4 and obtained after conversion from D_S) obtained from the bootstrapping analysis of the simulation FRF 2 shown in Figure 7.8A. The distribution was approximately normal with a kurtosis of 4.08 and skewness of 0.72 . The peak of the distribution coincided with the median (yellow dashed line) of the parameter estimate and was within 35 % of the noise variance simulated in the model. Table 7.2 shows the results for the same simulation.

Parameters		Expected	Estimated	
			Median	Percentile [2.5 97.5]
σ_s^2	30	39.31	[23.19 61.41]	

Table 7.2 Simulation Results for estimation of sensory noise (median, percentile [2.5 97.5])

Validation across the parameter space:

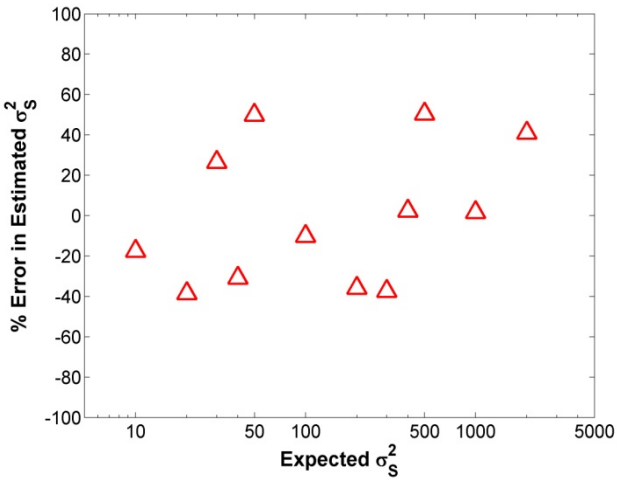

Figure 7.9 Validation of Exp. 4b used in conjunction with frequency response analysis to characterize sensory noise. The approach to estimate the sensory noise was tested over a range of values (σ_S^2= 10-2000 degree^2). The plot shows the percent error in the estimate (median) relative to the actual internal variance of the sensory noise. The percent error in estimation was less than 50% across simulations.

The method to estimate sensory noise, σ_S^2, was tested over a range of values (σ_S^2 = 10-2000 degree^2). Figure 7.9 shows the plot of percentage error in the estimation of σ_S^2. The error in the estimation was less than 50 % for all values of σ_S^2. No systematic trend in the error was observed (see Appendix A11 for simulation results).

7.4.2 Experimental Results

Figure 7.10A shows the magnitude of the noise frequency response function (FRF2) for Subject 10 (Exp. 4) obtained using the subtraction analysis outlined in Section 7.2. FRF2 was estimated over the frequency range of 0.0033-0.2 Hz for all subjects. For this subject, the correlation coefficient between FRF2 and the curve fit obtained using Eq. 5 was high (r^2=0.79), yielding an estimate of σ_S^2 = 1204.5 ± 294.9 deg^2 (obtained after conversion from D_S). The distribution was approximately normal (Figure 7.10B) having a kurtosis of 3.25 and a skewness of 0.04. When interpreting the internal source variance (in $degrees^2$) it is important to note that its value does not directly correspond to the level

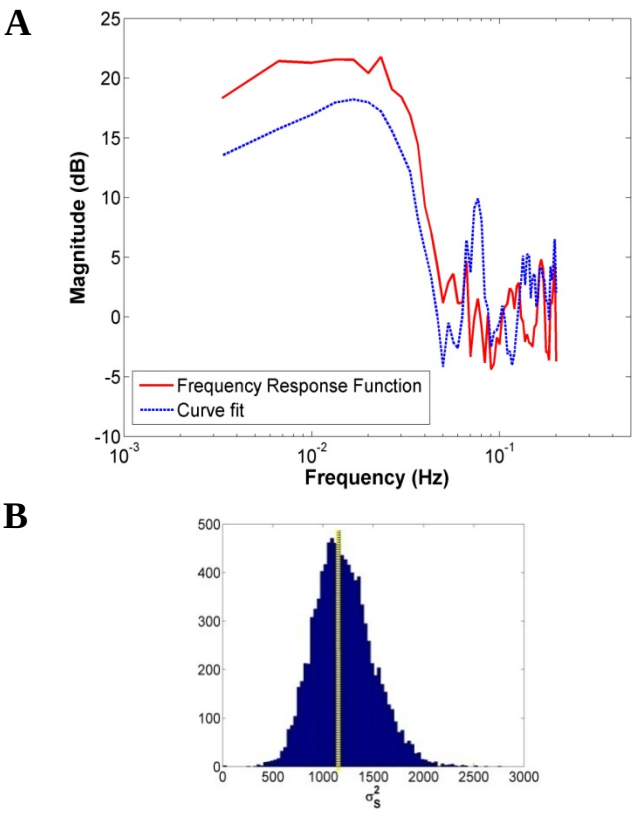

Figure 7.10 Characterization of the sensory noise using Exp. 4b for a subject. A) A typical Frequency Response Function (magnitude – FRF2) plot (red) for subject 10. The data was fitted (blue) in least squares sense to estimate D_S. The correlation coefficient was r^2=0.79. B) Distributions of σ_S^2 (obtained after conversion from D_S) obtained from Bootstrap analysis carried over 10000 iterations. The mean (yellow dashed line) of the distribution was 1204.5 $degrees^2$.

of variability seen in the position output of the system (see Section 7.4.1). For subject 10, the effective position variability was 41.9±8.59 deg^2. This variability was obtained by simulating the subject's position response, $\theta_a(t)$ (using the parameters estimate experimentally), with desired positions, $\theta_d(t)$, and external perturbation, $D_{ext}(t)$ set to 0.

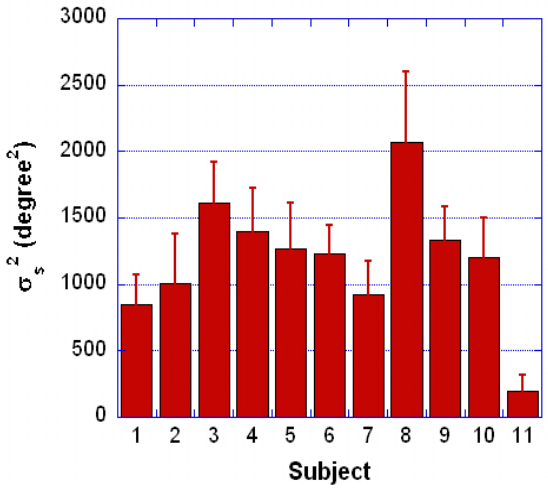

Figure 7.11 Sensory Noise across subjects. Estimate (mean ± std) of σ_S^2 across 11 subjects. The estimate of sensory noise was large and was set to zero for evaluating model's performance.

Figure 7.11 shows estimate of sensory noise (σ_S^2) for eleven subjects. For all subjects except one, the correlation coefficient between FRF2 and the least-squares fit to the internal noise transfer function (Eq. 5) was high (r^2>0.69; Appendix B). The distributions of the sensory noise estimate obtained from the bootstrapping analyses for all subjects were normally distributed with kurtosis value ranging from 2.59-3.84 and the skewness ranging from -0.53-0.51. Since the estimate of sensory noise was very large (see Appendix C), it was set to zero for all subjects when estimating variance accounted for by the model.

7.5 Discussion

7.5.1 Controller parameters

Based on sensory feedback signals, the neural controller processes the feedback information about the limb position and generates an output command to produce a desired movement. The current study implements a PID controller as a generalized surrogate for the processing and initiation of corrective movement in the brain. PID control is widely used in industrial applications and is capable of generating improved transient responses while simultaneously reducing steady state error; primary elements of online correction during goal-directed tasks encompassed by sensorimotor processing in the brain. That is not to say that PID control is implemented within a particular brain area, but rather that in the context of online error correction PID control is represented functionally as an aggregate control process within the brain. While this poses inherent challenges for interpretation of the controller parameters within a particular neural or cortical framework, it does provide a quantitative first approximation of the systems-level function that can be compared across subjects and task conditions.

Experiment 4 demonstrated the efficacy of using frequency response analysis in of subjects' correction to visual perturbations to estimate the controller parameters. Exploration of the 3D parameter space via simulation identified a gain region, K_d (<0.0005), K_{pr} (<0.01) and K_i (<0.1), in which the accuracy of the parameters estimated via the bootstrap analysis began to systematically degrade as the overall system response to perturbations decayed to zero (Figure 7.3). At high values of K_i (>1), the system became unstable, resulting in inaccurate parameter estimates. We return to this point later. Here also, the sampling of the parameters was coarse, and more simulations (with

fine sampling of parameter values) are required to more accurately determine the range beyond which estimation using the proposed experiments begins to break down. For the range of controller gains estimated experimentally, (K_d = 0.0001 – 0.0034 Nms/deg, K_{pr} = 0.019 - 0.086 Nm/deg, and K_i = 0.02 – 2.75 Nm/deg.s), the percentage error in estimation (for simulations) was less than 20 % (see Figure 7.3 and Appendices A6, A7 & A8), thereby giving confidence in the experimental results. The quantification of PID controller parameters during goal-directed wrist stabilization is novel, preventing meaningful comparisons with the literature.

For all subjects, the coherence between the variability in the input and output response spectra decreased dramatically for frequencies greater than 1 Hz, suggesting the presence of either a non-linearity or noise. What could account for a non-linearity? As the frequency of the perturbation increased the task became harder, forcing subjects to utilize alternative mechanisms which may not typically be required for low frequency perturbations. As the frequency of perturbations increased, several subjects noted an increased tendency to rely on their memory to average across recent perturbations and make approximate (lower frequency) corrections. Previously, studies have shown that the occulo-motor smooth pursuit system operates best at frequencies below 1 Hz (Stark et al. 1962; Leist et al. 1987; Hefter and Langenberg 1998), and switches to saccadic movements at higher frequencies (Hefter and Langenberg 1998) and this transition could potentially make a system non-linear.

Alternatively the reduction in coherence could be driven by an increase in noise in the system associated with the need to make high frequency corrections. High frequency movements are more abrupt and abrupt changes require large driving signal (Harris and

Wolpert 1998). From the model, an increase in the driving signal at higher frequencies would lead to an increase in the multiplicative feedforward noise, reducing the co-variation between input and output power spectra.

Simulations showed that as K_i increased, a resonant peak formed at 2-3 Hz and for values of K_i >1, the system became unstable. Simulations also suggested that as K_{pr} increased, the amplitude at the resonant frequency peak decreased and stability increased. This suggests that in order to produce stable movements, a high value of K_i must be accompanied by a high value of K_{pr}. Interestingly, for the experimental data, a strong correlation ($r^2 = 0.67$; see Appendix D for co-variation across parameters) existed between the two parameters (K_{pr} and K_i), suggesting that a common modulating gain could be driving the two parameters. Whether this could be an inherent strategy adopted by neurologically intact subjects and whether this strategy changes in patients suffering from tremors (a kind of instability) would be an area for future investigation.

7.5.2 Feedback Gains

In neural control models, systems having multiple feedback paths typically have a weight to each path whose value depends on how precise the feedback path is, how much attention is allocated to each path and/or the type of task at hand. Many studies have tried to decipher this mystery. A study by Welch et al. (1979) suggested that the weights are determined by the precision of the information in each modality. According to another idea, they are related to the attention that is directed to each modality (Welch et al. 1979; Kelso et al. 1975; van Beers et al. 1996). According to model proposed by van Beers et al. (1999), weights of visual and proprioceptive feedback are direction-dependent. The current study has quantified the relative weighting of visual and proprioceptive feedback

during visually-guided target stabilization. Simulation results (Figure 7.3A) indicate that the estimation of feedback gains was very robust (with less than 20% error in estimation).

It was initially assumed, that for a visually guided movement, more weight would be assigned to the visual feedback pathway. Although we expected the visual feedback gain (K_v) to be high for all subjects, the variability in K_v across subjects (range = [0.43,1]) was unexpected. It suggests that there are many ways to setup the control system to achieve comparable performance across subjects. This could also suggest that the standard experimental approach of classifying tasks in terms of a common underlying mechanism across subjects may not be entirely appropriate in the context of high-dimensional sensorimotor control.

7.5.3 Sensory Noise

Sensory processing in the human brain is not exact, such that the representation of sensory information is often corrupted by noise. While the underlying sources of noise may vary, e.g., due to nonlinear transduction, synaptic transmission and network (neuron) interactions during cortical processing (Faisal et al. 2008), their effect on the representation of information is cumulative. Thus in the model, the various sources of noise, and their propagation through the system were lumped into a single source of sensory noise.

It is important to note that in the current study estimates of sensory noise are expressed in terms of the variability associated with the internal noise as opposed to end point variability (van Beers et al. 1998) which is normally used as an estimate to describe variability (noise) during sensorimotor tasks. Although an important measure, end point

variability is an aggregate of motor and sensory noise and their transformation by the controller and/or plant. As a result, end-point variability does not provide an independent estimate of the sensory noise. Using a visual stabilization task (Exp. 4) and subtraction analysis (see Section 7.2), the sensory noise was quantified in terms of its internal variance.

The robustness of the approach is demonstrated by the simulation results. Although, for the experimental results the curve fit had high correlation ($r^2 > 0.69$ for all subjects except one), the estimate of the sensory noise was too high. This may be due to the way in which the sensory noise was modeled, i.e., as an additive noise. Previous studies of visual processing and perceptual learning (Dosher and Lu 1999; Dosher and Lu 1998; Lu and Dosher 1998) have reported multiplicative, as well as additive, noise sources during visual processing. The lack of a multiplicative component to the sensory noise could account for such a large estimate of sensory noise obtained from human performance. When evaluating model performance (see section 9.2), the sensory noise was set to zero as the variability introduced due to the internal noise (estimated values) affected the model performance significantly. Although, estimation of internal sensory noise is important for understanding the sensorimotor control system, its presence when evaluating the model's performance is insignificant.

In the current study, the sensory noise was represented by a single source. Ideally, there should be separate sources for each feedback path. However, the current experimental design was limited in its ability to estimate the noise sources independently due to the use of visual perturbations to characterize the FRF. The characterization of separate sources requires two sources of perturbation (one visual and one visuo-

proprioceptive). For example, introducing external perturbation simultaneously within each (visual and proprioceptive) feedback path provides a second estimate of the sensory noise that can be used to differentiate estimates of the internal visual and proprioceptive noise. Such perturbations can be introduced using externally applied torques, however, in the context of the proposed model their application and experimental characterization via the FRF requires the incorporation of a reflex model to properly account for the subject's response. Future work is aimed towards addressing this limitation in the current model with an eye toward dissociating the two noise sources and incorporating multiplicative sensory noise.

8 EMG ANALYSIS

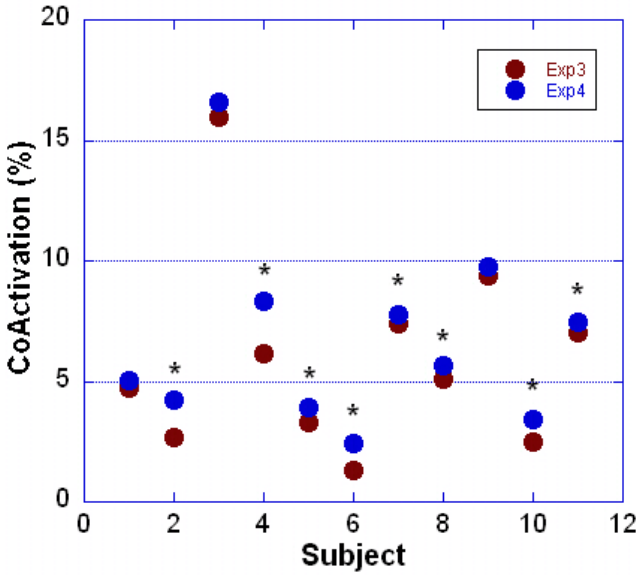

Figure 8.1 Comparison of EMG (CoActivation) across Exps. 3 and 4. CoActivity within wrist muscles (FCR and ECR) was measured for Exp. 3 (brown circles) and Exp. 4 (blue circles). CoA level was less than 10% of the maximum value achievable for all subjects except one. A two-sample t-tests with repeated measures was performed within subjects to test for significant differences between experiments (* denotes significance at the alpha=0.05 level). Error bars were less than the symbol size and are not shown for clarity.

Antagonist muscle co-activity (CoA) of the wrist (FCR and ECR) was measured for each subject across Exps. 3 and 4, to characterize the levels of co-contraction (achieved by stiffening the wrist joint) employed by subjects and to measure their similarity across experiments. Figure 8.1 shows CoA across subjects for Exp. 3 (averaged over 4 trials) and Exp.4 (averaged over 18 trials). Across subjects, co-activity was less than 10% for all subjects except one. A paired t-test across subjects showed that the CoA between experiments (3 and 4) was significantly different ($t(10) = -4.74$, $p<0.05$). A within-subject repeated measures analysis of CoA across experiments showed a small yet significant difference ($t(20) = -2.3$, $p<0.05$, two-tailed) in 8 out of 11 subjects. This is

due in part to the highly consistent average activity across trials within an experiment. The results of these analyses would seem to suggest a change in passive dynamic properties of the wrist across experiments, which would require separate estimates of B and K for each experiment. Separate studies of the biomechanical impact of changes in CoA indicate that the impact of a 1% change in overall CoA is small, which would tend to support the implicit assumption of constant biomechanical properties in the current tasks.

9 EXPERIMENTAL PERFORMANCE OF THE MODEL

9.1 Variance Accounted For

To measure the performance of the model, subjects' responses were compared with that of the model using the specific control parameters (delays, gains, neural controller, plant, and noise sources) estimated for each subject. For this, a different experiment involving visual stabilization was performed. The subject's task was same as described previously in Exp. 1a. However, a new set of ten trials of 20 seconds each were collected to measure the performance of the model. Variance Accounted For (VAF) was calculated to obtain a performance metric for the estimated parameters and the overall model. A VAF of 100% implies accurate prediction by the model. VAF of less than 100 % would indicate presence of unmodelled behavior, such as non-linearities and uncorrelated noise (Schouten et al. 2008).

To estimate VAF, the visual stabilization performance of the model (using the parameter estimates obtained from the experimental data analysis) was simulated for each subject in SIMULINK® and compared to subject's performance, $\theta_a(t)$, for the same visual perturbation, $D_{ext}(t)$.

$$VAF = \left[1 - \frac{\sum_n \left|\theta_a(t_n)|_{experimental} - \theta_a(t_n)|_{model}\right|^2}{\sum_n \left|\theta_a(t_n)|_{experimental}\right|^2}\right] \times 100$$

where n indexes the temporal samples. VAF was estimated for ten trials and averaged to evaluate mean and standard deviation of the estimate for each subject.

9.2 Model vs. Subject's Performance on wrist stabilization task

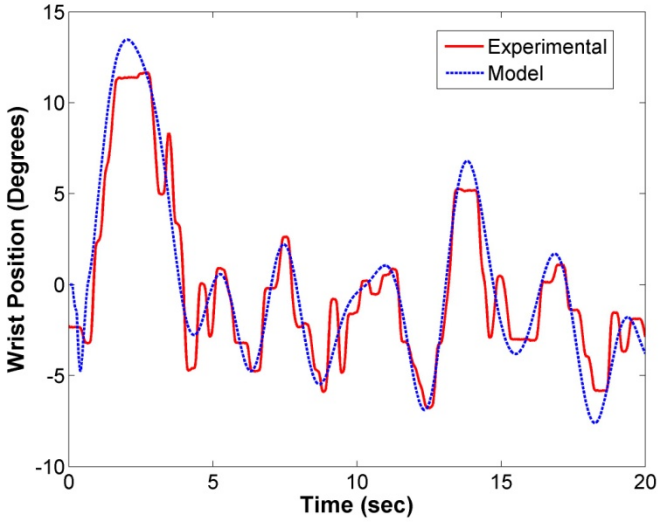

Figure 9.1 Model vs. Subject's Performance on wrist stabilization task. One trial of the visual stabilization performance of the model simulated for Subject 10 and compared to subject's performance for the same visual perturbation signal. For this trial the VAF was 86.5%

Figure 9.1 shows a time course of a subject's (#10) response to visual perturbations and model's prediction obtained using the sensorimotor control parameters measured for that subject. The predicted output was well matched to the subject's response, as suggested by the high variance accounted for (VAF = 86.5%) for the same trial. For this subject, the VAF averaged over 10 trials resulted in a mean of 80.2±5.8 %. Figure 9.2 shows the VAF for all eleven subjects. The VAF for all subjects was high, varying from 73.3% to 82.9% with a mean of 78.3±3.3 % (see Appendix E). While evaluating the performance of the model, the internal sensory noise (σ_S^2) was set to zero since the large values of the sensory noise estimates affected the model's performance dramatically.

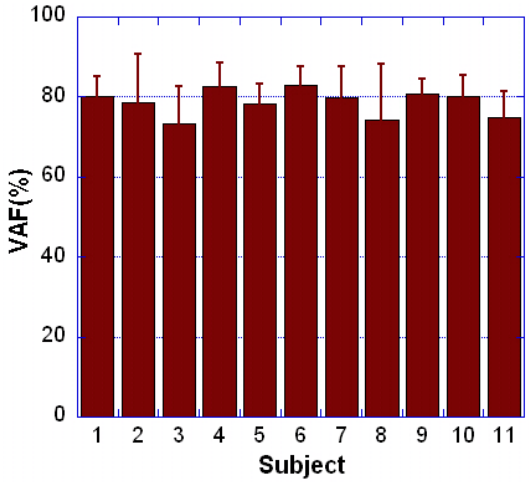

Figure 9.2 Variance Accounted For (VAF) across subjects. The VAF (mean ± std) for each subject was obtained by comparing subject's response with the model's prediction obtained using the sensorimotor control parameters measured for that subject. The VAF for all subjects was high, varying from 73.3% to 82.9% with a mean of 78.3±3.3 %.

9.3 Variance Accounted For (VAF) by the Model: Comparison across Sessions

Since the data was collected over two different sessions, we wanted to ensure that the system parameters did not change across these two sessions. Since Exp. 1a (designed to measure open loop visual delay) and Exp. 5 (designed to compare subject's performance with the model via VAF) were identical in nature and data for these two experiments were collected on different days (sessions), we compared the VAF by the model in Exp. 1a (Session 1) with that obtained in Exp. 5 (Session 2). Figure 9.3 shows this comparison in VAF across sessions for all subjects.

A within-subject two sample t-test (two-tailed, alpha=0.05) on repeated measures was performed to determine whether the VAF was significantly different between the two sessions. A significant difference in VAF between the two sessions (denoted by * in Figure 9.3) was observed in 3 of 11 subjects ($t(18) = -3.62$, $p<0.05$). For the subjects

whose difference in VAF across sessions was significant, no specific trends in the change in VAF were observed. A paired t-test across subjects revealed no significant difference in VAF between sessions ($t(10) = -0.219$, $p<0.05$). These results suggest that the sensorimotor control performance as a whole in most subjects did not vary significantly. However, no definitive comments about the time-invariant properties of the parameters can be made as VAF was an indirect measure and sensitivity of VAF to each parameter was not determined here.

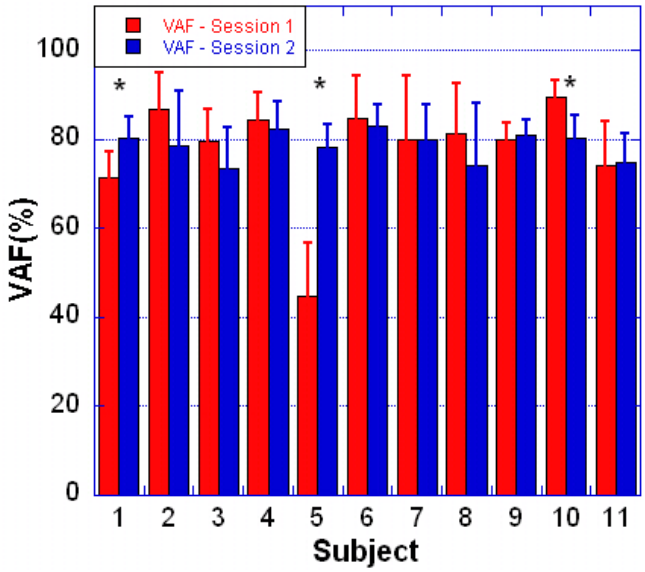

Figure 9.3 VAF comparison across sessions. VAF (mean ± std) for each subject across two sessions. A two-sample t-tests on repeated measures was performed within subjects to test for significant differences between sessions (* denotes significance at the alpha=0.05 level).

9.4 Discussion

The control parameters estimated for the human subjects resulted in accurate model prediction of position, as demonstrated by a high VAF for all subjects. This suggests that the proposed model accounts for human control of wrist movement. However, the fact that the VAF was less than 100% suggests the presence of additional

features inherent in the sensorimotor control system that was not accounted for by the model. Below we outline some possibilities which could account for the remaining 20-25% of the variance not accounted for by the model.

On examining the position response of human subjects, we found that subjects had a tendency to correct intermittently. It has been well established that visually guided tracking movements are not smooth (Miall et al. 1993a; Doeringer and Hogan 1998). Movement intermittency could be an inherent property of the central nervous system (CNS) which the current study failed to model. From the perspective of movement planning, the actual movement can be broken down into submovements (Miall et al. 1993a; Neilson et al. 1988) which could give rise to intermittent behaviors that increase for random target as opposed to rhythmic tracking. In our experiments, the visual perturbations were random in nature, which could have contributed to the intermittent behavior. Miall et al (1993) modeled this intermittent behavior by incorporating an error deadzone within a feedback control loop. It would be interesting to incorporate this intermittent behavior in our model to see if VAF increases.

Velocity, position and torque data also suggest that the robotic manipulandum had an inherent stiction (static friction) associated with it. The robotic manipulandum did not move if the torque command applied to it was less than 0.22Nm. This effect was most noticeable when changes in direction of the manipulandum occurred and likely contributed to the apparent intermittency of corrections to changes in position.

Another possibility for this intermittent behavior could reflect the presence of internal (neuromuscular) noise. Though sensory noise was incorporated into the model,

its value was set to zero when measuring the VAF since the accuracy of the noise estimates was uncertain in the human subjects. Increased sensory noise would manifest at the output as low-frequency modulations which could contribute to the apparent intermittency of subjects' responses by randomly opposing the subjects' movement. Finally, the intermittent behavior could be due to the increased inertia associated with using the robotic manipulandum, which could have altered the strategy used for stabilization. The incorporation of active compensation (to nullify this inertia effect) within the robotic manipulandum could be implemented to test this hypothesis.

EMG data was collected to measure the co-activation between FCR and ECR (flexor and extensor wrist muscles) while performing Exp.3 and Exp. 4. Statistical analysis across experimental conditions suggested that the co-activation across the two experiments was significantly different for 8 out of 11 subjects. This suggests that the dynamics of the wrist may have changed across experiments. To the extent that the assumption that wrist dynamics were constant was violated, the values of J, B and K may not have been optimal when estimating the parameters in Exp. 4, thereby affecting the VAF. Although, we used a more conservative approach by incorporating the variability of the wrist parameter estimates (J, B and K) when estimating the neural controller, feedback gain and noise sources in Exp. 4, the possibility that the wrist dynamics may have changed across experiments cannot be discarded.

Another important and compelling factor affecting the VAF could be the variability in the position response itself. By this, we mean that a VAF of 100% may not be possible because of the inherent variability (noise) present in the system. If a subject is asked to perform a visual stabilization task multiple times with the same input

perturbation sequence each time, the position response will vary across trials .This variability places an upper bound on the VAF that could be practically achieved. For example, with a 100 deg^2 internal variance in the position response, the maximum VAF that can be achieved is 90%. For the average VAF shown here (80%), the normalized VAF obtained by comparing model response to the subject's response would be 88.89%.

10 DISCUSSION

10.1 Summary

In this study, a methodology was developed which utilizes systems identification techniques together with experimental measurements of wrist control to systematically characterize the sensorimotor control system for visually-directed wrist movements in neurologically-intact subjects. Fully characterizing the sensorimotor control system is a necessary step toward understanding of how different elements of the system interact to produce intended movement.

The proposed model of sensorimotor control contained 13 parameters (including temporal delays, internal noises, feedback gains, wrist dynamics and controller gains) and was structurally similar to several qualitative models of sensorimotor control proposed in the literature (Kawato 1999; Miall et al. 1993b; Wolpert and Miall 1996a; Mehta and Schaal 2002; Peterka 2002). The parameters defining the model were characterized experimentally through a series of four stabilization tasks designed specifically to isolate elements of the control system and estimate the underlying parameters. In Exp. 1, cross-correlation analysis was employed to measure the implicit and explicit delays in the control system. Exp. 2 used isometric force contractions to estimate the signal-dependent (multiplicative) feedforward noise. In Exp. 3 and 4, wrist dynamics, controller parameters, feedback gains and sensory noise were quantified by fitting the model to the frequency response functions obtained from the subjects' position response to input perturbations (visual and torque).

A cross-validation approach was used to simultaneously assess the ability of our

approach to estimate the underlying model parameters and accurately reproduce subject responses to stabilization and tracking tasks. The experimental paradigm was validated by simulating the sensorimotor control model and experiments in SIMULINK® over a range of values for each parameter to characterize the robustness of the approach. Model validation was performed by characterizing the sensorimotor control system in human subjects, and subsequently using the estimated parameters in the model to predict subject-specific performance on stabilization (and tracking) tasks. All but one parameter (σ_S^2) was found to be estimated reliably. The control parameters estimated for human subjects resulted in accurate model prediction of position, as demonstrated by a high VAF for all subjects.

10.2 Model Assumptions

Previous studies have estimated components of the sensorimotor control system in isolation (van Beers et al. 1999; Jones et al. 2002a; Notley et al. 2007), thereby making it difficult to make interpretations about the sensorimotor control system as a whole. To model a sensorimotor control system as a whole and study its interaction while performing a task, it was therefore necessary to characterize all the parameters of the model simultaneously in one experimental session. Further, based on the complexity of the sensorimotor system, it was necessary to make several simplifying assumption for the model and the parameters, which warrant further discussion.

As a first order approximation, the model as a whole was assumed to be a linear time-invariant (LTI) system (Mehta and Schaal 2002; Peterka 2002) . The process of proprioception combines information from multiple sources including muscle stretch, force receptors, tactile receptors and the Golgi tendon. Visual processing is a complex

process spanning multiple cortical areas that systematically build up a representation of the visual space through a distributed hierarchy of processing stages. In our study, these feedback paths were highly simplified into lumped parameter models, each consisting of a weight, delay and a noise term based on an implicit assumption that the position information propagated through the feedback paths is an exact estimate of the limb's actual position, and this position information is weighted, delayed and corrupted by sensory noise as it propagates through the sensory system. Similarly, the neural controller was modeled as a PID controller (Peterka 2002), which as generalized and robust controller has been widely used in control theory applications.

The forward model was implemented as a Smith Predictor (Miall et al. 1993b), first developed for use in industrial control systems to predict large feedback delays. A Smith predictor in its truest sense is static (i.e. non-adaptive). However, previous studies have shown that the forward model is adaptive and its response can be altered or changed through learning (Miall and Jackson 2006). Our study assumes that over the realm of the experimental session, the forward model and in fact all the parameters in the model are time-invariant. This assumption is reasonable, as during the experimental session none of the sensorimotor behavior was changed or altered via learning. The task on which subjects were provided practice was different than the task used for characterizing the parameters, thereby making sure that no learning occurs. Also, fatigue effects were minimized by providing breaks between trials and experiments. These simplifying assumptions allowed us to model the dynamic behavior of the sensorimotor system for wrist movements.

Four experiments were developed to estimate the 13 parameters that together

characterize the model. The model parameters were estimated successively across experiments such that the parameters estimated in Exps. 1 & 2 were used as constants to estimate the subsequent groups of parameters in Exps. 3 & 4. All the parameters (except K_{pr} and K_i) were independent of each other. This was observed from the co-variation matrix calculated across parameter estimates across subjects. Except for K_{pr} and K_i, co-variation across parameters was less than 0.42 (refer Appendix D).

10.3 Feedforward conduction delay

Subject #	T_{eff} (ms) (Exp. 1c)	T_{cp} (ms) (measured from the model)	T_{ff} (ms) (T_{eff} - T_{cp})
1	66.4	37.9	28.5
2	70.9	29.5	41.4
3	59.4	213	-153.6
4	49	58.8	-9.8
5	65.3	81.8	-16.5
6	79.7	11.4	68.3
7	55	25	30
8	67.7	16.7	51
9	50.9	121	-70.1
10	54.8	14	40.8
11	52.2	199.9	-147.7

Table 10.1 Feedforward conduction delay across subjects. Feedforward conduction delay was estimated using an indirect method by subtracting T_{cp} from T_{eff}.

Using the model, we were able to indirectly measure the feedforward conduction delay by subtracting out the phase shift induced by the controller and the plant (T_{cp}) from the estimate of effective feedforward delay (T_{eff}). This was achieved by using the parameter estimates (measured experimentally) for each individual subject in the model, with all the delays (T_v, T_p and T_{ff}) set to zero, and simulating Exp. 1c to measure the delay (i.e. T_{cp}) between the input and the output. Results of the above approach are shown in Table 10.1.

The feedforward delay estimate obtained using above approach ranged from 28 to 68 ms across subjects (6 out of 11). Although, this range seems plausible, one might potentially use other noninvasive methods such as EEG or MEG to obtain more accurate estimates. Surprisingly, the feedforward delay for the remaining 5 subjects was negative. Of these 5 subjects, 4 subjects (# 3, 5, 9 and 11) had a low K_i (< 0.26) estimated from Exp. 4. It should be noted that the error in estimation of K_i was high for lower values of K_i (refer section 7.3.1). This would suggest that the negative feedforward delays could be an artifact due to inaccurate measurement of K_i.

10.4 Forward Model

Evidence in support of a forward model in sensorimotor control has been indirect, however, a number of studies point to its presence and use during goal-oriented tasks (Miall et al. 1993b; Wolpert and Miall 1996a; Mehta and Schaal 2002; Miall and Reckess 2002). The forward model's output can rarely be observed explicitly making it hard to fully characterize. In the current study, the forward model was based on a Smith Predictor topology (Miall et al. 1993b), such that instantaneous limb position was predicted based on the descending motor commands to make online corrections. In the model, the Smith Predictor was assumed to be quasi-static in nature and to perfectly predict the output of the sensory feedback based on the current torque commands. By perfect prediction we mean that the parameters values (J, B, K, T_v, T_p, T_{ff}, K_p and K_v) in the Smith Predictor were identical to those of sensory and motor paths, and hence no additional experiments were required for its characterization. By quasi-static we mean that for the specified task and/or the duration of experimental session, the forward model did not change significantly unless forced to change via learning or adaptation. Miall et al. (2006)

showed that adaptation altered the properties of the forward model and argued against the forward model acting as a Smith Predictor, whose parameters are constant by definition. We do not claim that the Smith predictor is “the forward model” and that it cannot be altered. However, our results suggest that Smith predictor is a good quasi-static approximation of a forward model that has an inherent property to adapt with learning.

An interesting hypothesis is that sensorimotor deficits in certain types of neurological disease could reflect an inability of the forward model to adapt, causing a mismatch in one or more parameters. Miall et al. (2000) demonstrated that closed-loop system can become unstable as a result of this kind of mismatch. A potential application of this study will be to test for this hypothesis in the context of deficits such as tremor.

10.5 Importance of the Study and possible applications

The accurate model prediction of position (suggested by a high VAF) provides support for the proposed model of 1-D wrist movement and suggests that the experimentally measured model parameters can be used to investigate the characteristics of sensorimotor control for wrist movements specifically, and may be for goal-oriented tasks more generally. While we acknowledge that the model does not fully account for all aspects of sensorimotor processing involved in performing 1-D wrist movements, we are hopeful that this research will provide the framework for developing more sophisticated approaches to characterize sensorimotor control in the future.

This finding could be easily translated to other 1-D movements (about elbow or shoulder joint) and can be even extended to decode the sensorimotor integration for 2-D movements. Further, characterizing the sensorimotor control for a tracking paradigm,

and comparing the parameters across tracking and stabilization paradigms can help differentiate the strategies used in these paradigms. Another application of the proposed method would be to characterize the changes in the sensorimotor control system that occurs with aging.

The incorporation and quantification of the forward model, internal noises and temporal delays (as opposed to a single delay term) is a novel aspect of the research and one which we believe will facilitate identification of the sources of sensorimotor deficits resulting from neurological impairment. An underlying motivation of the project has been to study ataxia and tremor in Multiple Sclerosis (MS). Changes in the temporal delay of feedback signals is of special interest because it has been shown previously that these deficits slow down the responses of the patients having these symptoms (Demaree et al. 1999). In case of MS patients, sensory delays (T_v and/or T_p) may be significantly greater than for neurologically intact subjects. In cases where the forward model is unable to update the increased sensory delay in patients suffering from Multiple Sclerosis, the subsequent mismatch in delays can lead to tremor.

Figure 10.1shows the results of a simulation wherein kinetic tremor was obtained by creating a mismatch between the predicted (forward model) and actual visual delays. As seen the figure, the system becomes unstable as the mismatch between the two delays increases. This instability leads to tremulous response by the model. Interestingly, the frequency of the simulated tremors lies between from 2.5 – 3.5 Hz, which is one of the frequency bands of tremors reported for MS patients (Alusi et al. 2001). Given the complexity of the sensorimotor control system, variations in other parameters could lead to similar functional impairments in persons with MS. Therefore, the above approach will

be used to characterize the contributions of impaired sensory and motor processing to the phenomena of tremor and ataxia during goal-directed movement.

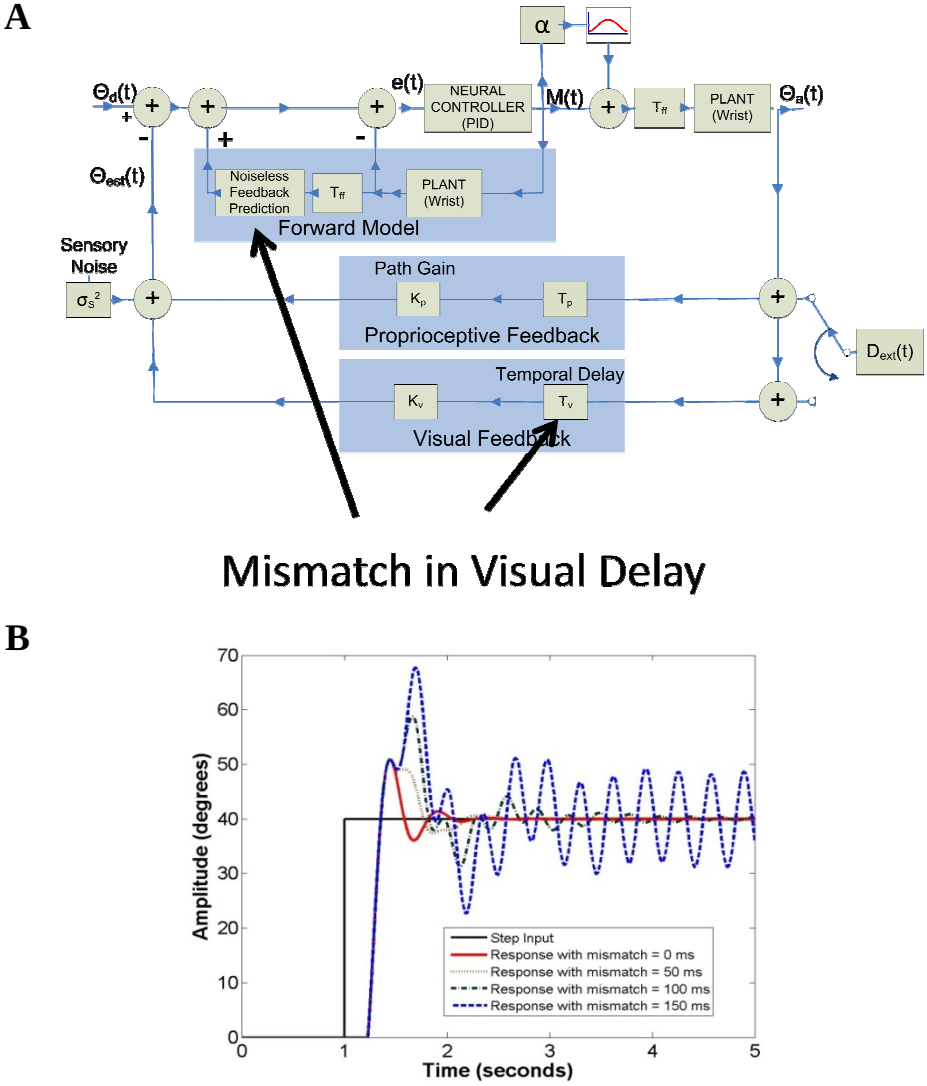

Figure 10.1 Simulating Tremors. A) A mismatch in the two visual delay blocks (one each in the visual feedback path and the forward model) is created, while the other parameters were set to nominal values (measured experimentally in normal subjects). B) Step response of the model is measured with varying levels of mismatch. This mismatch causes the system to become unstable and the level of instability increases as the mismatch increases.

11 FUTURE DIRECTIONS

In Experiment 4, the additive source for sensory noise used in the model was not able to account for the experimental data. Future work will model the sensory noise as combination of additive and multiplicative noise in line with the model proposed by Dosher and Lu (1999) for visual perception. The lack of a multiplicative component to the sensory noise could account for the inability of the model to account for human performance.

For the current study, the sensory noise was represented by a single source. Ideally, there should be two noise sources; one corresponding to each feedback path. However, the current methodology had a limitation in estimating these noise sources independently. An additional experimental condition would be required to be implemented that could help in dissociating the two sources. One such experimental condition could be visuo-proprioceptive stabilization. The subject's task would be to stabilize against the torque perturbations applied to the wrist manipulandum in the presence of visual and proprioceptive feedback. This experimental condition would provide a second estimate of the sensory noise sources, which could be used to separately estimate the noise source. Preliminary results suggest that reflexes may contribute to subjects' overall position response. Accounting for these effects will require the incorporation and experimental characterization of a reflex pathway in the model.

Hence it is important to incorporate a reflex path within the plant (wrist) in order to model the reflex action generated in response to the torque perturbations applied to the wrist. Incorporation of reflex path will solve two problems. Firstly, it would help to

rectify the negative viscosity that was measured experimentally using Exp. 3 (if our hypothesis that the negative viscosity was due to reflex action is correct). Secondly, it would help us to implement stabilization task involving torque perturbations.

Stabilization against torque perturbation could be implemented under two different conditions, visuo-proprioceptive stabilization (in presence of visual feedback) and proprioceptive stabilization (no visual feedback available). Using subtraction analysis (refer Section 7.2), the controller parameters and the feedback gains could be estimated for each of the experimental condition. A comparison of these estimates across three experimental conditions (visual stabilization, proprioceptive stabilization and visuo-proprioceptive stabilization) will help decipher different strategies used when external perturbations are applied to a single and/or both feedback paths.

The current study employed stabilization task as a means to estimate system parameters. Will the strategy used remain the same for a tracking task? To answer this question, all the experiments used in the current study could be replicated to incorporate a tracking task. The target will be moving back and forth in random manner (as opposed to the current study where it was static) and the subject's task would be to try to keep the cursor onto the target in presence of external perturbations. The estimates obtained from tracking paradigm could then be compared to those obtained from stabilization paradigm for the same subject. This will help to compare the strategies used for each paradigm.

BIBLIOGRAPHY

Alusi SH, Worthington J, Glickman S and Bain PG. A study of tremor in multiple sclerosis. *Brain* 124: Pt 4: 720-730, 2001.

Becker JD and Mote CD,Jr. Identification of a frequency response model of joint rotation. *J Biomech Eng* 112: 1: 1-8, 1990.

Bennett DJ. Stretch reflex responses in the human elbow joint during a voluntary movement. *J Physiol* 474: 2: 339-351, 1994.

Bennett DJ, Hollerbach JM, Xu Y and Hunter IW. Time-varying stiffness of human elbow joint during cyclic voluntary movement. *Exp Brain Res* 88: 2: 433-442, 1992.

Beppu H, Suda M and Tanaka R. Analysis of cerebellar motor disorders by visually guided elbow tracking movement. *Brain* 107 (Pt 3): Pt 3: 787-809, 1984.

Binsted G and Elliott D. Ocular perturbations and retinal/extraretinal information: the coordination of saccadic and manual movements. *Exp Brain Res* 127: 2: 193-206, 1999.

Bock O and Girgenrath M. Relationship between sensorimotor adaptation and cognitive functions in younger and older subjects. *Exp Brain Res* 169: 3: 400-406, 2006.

Boff KR, Kaufman L and Thomas JP. Intersensory interactions. In: *Handbook of Perception and Human Performance*, edited by Welch RB and Warren DH. New York: Wiley, 1986, p. 25.1-25.36.

De Serres SJ and Milner TE. Wrist muscle activation patterns and stiffness associated with stable and unstable mechanical loads. *Exp Brain Res* 86: 2: 451-458, 1991.

Demaree HA, DeLuca J, Gaudino EA and Diamond BJ. Speed of information processing as a key deficit in multiple sclerosis: implications for rehabilitation. *J Neurol Neurosurg Psychiatry* 67: 5: 661-663, 1999.

Deuschl G, Bain P and Brin M. Consensus statement of the Movement Disorder Society on Tremor. Ad Hoc Scientific Committee. *Mov Disord* 13 Suppl 3: 2-23, 1998.

Doeringer JA and Hogan N. Intermittency in preplanned elbow movements persists in the absence of visual feedback. *J Neurophysiol* 80: 4: 1787-1799, 1998.

Dosher BA and Lu ZL. Mechanisms of perceptual learning. *Vision Res* 39: 19: 3197-3221, 1999.

Dosher BA and Lu ZL. Perceptual learning reflects external noise filtering and internal

noise reduction through channel reweighting. *Proc Natl Acad Sci U S A* 95: 23: 13988-13993, 1998.

Elliott D, Helsen WF and Chua R. A century later: Woodworth's (1899) two-component model of goal-directed aiming. *Psychol Bull* 127: 342-357, 2001.

Faisal AA, Selen LP and Wolpert DM. Noise in the nervous system. *Nat Rev Neurosci* 9: 4: 292-303, 2008.

Feys P, Helsen WF, Lavrysen A, Nuttin B and Ketelaer P. Intention tremor during manual aiming: a study of eye and hand movements. *Mult Scler* 9: 1: 44-54, 2003a.

Feys P, Helsen WF, Liu X, Lavrysen A, Loontjens V, Nuttin B and Ketelaer P. Effect of visual information on step-tracking movements in patients with intention tremor due to multiple sclerosis. *Mult Scler* 9: 5: 492-502, 2003b.

Fitzpatrick R, Burke D and Gandevia SC. Loop gain of reflexes controlling human standing measured with the use of postural and vestibular disturbances. *J Neurophysiol* 76: 6: 3994-4008, 1996.

Flanders M and Cordo PJ. Kinesthetic and visual control of a bimanual task: specification of direction and amplitude. *J Neurosci* 9: 2: 447-453, 1989.

Foulkes AJ and Miall RC. Adaptation to visual feedback delays in a human manual tracking task. *Exp Brain Res* 131: 1: 101-110, 2000.

Ghez C, Scheidt R and Heijink H. Different learned coordinate frames for planning trajectories and final positions in reaching. *J Neurophysiol* 98: 6: 3614-3626, 2007.

Gielen CC, Houk JC, Marcus SL and Miller LE. Viscoelastic properties of the wrist motor servo in man. *Ann Biomed Eng* 12: 6: 599-620, 1984.

Grey MJ. Viscoelastic Properties of the Human Wrist During the Stabilization Phase of a Targeted Movement. 1997.

Halaki M, O'Dwyer N and Cathers I. Systematic nonlinear relations between displacement amplitude and joint mechanics at the human wrist. *J Biomech* 39: 12: 2171-2182, 2006.

Harris CM and Wolpert DM. Signal-dependent noise determines motor planning. *Nature* 394: 6695: 780-784, 1998.

Hefter H and Langenberg U. Sinusoidal forearm tracking with delayed visual feedback. II. Dependence of the relative phase on the relative delay. *Exp Brain Res* 118: 2: 171-179, 1998.

Helsen WF, Starkes JL, Elliott D and Buekers MJ. Manual asymmetries and saccadic eye movements in right-handers during single and reciprocal aiming movements.

Cortex 34: 4: 513-529, 1998.

Hogan N and Sternad D. On rhythmic and discrete movements: reflections, definitions and implications for motor control. *Exp Brain Res* 181: 1: 13-30, 2007.

Ito M. Neurophysiological aspects of the cerebellar motor control system. *Int J Neurol* 7: 2: 162-176, 1970.

Izawa J and Shadmehr R. On-line processing of uncertain information in visuomotor control. *J Neurosci* 28: 44: 11360-11368, 2008.

Jones KE, Hamilton AF and Wolpert DM. Sources of signal-dependent noise during isometric force production. *J Neurophysiol* 88: 3: 1533-1544, 2002.

Kawato M. Internal models for motor control and trajectory planning. *Curr Opin Neurobiol* 9: 6: 718-727, 1999.

Keele SW and Posner MI. Processing of visual feedback in rapid movements. *J Exp Psychol* 77: 1: 155-158, 1968.

Kelso JA, Cook E, Olson ME and Epstein W. Allocation of attention and the locus of adaptation to displaced vision. *J Exp Psychol Hum Percept Perform* 1: 3: 237-245, 1975.

Kornecki S. Mechanism of muscular stabilization process in joints. *J Biomech* 25: 3: 235-245, 1992.

Kotovsky J and Rosen MJ. A wearable tremor-suppression orthosis. *J Rehabil Res Dev* 35: 4: 373-387, 1998.

Laidlaw DH, Bilodeau M and Enoka RM. Steadiness is reduced and motor unit discharge is more variable in old adults. *Muscle Nerve* 23: 4: 600-612, 2000.

Leist A, Freund HJ and Cohen B. Comparative characteristics of predictive eye-hand tracking. *Hum Neurobiol* 6: 1: 19-26, 1987.

Lu Z and Dosher BA. External noise distinguishes attention mechanisms. *Vision Res* 38: 9: 1183-1198, 1998.

McRuer DT and Krendel ES. The human operator as a servo system element, *J. Franklin Inst.*, 267: 381-403, May 1959; 511-536, June 1959.

McRuer DT, Graham D, Krendel ES, and Reisener W, Jr. Human pilot dynamics in compensatory systems-theory, models, and experiments with controlled element and forcing function variations, *AFFDL-TR-65-15*, 1965.

Mehta B and Schaal S. Forward models in visuomotor control. *J Neurophysiol* 88: 2: 942-953, 2002.

Miall RC and Jackson JK. Adaptation to visual feedback delays in manual tracking: evidence against the Smith Predictor model of human visually guided action. *Exp Brain Res* 172: 1: 77-84, 2006.

Miall RC and Reckess GZ. The cerebellum and the timing of coordinated eye and hand tracking. *Brain Cogn* 48: 1: 212-226, 2002.

Miall RC, Weir DJ and Stein JF. Intermittency in human manual tracking tasks. *J Mot Behav* 25: 1: 53-63, 1993a.

Miall RC, Weir DJ, Wolpert DM and Stein JF. Is the Cerebellum a Smith Predictor? *J Mot Behav* 25: 3: 203-216, 1993b.

Mon-Williams M, Wann JP, Jenkinson M and Rushton K. Synaesthesia in the normal limb. *Proc Biol Sci* 264: 1384: 1007-1010, 1997.

Morgan MH, Hewer RL and Cooper R. Application of an objective method of assessing intention tremor - a further study on the use of weights to reduce intention tremor. *J Neurol Neurosurg Psychiatry* 38: 3: 259-264, 1975.

Neilson PD, Neilson MD and O'Dwyer NJ. Internal models and intermittency: a theoretical account of human tracking behavior. *Biol Cybern* 58: 2: 101-112, 1988.

Notley SV, Turk R, Pickering R, Simpson DM and Burridge JH. Analysis of the quality of wrist movement during a simple tracking task. *Physiol Meas* 28: 8: 881-895, 2007.

Oldfield RC. The assessment and analysis of handedness: the Edinburgh inventory. *Neuropsychologia* 9: 1: 97-113, 1971.

Osafo-Charles F, Agarwal GC, O'neill WD and Gottlieb GL. Application of Time-Series Modeling to Human Operator Dynamics. *Systems, Man and Cybernetics, IEEE Transactions on* 10: 12: 849-860, 1980.

Paillard J. Fast and slow feedback loops for the visual correction of spatial errors in a pointing task: a reappraisal. *Can J Physiol Pharmacol* 74: 4: 401-417, 1996.

Peterka RJ. Sensorimotor integration in human postural control. *J Neurophysiol* 88: 3: 1097-1118, 2002.

Pick HL, Warren DH and Hay JC. Sensory conflict in judgments of spatial direction. *Perception & Psychophysics* 6: 4: 203-205, 1969.

Plooy A, Tresilian JR, Mon-Williams M and Wann JP. The contribution of vision and proprioception to judgements of finger proximity. *Exp Brain Res* 118: 3: 415-420, 1998.

Rocon E, Belda-Lois JM, Sanchez-Lacuesta JJ and Pons JL. Pathological tremor

management: Modelling, compensatory technology and evaluation. 16: 1: 3-18, 2004.

Scheidt RA and Ghez C. Separate adaptive mechanisms for controlling trajectory and final position in reaching. *J Neurophysiol* 98: 6: 3600-3613, 2007.

Schouten AC, de Vlugt E, van Hilten JJ and van der Helm FC. Quantifying proprioceptive reflexes during position control of the human arm. *IEEE Trans Biomed Eng* 55: 1: 311-321, 2008.

Shinners SM. Modeling of Human Operator Performance Utilizing Time Series Analysis. *Systems, Man and Cybernetics, IEEE Transactions on* 4: 5: 446-458, 1974.

Slifkin AB and Newell KM. Variability and noise in continuous force production. *J Mot Behav* 32: 2: 141-150, 2000.

Smaga S. Tremor. *Am Fam Physician* 68: 8: 1545-1552, 2003.

Stark L, Vossius G and Young L. Predictive Control of Eye Tracking Movements. *IRE Trans HFE 3* 52-57, 1962.

Stein JF and Glickstein M. Role of the cerebellum in visual guidance of movement. *Physiol Rev* 72: 4: 967-1017, 1992.

Uhlarik JJ and Canon LK. Influence of concurrent and terminal exposure conditions on the nature of perceptual adaptation. *J Exp Psychol* 91: 2: 233-239, 1971.

van Beers RJ, Haggard P and Wolpert DM. The role of execution noise in movement variability. *J Neurophysiol* 91: 2: 1050-1063, 2004.

van Beers RJ, Sittig AC and Denier van der Gon JJ. The precision of proprioceptive position sense. *Exp Brain Res* 122: 4: 367-377, 1998.

van Beers RJ, Sittig AC and Denier van der Gon JJ. How humans combine simultaneous proprioceptive and visual position information. *Exp Brain Res* 111: 2: 253-261, 1996.

van Beers RJ, Sittig AC and Gon JJ. Integration of proprioceptive and visual position-information: An experimentally supported model. *J Neurophysiol* 81: 3: 1355-1364, 1999.

van Donkelaar P and Lee RG. Interactions between the eye and hand motor systems: disruptions due to cerebellar dysfunction. *J Neurophysiol* 72: 4: 1674-1685, 1994.

Warren DH and Schmitt TL. On the plasticity of visual-proprioceptive bias effects. *J Exp Psychol Hum Percept Perform* 4: 2: 302-310, 1978.

Welch RB, Widawski MH, Harrington J and Warren DH. An examination of the relationship between visual capture and prism adaptation. *Percept Psychophys* 25: 2: 126-132, 1979.

Wolpert DM, Ghahramani Z and Jordan MI. An internal model for sensorimotor integration. *Science* 269: 5232: 1880-1882, 1995.

Wolpert DM and Miall RC. Forward Models for Physiological Motor Control. *Neural Netw* 9: 8: 1265-1279, 1996.

Wolpert DM, Miall RC and Kawato M. Internal models in the cerebellum. 2: 9: 338-347, 1998.

Woodworth RS. The accuracy of voluntary movement. *Psychol Rev* 3: 1-119, 1899.

APPENDICES

APPENDIX A1

Simulation Results for Experiment 1a. The experimental approach to estimate the open loop visual delay (T_v+T_{eff}) was tested over a range of values of T_v = 50-600 ms. For the simulation feedforward conduction delay (T_{ff}) was set to 30 ms and the delay associated with the plant and the controller (T_{cp}) was 40 ms corresponding to an effective feedforward delay (T_{eff}) of 70 ms. Table below shows the estimated open loop visual delay and correlation between the visual perturbation and wrist response.

Sim #	Expected (T_v + T_{eff})	Estimated (T_v + T_{eff})		r^2
		Mean	SD	
1	120	120.7	1.83	0.99
2	170	171.0	1.05	0.99
3	220	219.5	2.92	0.99
4	270	270.6	2.63	0.98
5	320	320.2	1.69	0.98
6	370	369.7	4.30	0.97
7	420	421.0	1.63	0.97
8	470	471.5	1.18	0.98
9	520	520.6	1.71	0.97
10	570	570.3	2.06	0.97
11	620	619.5	4.38	0.95
12	670	670.7	1.70	0.96

APPENDIX A2

Simulation Results for Experiment 1b. The experimental approach to estimate the open loop proprioceptive delay (T_p+T_{eff}) was tested over a range of values of T_v = 20-240 ms. For the simulation feedforward conduction delay (T_{ff}) was set to 30 ms and the delay associated with the plant and the controller (T_{cp}) was 40 ms corresponding to an effective feedforward delay (T_{eff}) of 70 ms. Table below shows the estimated open loop proprioceptive delay and correlation between the torque perturbation and counter torque produced by the wrist.

Sim #	**Expected (T_p + T_{eff})**	**Estimated (T_p + T_{eff})**		**r^2**
		Mean	**SD**	
1	90	92.5	10.07	0.88
2	110	114.1	12.76	0.88
3	130	131.3	6.88	0.88
4	150	150.7	6.34	0.88
5	170	168.8	10.20	0.87
6	190	190.2	4.61	0.88
7	210	212.4	11.56	0.86
8	230	231.8	9.34	0.89
9	250	248.1	8.67	0.88
10	270	271.1	5.59	0.88
11	290	293.3	11.34	0.88
12	310	311.3	9.52	0.88

APPENDIX A3

Simulation Results for Experiment 1c. The experimental approach to estimate the effective feedforward delay (T_{eff} = T_{ff} + T_{cp}) was tested over a range of values of T_{ff} = 10-100 ms. For the simulation the delay associated with the plant and the controller (T_{cp}) was 40 ms. Table below shows the estimated effective feedforward delay and correlation between the sinusoid tracking signal and wrist position.

Sim #	Expected (T_{eff})	Estimated (T_{eff})		r^2
		Mean	SD	
1	50	50	0.00	1.00
2	60	60	0.00	1.00
3	70	70	0.00	1.00
4	80	79.6	0.52	1.00
5	90	89.2	0.42	1.00
6	100	99	0.00	1.00
7	110	109	0.00	1.00
8	120	119	0.00	1.00
9	130	129	0.00	1.00
10	140	139	0.00	1.00

APPENDIX A4

Simulation Results for Experiment 2. The experimental approach to estimate the multiplicative feedforward noise (α) was tested over a range of values of α = 0.01-1. Table below shows the estimated multiplicative feedforward noise and correlation between the data (SD vs. Mean Torque level) and a line having a slope of estimated α passing through origin.

Sim #	Expected (α)	Estimated (α)	r^2
1	0.01	0.0101	1.00
2	0.02	0.0201	1.00
3	0.03	0.0299	1.00
4	0.04	0.0401	1.00
5	0.05	0.0500	1.00
6	0.06	0.0596	1.00
7	0.07	0.0697	1.00
8	0.08	0.0801	1.00
9	0.09	0.0889	1.00
10	0.1	0.1006	1.00

APPENDIX A5

Simulation Results for Experiment 3. The approach to estimate passive wrist dynamics was tested over a range (J = 0.005-0.05; B = 0.03-0.7; K = 0.5-5) of values. Figure below shows the surface plot of error estimation in one parameter as function of the other two parameters for one value of J (0.05), B (0.03) and K (0.5) for which the error is estimation was highest.

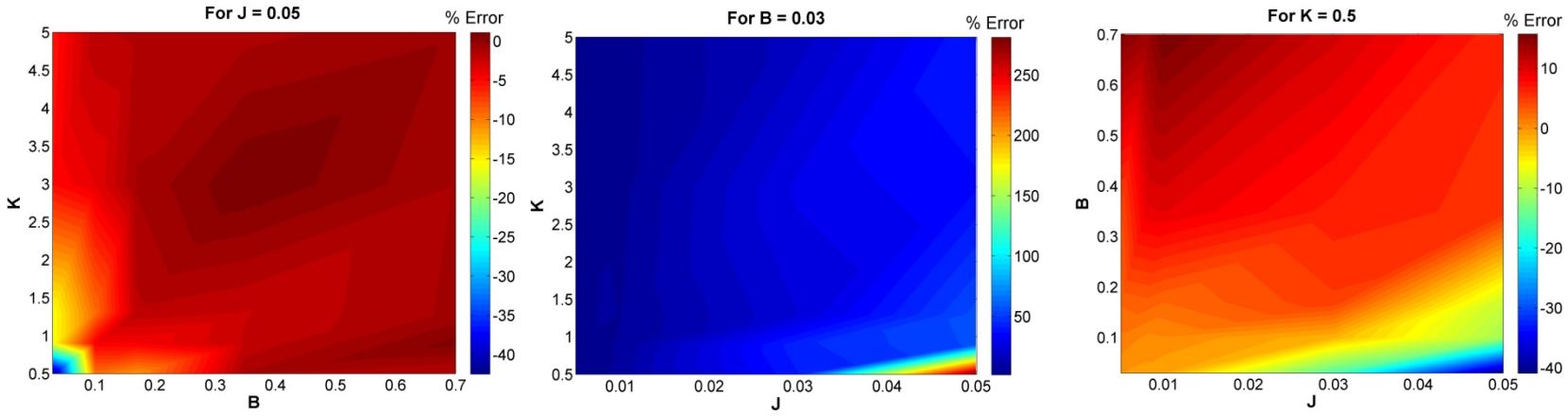

APPENDIX A6

Simulation Results for Experiment 4 (K_d). The approach to estimate controller parameters was tested over a range (K_v = 0.5, 0.75 and 1; K_d = 0.0001-0.01; K_{pr} = 0.005-0.5; K_i = 0.02-5) of values. Figure below shows the surface plot of error estimation in K_d as function of the K_{pr} and K_i for all values of K_d. White space denotes that the system became unstable for these values of K_d, K_{pr} and K_i.

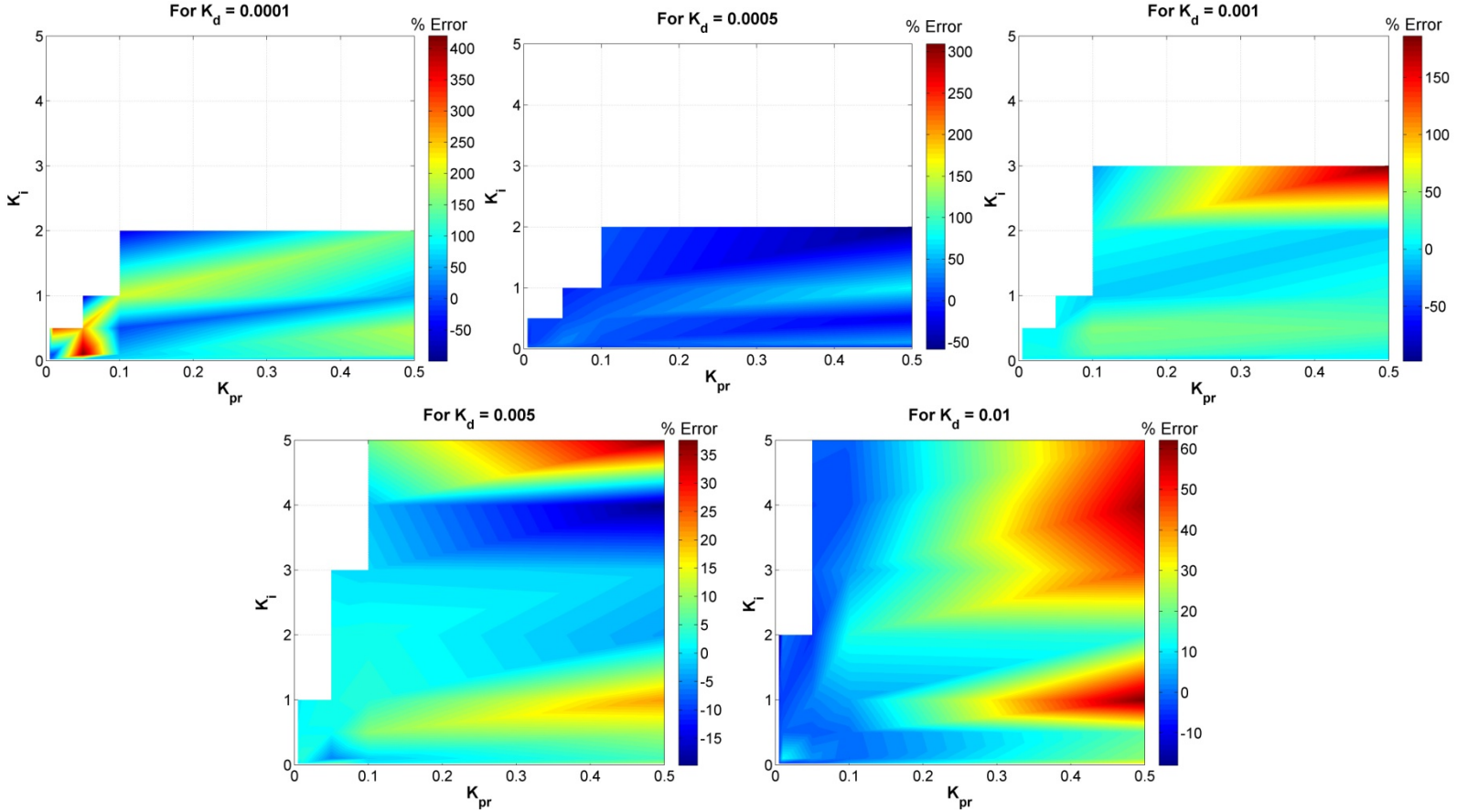

APPENDIX A7

Simulation Results for Experiment 4 (K_{pr}). The approach to estimate controller parameters was tested over a range (K_v = 0.5, 0.75 and 1; K_d = 0.0001-0.01; K_{pr} = 0.005-0.5; K_i = 0.02-5) of values. Figure below shows the surface plot of error estimation in K_{pr} as function of the K_d and K_i for all values of K_{pr}. White space denotes that the system became unstable for these values of K_d, K_{pr} and K_i.

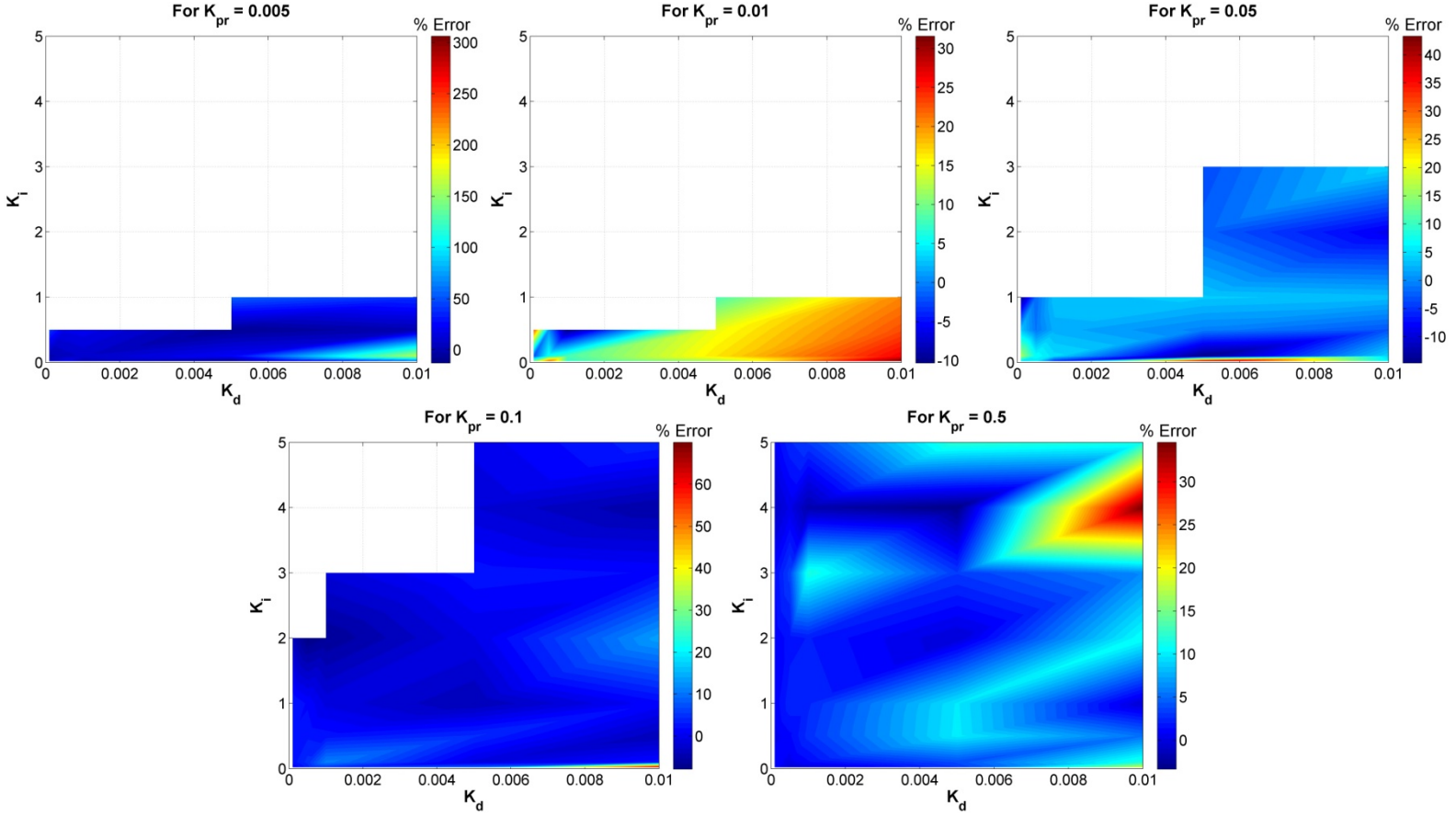

APPENDIX A8

Simulation Results for Experiment (K_i). The approach to estimate controller parameters was tested over a range (K_v = 0.5, 0.75 and 1; K_d = 0.0001-0.01; K_{pr} = 0.005-0.5; K_i = 0.02-5) of values. Figure below shows the surface plot of error estimation in K_i as function of the K_d and K_{pr} for all values of K_i. White space denotes that the system became unstable for these values of K_d, K_{pr} and K_i.

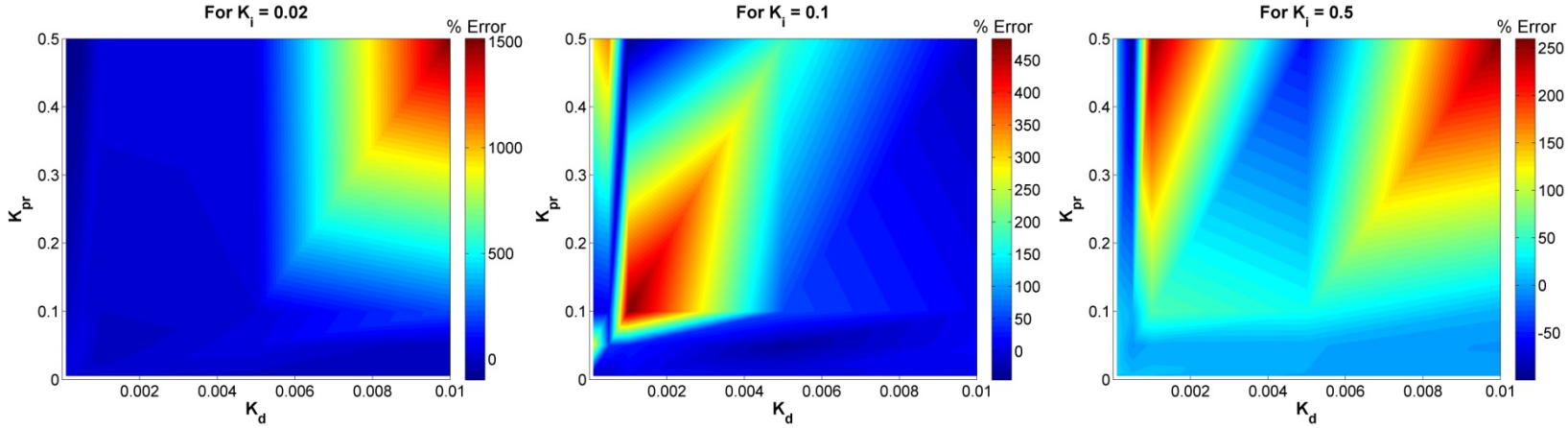

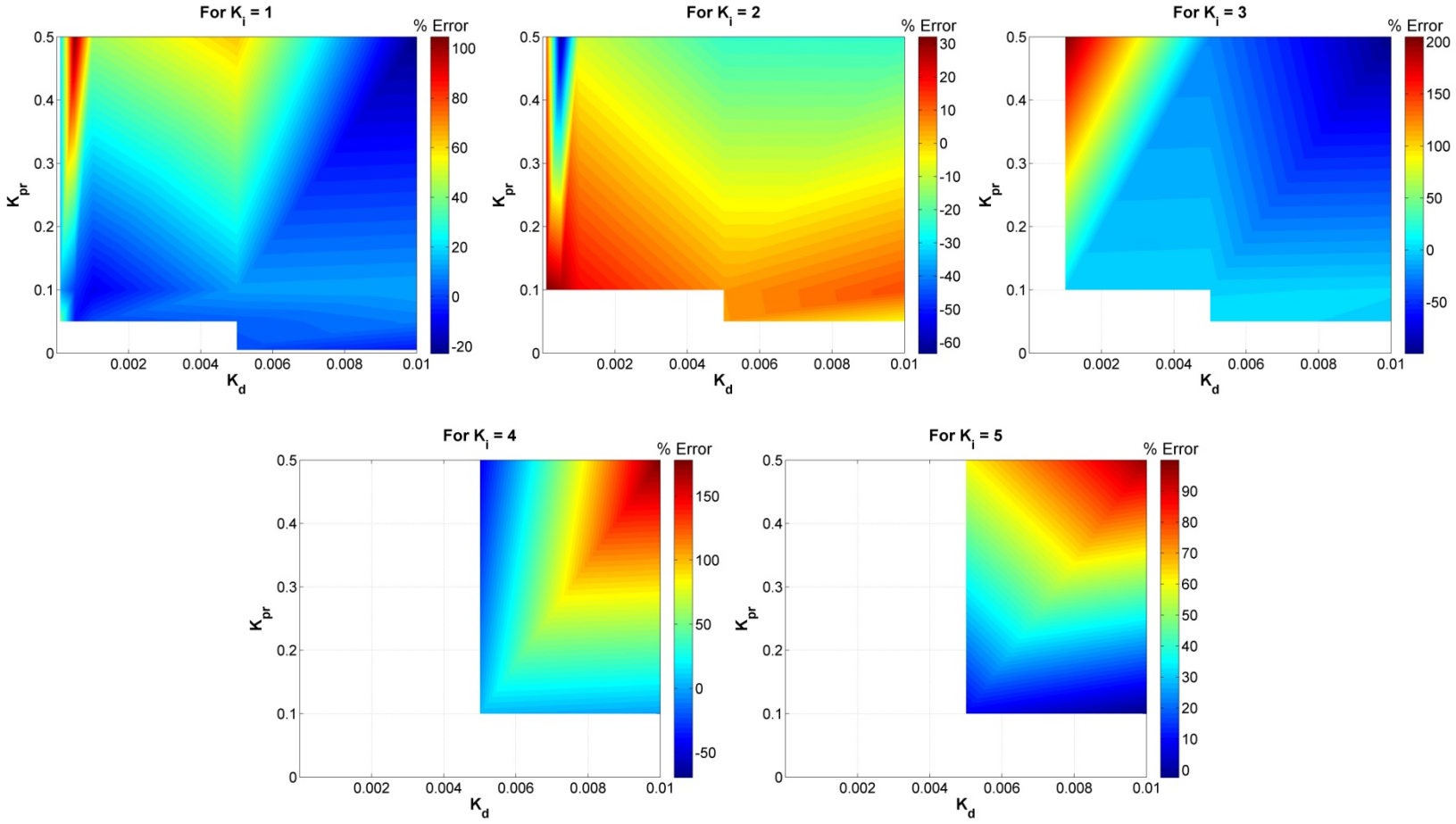
For K_i = 1
% Error
100
80
60
40
20
0
-20
K_pr
K_d
0.5
0.4
0.3
0.2
0.1
0
0.002
0.004
0.006
0.008
0.01
For K_i = 2
% Error
30
20
10
0
-10
-20
-30
-40
-50
-60
For K_i = 3
% Error
200
150
100
50
0
-50
For K_i = 4
% Error
150
100
50
0
-50
For K_i = 5
% Error
90
80
70
60
50
40
30
20
10
0

APPENDIX A9

Simulation Results for Experiment 4. The approach to estimate controller parameters was tested for K_v = 0.5, 0.75 and 1 Figure below show percent error in the median estimates of the K_v, K_d, K_{pr}, and K_i for K_v = 0.75.

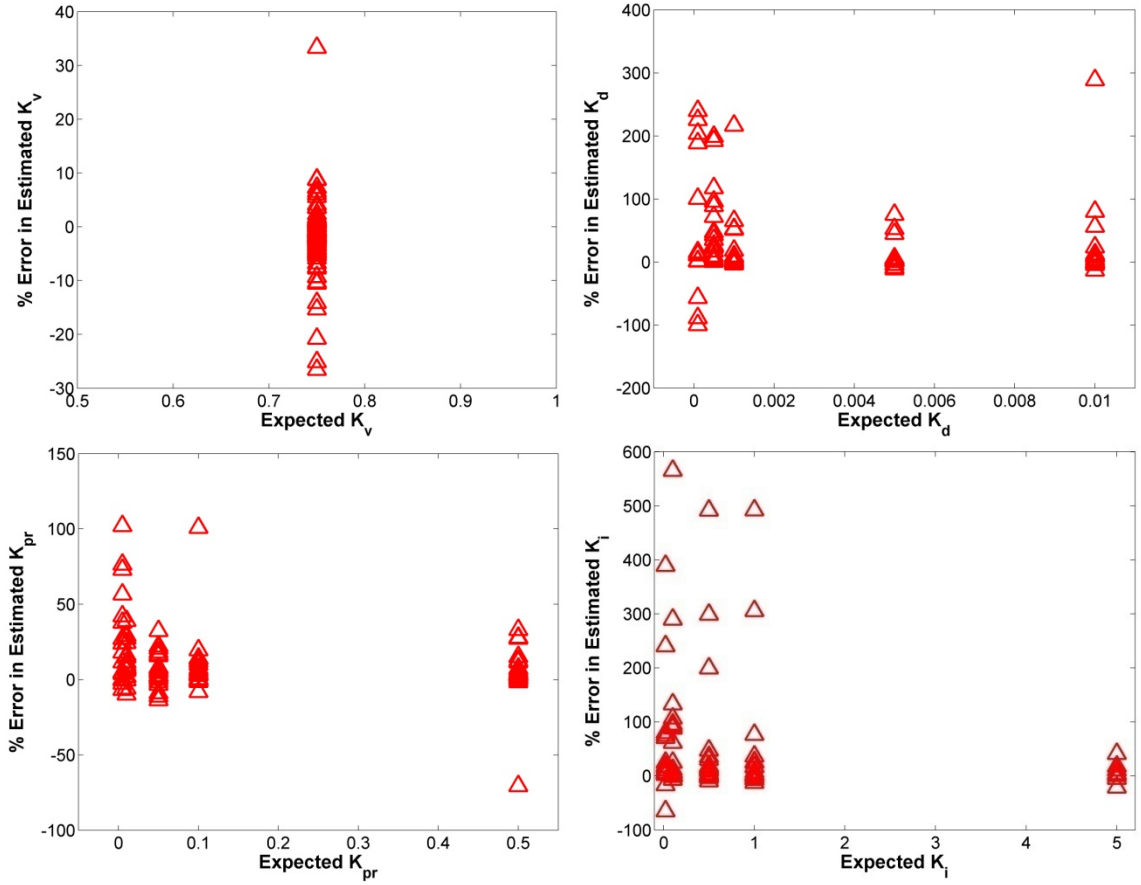

APPENDIX A10

Simulation Results for Experiment 4. The approach to estimate controller parameters was tested for K_v = 0.5, 0.75 and 1 Figure below show percent error in the median estimates of the K_v, K_d, K_{pr}, and K_i for K_v = 1.

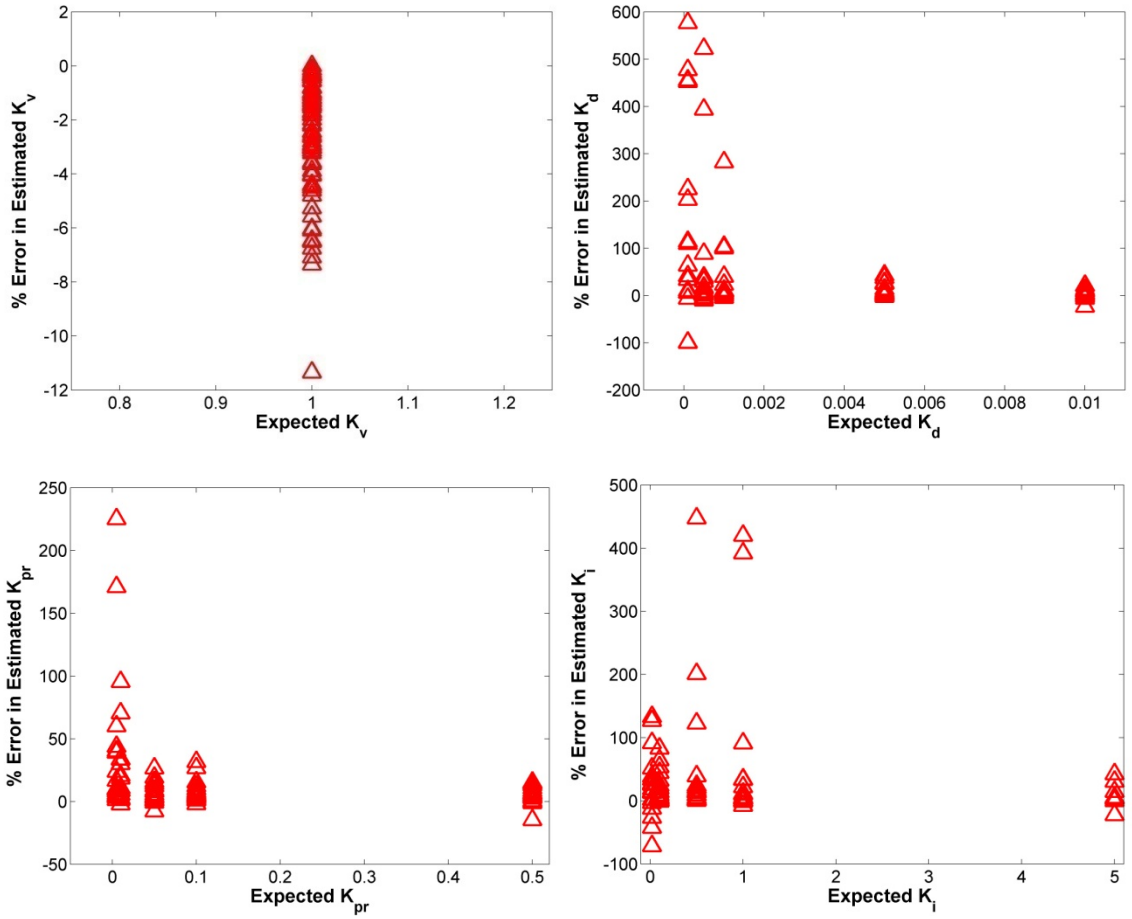

APPENDIX A11

Simulation Results for Experiment 4. The approach to estimate sensory noise was tested over a range (σ_S^2 = 10-2000 degree^2. Table below shows the estimated sensory noise and r^2 values.

Sim #	Expected	Estimated		r^2
		Mean	STD	
1	10	8.25	2.85	0.98
2	20	12.30	5.02	0.98
3	30	37.96	10.67	0.94
4	40	27.68	13.60	0.96
5	50	74.92	14.94	0.96
6	100	89.87	72.90	0.94
7	200	128.15	31.87	0.94
8	300	187.78	48.79	0.93
9	400	409.70	121.39	0.88
10	500	752.20	281.95	0.87
11	1000	1017.20	237.21	0.76
12	2000	2819.95	629.08	0.70

APPENDIX B

Experimental Results. Table below shows the experimental results across all experiments for 11 subjects

Experiments	Parameters	Subject 1					Subject 2				
		μ	r^2	σ	γ	κ	μ	r^2	σ	γ	κ
Experiment 1	$T_v + T_{eff}$ (ms)	239.4	0.7056	22.2	-	-	241.6	0.8649	27.2	-	-
	$T_p + T_{eff}$ (ms)	80.6	0.7744	25.2	-	-	129.2	0.8464	52.9	-	-
	T_{eff} (ms)	66.4	0.9801	13.9	-	-	70.9	0.9604	10.3	-	-
Experiment 2	α	0.0207	-	-	-	-	0.0354	-	-	-	-
Experiment 3	J (kgm^2)	0.0098	0.964	0.0004	0.09	2.97	0.0096	0.969	0.0004	0.09	2.98
	B (Nms/rad)	0.248		0.037	0.56	3.57	0.254		0.037	0.44	3.27
	K (Nm/rad)	2.189		0.165	0.05	3.09	1.095		0.127	0.3	3.28
Experiment 4	K_v	0.998	0.703	0.0118	-6.15	48.27	0.774	0.697	0.0451	0.69	4.23
	K_p	0.002		0.0118	6.15	48.27	0.226		0.0451	-0.69	4.23
	K_d (Nms/deg)	0.0024		0.0002	0.36	3.6	0.0034		0.0004	0.27	3.14
	K_{pr} (Nm/deg)	0.0518		0.0084	0.4	3.24	0.0375		0.008	0.46	3.28
	K_i (Nm/deg.s)	1.085		0.1452	0.36	3.17	0.779		0.1799	0.55	3.48
	σ_S^2 ($degree^2$)	851.4	0.92	217.8	0.36	3.14	1009.9	0.84	373.71	-0.53	3.84

Experiments	Parameters	Subject 3					Subject 4				
		μ	**r^2**	**σ**	**γ**	**κ**	**M**	**r^2**	**σ**	**γ**	**κ**
Experiment 1	**$T_v + T_{eff}$ (ms)**	280.8	0.8836	27.5	-	-	232.6	0.8281	27.5	-	-
	$T_p + T_{eff}$ (ms)	118.5	0.8281	56.3	-	-	106.9	0.8464	56.3	-	-
	T_{eff} (ms)	59.4	0.9604	19.6	-	-	49.0	0.9604	19.6	-	-
Experiment 2	**α**	0.0210	-	-	-	-	0.0354	-	-	-	-
Experiment 3	**J (kgm^2)**	0.0090	0.977	0.0004	0.09	2.95	0.0090	0.953	0.0004	0.09	3.01
	B (Nms/rad)	0.183		0.024	0.63	3.72	0.322		0.036	0.45	3.29
	K (Nm/rad)	2.912		0.205	0.08	2.98	2.940		0.266	0.12	2.98
Experiment 4	**K_v**	0.993	0.792	0.0285	-4.72	28.14	0.906	0.875	0.0625	-0.19	2.28
	K_p	0.007		0.0285	4.72	28.14	0.094		0.0625	0.19	2.28
	K_d (Nms/deg)	0.0002		0.0001	-0.04	2.35	0.0001		0.0002	1.28	2.49
	K_{pr} (Nm/deg)	0.0184		0.0024	0.51	3.75	0.0424		0.0055	0.49	3.05
	K_i (Nm/deg.s)	0.164		0.0248	0.22	3.04	0.929		0.1657	0.67	3.54
	σ_S^2 ($degree^2$)	1608.2	0.92	311.0	0.21	3.02	1393.3	0.69	335.1	0.51	3.66

Experiments	Parameters	Subject 5					Subject 6				
		M	**r^2**	**σ**	**γ**	**κ**	**μ**	**r^2**	**σ**	**γ**	**κ**
Experiment 1	**$T_v + T_{eff}$ (ms)**	301.9	0.4761	22.5	-	-	285.3	0.8649	40.7	-	-
	$T_p + T_{eff}$ (ms)	125.4	0.8836	48.7	-	-	124.9	0.8836	37.7	-	-
	T_{eff} (ms)	65.3	0.9409	19.1	-	-	79.7	0.9216	24.4	-	-
Experiment 2	**α**	0.0592	-	-	-	-	0.0280	-	-	-	-
Experiment 3	**J (kgm^2)**	0.0095	0.939	0.0004	0.13	2.97	0.0092	0.962	0.0004	0.14	2.96
	B (Nms/rad)	0.264		0.043	0.53	3.54	0.245		0.035	0.56	3.59
	K (Nm/rad)	0.680		0.102	0.58	3.42	1.607		0.163	0.11	2.96
Experiment 4	**K_v**	0.985	0.786	0.0308	-2.62	10.3	0.633	0.838	0.0475	0.38	3.07
	K_p	0.015		0.0308	2.62	10.3	0.367		0.0475	-0.38	3.07
	K_d (Nms/deg)	0.0003		0.0002	-0.17	2.42	0.0027		0.0006	0.61	3.51
	K_{pr} (Nm/deg)	0.0339		0.0044	0.24	3.45	0.0598		0.0152	-0.25	3.47
	K_i (Nm/deg.s)	0.203		0.0715	0.52	3.75	2.746		0.5999	0.74	3.62
	σ_S^2 ($degree^2$)	1265.9	0.84	349.13	0.28	3.24	1228.0	0.92	218.6	0.25	3.16

Experiments	Parameters	Subject 7					Subject 8				
		μ	**r^2**	**σ**	**γ**	**κ**	**M**	**r^2**	**σ**	**γ**	**κ**
Experiment 1	**$T_v + T_{eff}$ (ms)**	330.6	0.8836	65.3	-	-	374.6	0.8464	64.5	-	-
	$T_p + T_{eff}$ (ms)	109.5	0.9025	23.7	-	-	155.2	0.8836	22.9	-	-
	T_{eff} (ms)	55.0	0.9409	17.1	-	-	67.7	0.9409	39.5	-	-
Experiment 2	**α**	0.0378	-	-	-	-	0.0270	-	-	-	-
Experiment 3	**J (kgm^2)**	0.0097	0.949	0.0004	0.13	2.98	0.0098	0.966	0.0004	0.11	2.97
	B (Nms/rad)	0.252		0.036	0.55	3.56	0.266		0.036	0.52	3.52
	K (Nm/rad)	1.390		0.176	0.19	2.89	1.768		0.165	0.13	3.02
Experiment 4	**K_v**	0.411	0.767	0.0607	0.46	3.37	1	0.822	0	-1.71	5.41
	K_p	0.589		0.0607	-0.46	3.37	0		0	1.71	5.41
	K_d (Nms/deg)	0.0023		0.0008	0.39	3.74	0.0018		0.0003	-0.42	3.73
	K_{pr} (Nm/deg)	0.0547		0.012	0.34	3.11	0.0796		0.0092	0.11	2.85
	K_i (Nm/deg.s)	1.081		0.6215	0.57	3.37	2.0006		0.2389	0.59	3.65
	σ_S^2 ($degree^2$)	921.9	0.88	251.5	2.59	-0.02	2071.5	0.90	525.35	2.53	-0.15

Experiments	Parameters	Subject 9					Subject 10				
		M	**r^2**	**σ**	**γ**	**κ**	**μ**	**r^2**	**σ**	**γ**	**κ**
Experiment 1	**$T_v + T_{eff}$ (ms)**	271.9	0.7921	35.8	-	-	293.5	0.9216	23.9	-	-
	$T_p + T_{eff}$ (ms)	122.9	0.9025	22.9	-	-	130.4	0.9216	47.3	-	-
	T_{eff} (ms)	50.9	0.9409	23.5	-	-	54.8	0.9604	21.2	-	-
Experiment 2	**α**	0.0152	-	-	-	-	0.0170	-	-	-	-
Experiment 3	**J (kgm^2)**	0.0097	0.952	0.0004	0.10	2.97	0.0080	0.911	0.0003	0.10	2.97
	B (Nms/rad)	0.270		0.036	0.53	3.48	0.256		0.035	0.49	3.43
	K (Nm/rad)	1.966		0.179	0.13	3.03	1.212		0.244	0.04	3.11
Experiment 4	**K_v**	0.693	0.795	0.1043	0.66	3.41	0.629	0.722	0.0375	0.36	3.26
	K_p	0.307		0.1043	-0.66	3.41	0.371		0.0375	-0.36	3.26
	K_d (Nms/deg)	0.0002		0.0001	0.54	2.65	0.0023		0.0004	0.25	3.23
	K_{pr} (Nm/deg)	0.0408		0.0073	0.36	3.1	0.083		0.0122	0.16	2.87
	K_i (Nm/deg.s)	0.258		0.078	0.52	3.69	1.741		0.3664	0.51	3.32
	σ_S^2 ($degree^2$)	1332.1	0.69	251.9	0.29	3.18	1204.5	0.79	294.9	0.04	3.25

Experiments	Parameters	Subject 11				
		μ	**r^2**	**Σ**	**γ**	**κ**
Experiment 1	**$T_v + T_{eff}$ (ms)**	305.9	0.8281	23.9	-	-
	$T_p + T_{eff}$ (ms)	137.8	0.8836	47.3	-	-
	T_{eff} (ms)	52.2	0.9604	15.1	-	-
Experiment 2	**α**	0.0196	-	-	-	-
Experiment 3	**J (kgm^2)**	0.0073	0.908	0.0003	0.06	3.00
	B (Nms/rad)	0.269		0.045	0.61	3.64
	K (Nm/rad)	0.876		0.137	0.37	2.96
Experiment 4	**K_v**	0.923	0.813	0.1195	-1.38	3.71
	K_p	0.077		0.1195	1.38	3.71
	K_d (Nms/deg)	0.0003		0.0001	-0.63	6.29
	K_{pr} (Nm/deg)	0.019		0.0057	1.34	5.16
	K_i (Nm/deg.s)	0.023		0.0068	0.81	3.7
	σ_S^2 ($degree^2$)	200.2	0.35	115.72	0.56	3.37

APPENDIX C

Sensory Noise. Experimental results across 11 subjects showing Internal Variance (σ_S^2) and corresponding end point variability (E.V.)

Sub #	σ_S^2 (degree^2)		E.V. (degree^2)	
	Mean	**STD**	**Mean**	**STD**
1	851.4	217.8	16.6	4.9
2	1009.9	373.7	26.7	9.2
3	1608.2	311.0	3.1	0.7
4	1393.3	335.1	12.1	2.8
5	1265.9	349.1	7.5	2.0
6	1228.0	218.6	84.4	13.6
7	921.9	251.5	17.8	5.3
8	2071.5	525.4	61.3	14.9
9	1332.1	251.9	5.8	1.1
10	1204.5	294.9	41.9	8.6
11	200.2	115.7	0.24	0.2

APPENDIX D

Covariance Matrix. Table below shows the co-variation in one parameter with respect to other parameter(s) for all 13 parameters of the model

	T_v+T_{eff}	T_p+T_{eff}	T_{eff}	α	J	B	K	K_v	K_p	K_d	K_{pr}	K_i	σ_S^2
T_v+T_{eff}	1.00	0.42	0.00	0.01	0.00	0.02	0.13	0.01	0.01	0.00	0.14	0.06	0.08
T_p+T_{eff}	0.42	1.00	0.01	0.00	0.08	0.00	0.19	0.00	0.00	0.00	0.03	0.02	0.08
T_{eff}	0.00	0.01	1.00	0.06	0.16	0.12	0.05	0.01	0.01	0.40	0.05	0.32	0.04
α	0.01	0.00	0.06	1.00	0.12	0.05	0.12	0.00	0.00	0.00	0.02	0.01	0.01
J	0.00	0.08	0.16	0.12	1.00	0.00	0.05	0.00	0.00	0.07	0.04	0.03	0.26
B	0.02	0.00	0.12	0.05	0.00	1.00	0.01	0.00	0.00	0.03	0.04	0.00	0.01
K	0.13	0.19	0.05	0.12	0.05	0.01	1.00	0.07	0.07	0.09	0.01	0.00	0.20
K_v	0.01	0.00	0.01	0.00	0.00	0.00	0.07	1.00	1.00	0.19	0.12	0.11	0.04
K_p	0.01	0.00	0.01	0.00	0.00	0.00	0.07	1.00	1.00	0.19	0.12	0.11	0.04
K_d	0.00	0.00	0.40	0.00	0.07	0.03	0.09	0.19	0.19	1.00	0.31	0.42	0.01
K_{pr}	0.14	0.03	0.05	0.02	0.04	0.04	0.01	0.12	0.12	0.31	1.00	0.67	0.16
K_i	0.06	0.02	0.32	0.01	0.03	0.00	0.00	0.11	0.11	0.42	0.67	1.00	0.12
σ_S^2	0.08	0.08	0.04	0.01	0.26	0.01	0.20	0.04	0.04	0.01	0.16	0.12	1.00

APPENDIX E

Variance Accounted For (VAF) by the Model. Table below shows the VAF (mean ± std) for all subject obtained by comparing subject's response with the model's prediction obtained using the sensorimotor control parameters measured for that subject.

Subject #	VAF (%)	
	Mean	**SD**
1	80.130	5.0100
2	78.480	12.250
3	73.320	9.2000
4	82.490	6.0100
5	78.310	4.9200
6	82.920	4.7600
7	79.890	7.8000
8	74.190	14.010
9	80.840	3.5400
10	80.200	5.2900
11	74.940	6.3100

APPENDIX F

Model implementation in SIMULINK. Figure below shows the model as implemented in SIMULINK for performing simulations.